CHAOTIC VORTICAL MOTION IN THE NEAR REGION OF A PLANE JET

By

JAMES W. CUTBIRTH

Bachelor of Science in Aerospace Engineering
University of Texas
Austin, Texas
1969

Master of Science in Engineering
University of Texas
Austin, Texas
1973

Submitted to the Faculty of the
Graduate College of the
Oklahoma State University
in partial fulfillment of
the requirements for
the Degree of
DOCTOR OF PHILOSOPHY
December, 1991

CHAOTIC VORTICAL MOTION IN

THE NEAR REGION OF

A PLANE JET

Thesis Approved:

Thesis Adviser

Dean of the Graduate College

ACKNOWLEDGMENTS

I would like to express my sincere appreciation to Dr. F. O. Thomas for his patient guidance during the research and his invaluable assistance in understanding the data. Dr. Mihir Sen provided significant insight for the chaos analysis. Further, I thank my graduate committee for their patience and for their encouragement. Dr Frank Chambers deserves special thanks for his assistance in the final revisions if the thesis. Especially, I want to thank Dr. Jerald Parker and Dr. P. M. Moretti for their continual reassurance and support.

Finally, I want to thank my wife Denise Cutbirth for her patience and for her assistance in typing and assembling this thesis.

TABLE OF CONTENTS

LIST OF TABLES

LIST OF FIGURES

NOMENCLATURE

A	constant in equation 2.2
B	constant in equation 2.2
b	mean velocity half-width (in)
C1	constant in equation 2.3
C2	constant in equation 2.4
C(r)	correlation function in equation 3.2
D	nozzle width (in)
E	mean anemometer D. C. bridge voltage (volts)
fc	jet column mode frequency (Hz)
fe	excitation frequency (Hz)
fu	shear layer most unstable frequency (Hz)
k1	constant in equation 2.3
k2	constant in equation 2.4
P	pressure
r	constant used in equation 1.1 and 1.2; distance between data points in equation 3.2
Re	Reynold's number based on the nozzle width
t	time (sec)
U	mean velocity (ft/sec)
Um	centerline velocity (ft/sec)
U_0	centerline velocity at the nozzle exit (ft/sec)
V	velocity vector (ft/sec)

x	longitudinal distance measured from the nozzle exit (in)
X	iteration variable in equation 1.1
y	Lateral distance measured from the nozzle exit (in)
z	Distance parallel to the nozzle exit (in)
ν	kinematic viscosity
λ_n	location of a bifurcation;
λ	Lyapunov Exponent
λ_∞	location of the onset of chaos
δ	Feigenbaum number

CHAPTER I

INTRODUCTION

It is well known that most flows of practical interest are turbulent and an understanding of these flows is essential in many fields of engineering. Successful analysis of the flow over bodies such as airfoils, turbine and compressor blades, and underwater (and surface) vessels requires a knowledge of 'free turbulent shear layer' flow (Ramaprian, Patel and Sastry (1982)). McInville, Gatske and Hassan (1985) have studied these types of flow fields in order to reduce overall vehicle drag and increase fuel economy for long-range transports and general aviation jets. Traditional jet and rocket engine flows have been modeled as axisymmetric or elliptic jets, while high lift aircraft engine exits and vectored thrust exits may be modeled as finite planar jets. Other applications include most combustion processes, jet streams in the upper troposphere, water currents below the surface of the ocean and the wakes of cars and ships. In all of these real flows, the evolution of vorticity and the motion of vortices are essential ingredients (Aref, 1983).

Several studies have been performed in turbulent jets with the objective of enhancing or suppressing turbulence

generation through manipulation of coherent structures in the flow field by means of external excitation. This manipulation involves intricate couplings of various instability and feedback modes. Most of these experimental studies have used 'time-averaged' data and perhaps some kind of 'conditional sampling' technique to obtain data for purely statistical flow models. While valuable information is gained from these analyses, substantial insight into the physical mechanisms inherent in the flow field may be lost. Turbulence research on coherent structures has put vortex dynamics at the heart of the 'turbulence problem'. An increasing emphasis is being placed on deterministic models of vortex interactions with the hope of gaining a better understanding of the seemingly random vortex motions. Purely statistical models and experiments tend to average out these 'random' motions, thus losing what may turn out to be some of the keys to a better understanding of complex fluid flows (Aref, 1988).

The current study concentrates on analyses involving free shear flows. Of particular interest is the motion and interaction of vortices in the near region of a planar jet. In recent years, a substantial number of studies have been performed in mixing layers, axisymmetric jets, wakes and the similarity region of planar jets. Very little research has centered on the near region of planar jets and the subsequent interaction between the shear layers.

In the following discussion, a brief introduction of the planar jet flow field is presented. Following sections present a literature review of some important concepts relating to the current study and the objectives of this study.

The Planar Turbulent Jet Flow Field

The flow field coordinate system is defined with 'x' denoting the streamwise spatial coordinate (perpendicular to the nozzle exit), 'y' denoting the lateral spatial coordinate, and 'z' denoting the direction of mean flow homogeneity (along the slot) (Fig 1). The coordinate origin is located at the center of the nozzle exit. The planar jet flow field can be divided into three basic regions with the first region (near or initial region) consisting of a core of irrotational fluid (referred to as the potential core) at velocity U0 exiting through a two-dimensional slot of width 'D' into a quiescent environment. Planar mixing layers in which structures form and pair at similar longitudinal locations(symmetric shear layers) are formed on each side of the two-dimensional jet and bound the potential core and the surrounding fluid. These layers are initially very thin but widen with downstream distance. Thomas and Brehob (1986) find that for a planar jet with Re=7700 the shear layers merge and effectively end the potential core at a longitudinal distance x of 4 to 7 times the jet slot width

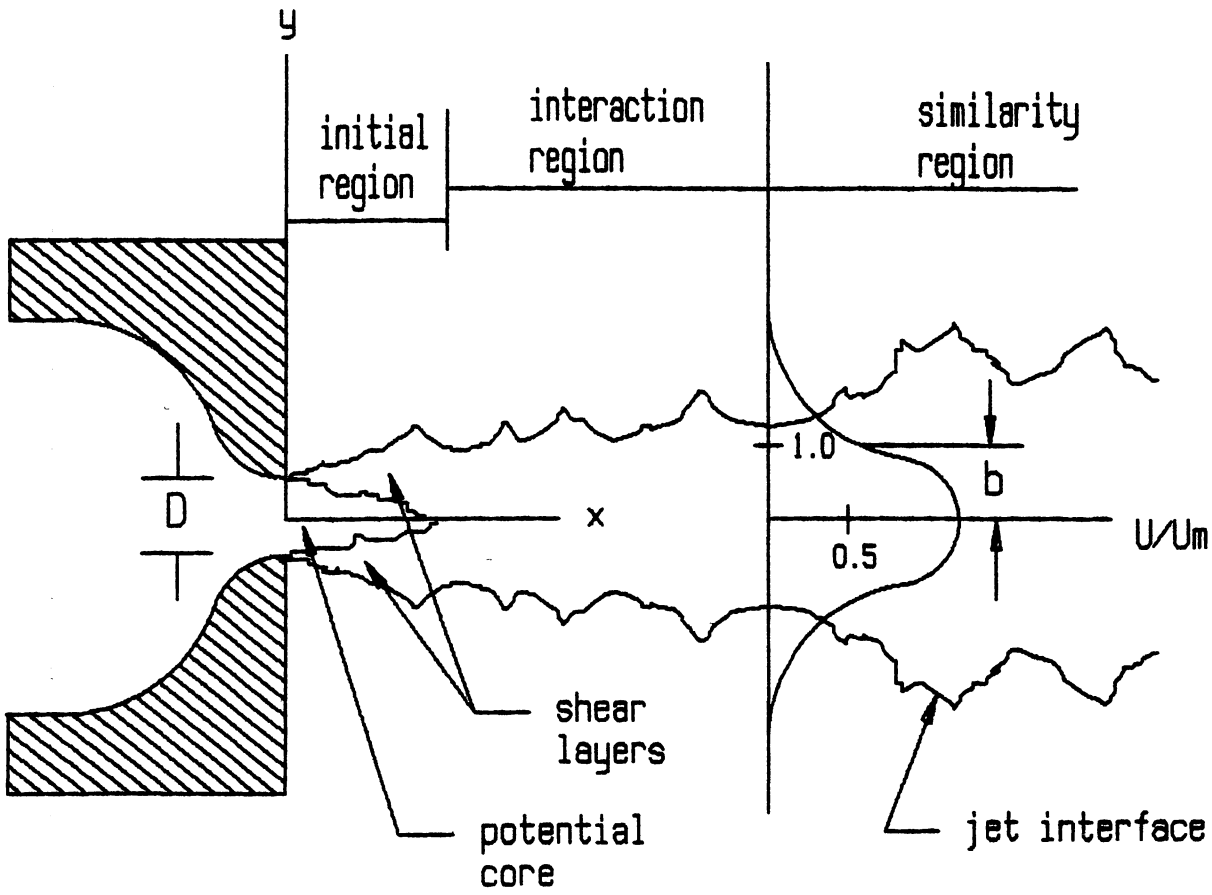

Figure 1. Two-dimensional Turbulent jet

D. This signifies the end of the initial region. Between x/D of approximately 5 to 11, the merged shear layers adjust to form a dynamical equilibrium condition and is termed the interaction region. Beyond x/D = 11, the jet is fully developed and all mean velocity profiles collapse onto one curve when normalized using the centerline mean velocity Um and the mean velocity half-width b as the length scale. Mean velocity half-width b is defined as the lateral position where the mean velocity U drops to half of the local centerline velocity. Since the jet has become self-similar, this region is labeled the similarity or self-preserving region. Typically, profiles of turbulence quantities require larger downstream distances to develop self-preserving characteristics.

Numerous experimental investigations have been performed on planar jets and a substantial body of experimental data is currently available which describes the basic characteristics. A few of these references are Everitt and Robins (1978), Gutmark and Wygnanski (1976), and Bradbury (1965).

Brief Review of Background Work

Growth and Saturation of Two- and Three-Dimensional Modes

Of special importance is the mechanisms involved as the coherent two-dimensional structures breakdown and the

jet transitions from laminar to turbulent. The following sections present a brief review of coherent structures in free shear flows.

Visualization of Coherent Structures. Various methods have been used in attempts to visualize the mechanisms present in the near region of planar jets and other free shear layers (Rockwell, 1972; Rockwell and Niccolls, 1972; Monkewitz, 1988). Brown and Roshko (1974) performed a landmark study in which they took high-speed movies, instantaneous shadowgraphs and measurements of a turbulent mixing layer. A well organized and basically two-dimensional large scale structure is found in conjunction with other patterns which are suggestive of turbulence of smaller scale superimposed on the large structure. This coherent structure is a connected, large-scale turbulent fluid mass with a phase-correlated vorticity over its spatial extent. They conclude that these 'large-scale structures' are primarily responsible for the phenomenon of entrainment (the rate of ingestion of nonturbulent fluid into the turbulent region). The process of entrainment appears to be one in which nonturbulent fluid becomes 'entangled' in the formation of large coherent eddies and is 'enfolded' or 'gulped' into the turbulent region. Smaller instabilities (turbulence) appear to add little or nothing to the "basic ingestion of fluid, but only to its 'digestion'". Brown and Roshko (1974) concluded that the

coherent structures must 'amalgamate' in some way into larger structures and these structures are then convected downstream. This amalgamation is termed 'vortex pairing'; a process in which the vortices become unstable, rotate around each other briefly and unite. The combined structure then convects downstream until the next pairing. A discussion of the implications of these observed structures is included in the next section.

Formation and Interaction of Coherent Structures. Winant and Browand (1974), Peterson (1978), Ho and Huang (1982) and others have concluded that the turbulent shear layer consists of large-scale vortical structures which have their axes perpendicular to the direction of the mean flow. These structures derive their energy from the velocity difference between the two sides of the layer. Vortex pairing appears to be an instability initiated by irregularities in vortex spacing and strength and results in approximately doubling the spacing between vortices and in broadening the layer. Ho and Huerre (1984) also observed that the resulting wavelength and strength is doubled after each interaction and the passage frequency is halved. This interaction is not fixed in space. If a fixed element of the space which is occupied by the mixing layer is examined over a period of time, unpaired vortices, paired vortices and vortices in various stages of pairing will be seen (Browand and Weidman, 1976). This observation

leads to a perplexing question. Why does this irregular (apparently random) motion occur even when the flow is forced with a periodic oscillation? A review of some prominent studies and concepts regarding this irregular motion is presented. An experimental analysis for the planar jet is presented in Chapter 3.

Large-scale coherent structures have also been observed in jets. Becker and Massaro (1988), Crow and Champagne (1971), Ho and Huerre (1984) and Bruun (1977) noted the existence of coherent structures in the near field region of a round jet. Antonia, Brown, Rajagopalan and Chambers (1983), Oler and Goldschmidt (1982, 1984) and Thomas and Goldschmidt (1986) have observed coherent structures in both the near and far regions of two-dimensional jets. Thus, the existence of large scale structures in free shear flow is a well established phenomenon. The importance of these structures on the development and subsequent characteristics of the flow has also been well established. However, adequate physical interpretations of these structures, their interactions, and their relationships in the various flow regions are not readily available. Vortex interactions and instabilities not only dominate the dynamics of the flow field but appear to be the mechanism by which three-dimensional instabilities are introduced. It is clear that streamwise vortices are produced in a mixing layer. However, no information appears to be available for the near region of

a planar jet. Also, although Ho and Huang (1982) and others have determined the sensitivity of vortex formation and interaction on the initial conditions for shear layers, no data are available regarding the formation and subsequent three-dimensional movement of vortices in the near region of a planar jet.

Another concept which has been the topic of numerous investigations involves the observation of different pairing mechanisms. Hussain and Zaman (1985) and Hussain (1986) describe four types of pairing -- complete, fractional, partial, and tearing. Fractional pairing occurs when two independent structures are torn apart and two of the four resulting structures pair. Partial pairing is when one structure is torn apart and pairs with a whole structure. Tearing is simply when a coherent structure is torn apart or splits to form two separate structures. Monkewitz (1988) contends that vortex pairing is heavily favored as compared with vortex tearing (or shredding) with the bias being so strong that it may be impossible to isolate using conditional-sampling techniques. Rockwell and Niccolls (1972) describe two classes of vortex pairing in a planar jet. The first class is where adjacent vortices merge almost immediately after the initial roll-up. The second is a 'mature' pairing where two adjacent relatively mature vortices pair. Occasionally 'embryonic' vortices were observed 'stagnating and sliding' into each other with a motion which appeared to be a 'folding' (i.e.

no net rotation of the wave). Becker and Massaro (1988) observed similar pairing mechanisms occurring in an axisymmetric jet. Ho and Huang (1982) found an unusual type of pairing in a mixing layer which involved a simultaneous merging of 10 or more vortices. This was termed 'collective interaction'. A three-dimensional analysis of these mechanisms in the near region of a planar jet and their response to low amplitude external forcing frequencies is currently unavailable.

Chaos

One of the most dramatic influences on scientific thinking has been the fairly recent emergence of the 'theory of chaos'. An excellent historical background is presented by Gleick (1987). Chaos (deterministic chaos) is the seemingly unpredictable (apparently random) behavior of purely deterministic solutions to non-linear equations. Chaotic motion is a type of motion that is extremely sensitive to small changes in initial conditions. For example, May (1976) explored what appeared to be a simple equation known as the logistic equation

$$X_{n+1} = r\, X_n\, (1 - X_n) \qquad (1.1)$$

where r is the 'bifurcation parameter'

For values of r below 3, this is a well behaved equation where X_{n+1} approaches a single value for any starting value of X_n between zero and one. At r=3, a bifurcation (one equilibrium state changes to two stable equilibrium states)

occurs with this one solution becoming unstable but a two-cycle solution becoming stable (Moon, 1987). The next bifurcation occurs at 3.44949... with another occurring at 3.544090... (Lundqvist, March, and Tosi, 1988). This period-doubling process continues as r --> 3.56994.... An important number is obtained by taking the ratio of the values of r at which bifurcations occur.

$$\text{i.e.} \quad \lim_{n\to\infty} \frac{r_{n+1} - r_n}{r_n - r_{n-1}} = 4.66920... \qquad (1.2)$$

$$\text{where:} \quad \lim_{n\to\infty} r_n = 3.56694$$

This is named the Feigenbaum number after the physicist who discovered these properties. For values of r between 3.56694 and 4, chaotic iterations occur although there are small windows in which periodic motion exists. The really amazing observation is that even though the pattern appears to be totally random, it is repeatable implying the existence of some underling order.

Period doubling and Feigenbaum scaling have been observed in many fluids experiments. There seems to be an intense interest in chaotic dynamics primarily for its potential in unlocking some of the secrets of turbulence. The thought that apparently random fluctuations in turbulence may not be totally random at all, but may have some sort of order (the concept of chaos) is indeed intriguing.

Aref (1983) considered chaotic turbulent vortex motion

in two-dimension flows. He analyzed point vortices using a 'Hamiltonian dynamical system'. A 'threshold for chaotic behavior' is found to exist. For any flow geometry, there exists a maximum number (N^*) of vortices that has integrable dynamics. If $N < N^*$, the vortex motion is periodic or at worst quasi-periodic. However, if $N > N^*$, the dynamics become chaotic with extreme sensitivity to initial conditions. For free shear flows, it is found that the vortex roll-up is periodic in nature but 'time-stepping' errors destroy the exact periodicity. Since most of this work is theoretical, more experimental work is required for verification of these concepts. (See also the IUTAM symposium review by Aref, 1988.)

The fractal nature of turbulent flows has also been investigated. A fractal is defined as a geometric property of a set of points in an n-dimensional space having the quality of self-similarity at different length scales and having a noninteger fractal dimension less than n. A fractal (Hausdorff) dimension can be described by considering a set of points in n-dimensional space. This set is to be covered by a set of cubes of linear dimension ϵ. Let N be the smallest number of cubes required to cover the space. The fractal dimension d is defined by the limit (if it exists) of the ratio

$$d = \lim_{\epsilon \to 0} \frac{\ln N}{\ln (1/\epsilon)} \qquad 1.3$$

When the set is merely a single point, N=1 and d=0. This is equivalent to the Euclidean dimension of zero. If the set is a line segment of length L (Euclidean dimension of 1), then $N=L/\epsilon$ and d=1.

Prasad, Meneveau, and Sreenivasan (1988) investigated a section of the similarity region of a jet. Of primary interest was the multifractal nature of the dissipation field. A similar study was performed by Sreenivasan and Meneveau (1986) in the wake of a projectile. In this case, the fractal nature of the turbulent non-turbulent interface was the object to be investigated. It is concluded that turbulence can indeed be described as a fractal set. Unfortunately, it is not clear how to use the fractal set to reconstruct the turbulent flow. Mandelbrot (1983) investigated the fractal geometry of many physical phenomena including fluid flows.

Numerous other studies involving the chaotic nature of fluid flows have been performed. Chaotic advection was studied by Jones and Aref (1987). Studies have been conducted regarding thermal convection, Taylor-Couette flow between cylinders, pipe flow and surface waves (Moon, 1987).

Perhaps the most well known of all fluids experiments in chaos is the dripping faucet (Shaw, 1984). It is found that if droplets of water are allowed to fall from a faucet, the nature of the motion is highly dependent on the flow rate (i.e. initial conditions). For low flow rates,

the motion is periodic but for high flow rates, the motion bifurcates and eventually becomes chaotic. Shaw compares the motion to the logistic equation and finds that the Poincare sections are virtually identical.

Fundamental terms such as flows, Poincare maps, Poincare sections, and bifurcations are essential to a discussion of chaos and demand some additional explanation. A 'flow' is a set of differential equations such as

$$\frac{d}{dt} X(t) = F(X,t) \qquad 1.4$$

where: X is a vector in R^n

R^n is the phase space

phase space is a plot of velocity vs position

F is a vector field over R^n

Most of the time, the flow equation is not integrable and each solution must be studied by considering the flow trajectory in phase space. Due to the usual difficulties, Henri Poincare was prompted to develop a method to simplify this task. Instead of directly studying the solution to equation 1.4, information regarding the flow can be obtained by analyzing the points of intersection between the trajectory of the flow and a plane. The resulting two-dimensional graph is called a Poincare section. The transformation leading from one point to the next in the section is called the Poincare map. If each of the points in the map completely determines the next (i.e. p_1 uniquely

determines p_2) and the inverse is also true (i.e. p_2 uniquely determines p_1), the map is an 'invertible' map.

There are three basic kinds of Poincare sections. These encompass the classic types of dynamical motion (periodic, quasiperiodic) called attractors and a relatively new class of motion (aperiodic or chaotic) called a strange attractor. The first involves a periodic solution. In this case the phase trajectory is a closed orbit and the corresponding Poincare section simply reduces to a single point. The second kind involves a quasiperiodic solution. For a biperiodic solution with two fundamental frequencies f_1 and f_2, the attractor is a torus. Any trajectory on the surface of the torus can be visualized as the superposition of a rotation along the larger torus dimension and the other, a rotation about the axis of the 'cylinder' which forms the torus. If the ratio f_1/f_2 is irrational, the Poincare section consists of a dense set of points forming a closed curve. If the ratio is rational, the Poincare section consists of a finite set of points lying on the intersection of the torus and the plane. The third kind of Poincare section is aperiodic (chaotic) and the attractor is called 'strange'. If the flow is dissipative and results in a rapid contraction of areas, the Poincare section can be considered to be a set of points distributed along a curve (a one dimensional graph or map). Usually the study involves the analysis of the 'first return map'; i.e. a map of the iteration

$$X_{k+1} = f(X_k) \qquad 1.5$$

which expresses the relationship between the coordinates of a point and its predecessor.

The concept of bifurcations is immense and encompasses an entire branch of mathematics. As stated earlier in this section, a bifurcation occurs when the solution to an equation changes qualitatively at a fixed value (critical value) from one equilibrium state to two or more equilibrium states. The point at which the event occurs is defined to be a bifurcation point. The bifurcation parameter is the variable which is used to effect the change in dynamical motion. For values of the bifurcation parameter greater than the bifurcation point, two (or more) solution branches will emerge. These may be either stable or unstable. Two specific types of bifurcations will be of interest in Chapter III. The first is a saddle-node bifurcation (figure 2) and is encountered in equations of the form

$$dX/dt = \mu - X \qquad 1.6$$

where μ is the bifurcation parameter

The bifurcation is characterized by two non-linear (actually parabolic) branches of steady states emerging from the bifurcation point. One branch is stable and will continue as the bifurcation parameter is increased. The other is unstable which means that any (no matter how small) deviation in initial conditions will cause large

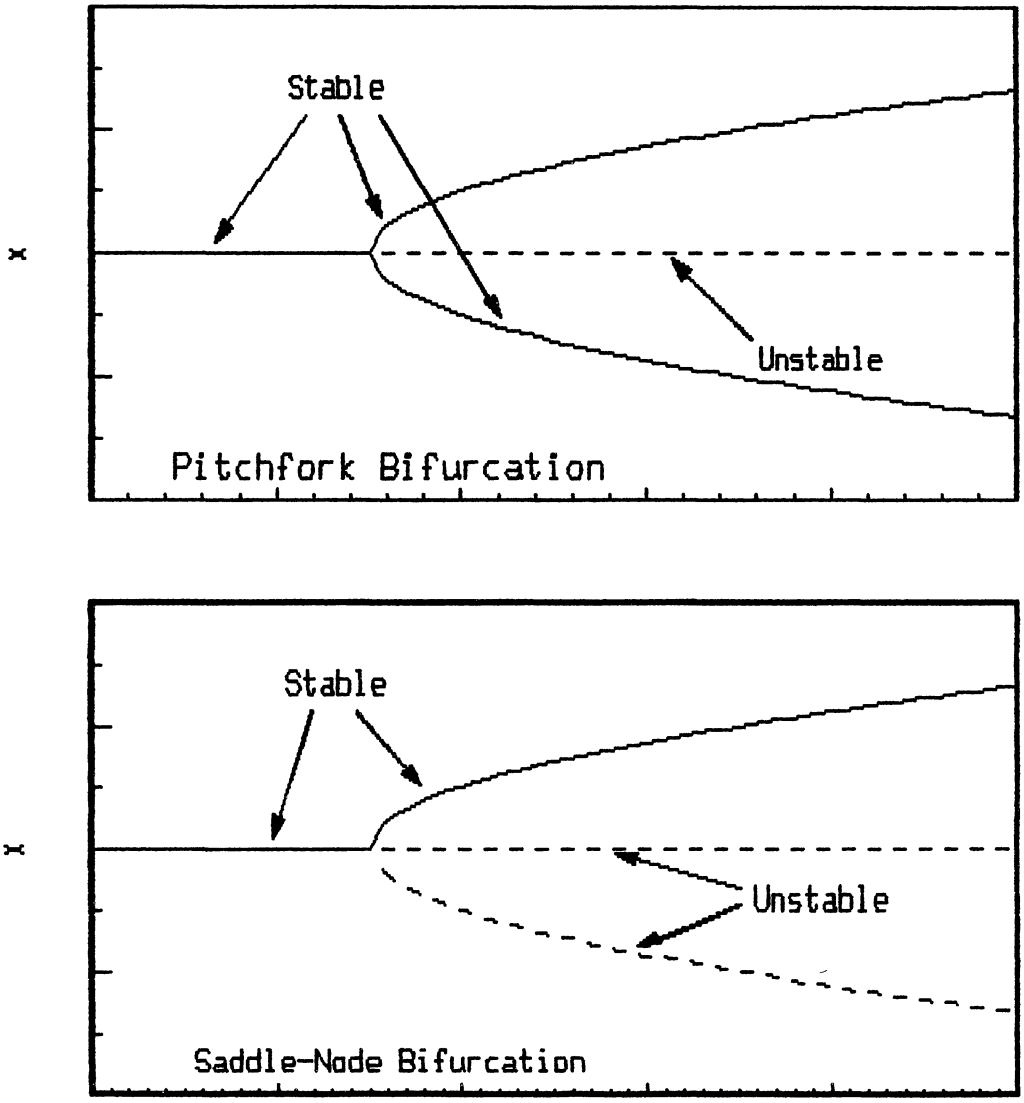

Figure 2. Schematic of Bifurcation types

fluctuations. No unstable branch will be observable. The second type associated with equations of the form

$$dX/dt = X * (\mu - X) \qquad 1.7$$

This type is similar to the saddle-node bifurcation except that both branches are stable and the original path (X=0) is theoretically possible but unstable. This is called a pitchfork bifurcation.

For more detailed information on chaos and related topics, the reader is referred to Moon (1987), Thompson and Stewart (1986), and Berge, Pomeau and Vidal (1984).

Objectives of the Research

The primary purpose of this research is to investigate physical mechanisms by which two-dimensional coherent structures form and interact with each other. Low amplitude, single frequency excitation is to be applied upstream of the nozzle exit to organize the initial instability wave and facilitate investigation of its downstream evolution. Frequencies are to be applied which emphasize particular spectral development patterns and isolate individual pairing mechanisms.

The major focus of this study is directed toward an answer to the following question. Why do motions of two-dimensional structures in the near region of a planar jet rapidly lose their periodicity with downstream distance? This perplexing phenomenon is observed even though the flow is forced with a regular, periodic oscillation. In

addition, flow visualization techniques will be used to isolate and identify various patterns of vortex roll-up and pairing.

CHAPTER II

EXPERIMENTAL FACILITIES AND MEASUREMENT TECHNIQUES

This chapter describes the water planar jet facility to be used in this study. Flow field validation for both the natural and externally forced conditions will be presented.

Description of Planar Water Jet Flow Field Facility

A schematic of the water jet facility is shown in Fig. 3. The water is recirculated through the jet by means of pump located below the tank. A drain located in the far end of the tank allows the water to be drained out of the tank, into the pump, and finally back into a 18 inch by 23 inch by 30 inch high plenum which is used for flow settling. A screen wire mesh separates the plenum from a 9 inch by 9 inch duct. The 30 inch long duct is used to filter and smooth the water in order to produce a 'clean' jet flow. Water first passes through plastic 'drinking type' tubes which act as flow straighteners and help remove any large scale turbulence. Two wire mesh screens are placed downstream of the plastic tubes to again reduce the

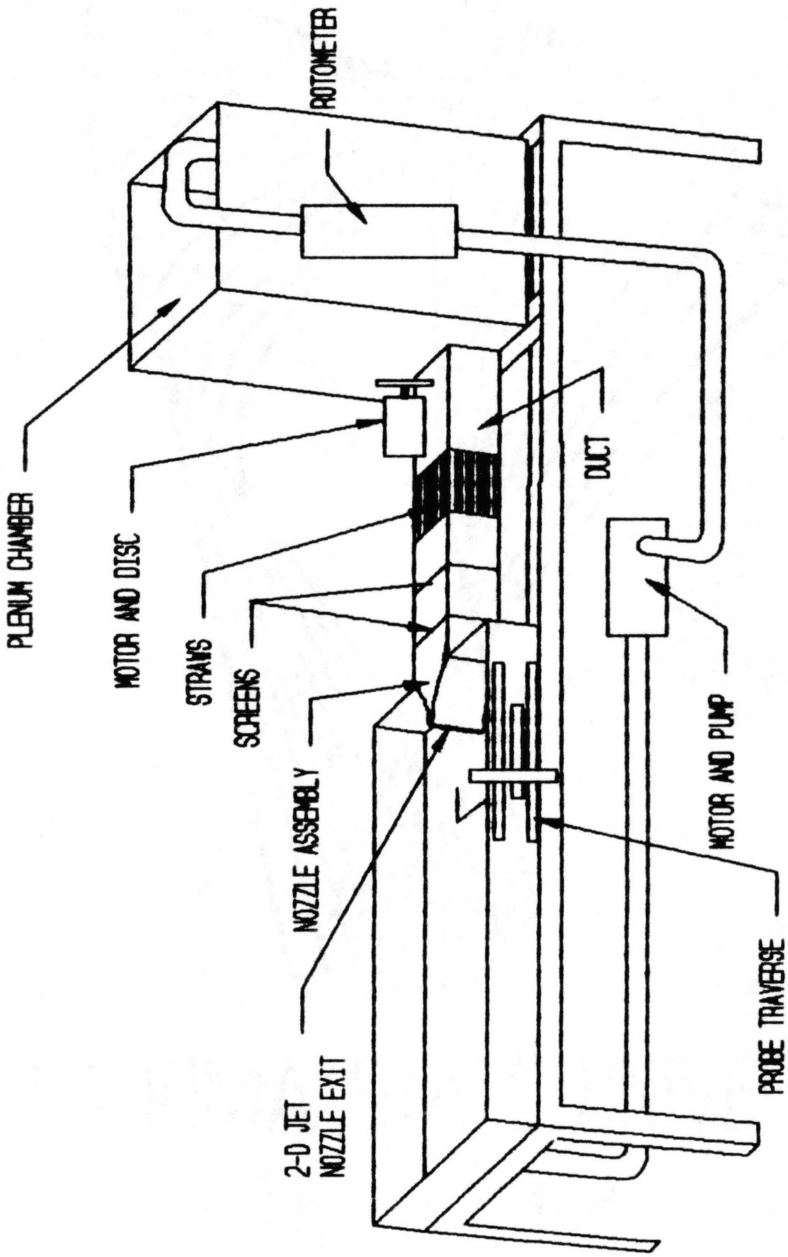

Figure 3. Schematic of Planar Water Jet

size of the turbulence and provide a clean inlet flow to the nozzle assembly. The two-dimensional nozzle has a contraction ratio of 16:1 and ends in a slot that is 0.5 inches in width and 5 inches in height. The nozzle contour is similar to that used in a similar air jet (Chu 1987). A slot perpendicular to the flow and one inch long was cut into each side of the nozzle wall to allow injection of dye into the layer of fluid immediately adjacent to the wall.

The water discharges from the nozzle exit into the flow field which is an enclosed plexiglass tank measuring 30 inches wide and 48 inches long and 5 inches high. The set-up is supported by a sturdy angle-iron and pipe frame.

A rotometer was mounted between the pump exit and the plenum chamber. The rotometer was calibrated so that the readings could be related to average nozzle exit flow velocity in ft/sec. The calibration was

$$\text{velocity} = (0.113 * \text{rotometer} + 0.0154)^{0.45} \quad \text{ft/s} \qquad (2.1)$$

In order to isolate the tank from vibrations of the pump, a rubber hose was used to connect the tank exit to the pump inlet. The tank sits on a rubber cushion to further isolate it from random vibrations.

Controlled perturbations were introduced into the flow between the plenum chamber and the straightener tubes. An electric motor with a Graham ball/disc variable speed transmission was connected to a circular disc. The disc had a slot cut in its center so that the degree of

eccentricity could be controlled. Thus the desired frequency and amplitude was set by adjusting the transmission and the degree of disc eccentricity. The disc was in contact with a rubber diaphragm which covered a hole in the upper surface of the plexiglass duct.

A two-dimensional traverse mechanism similar to the mechanism in the air jet (Chu, 1987) was used to control the location of the hot film probe. Several significant problems were encountered in the hot film measurement procedure. First, the hot film probe is extremely sensitive to water temperature. Changes on the order of 0.01 degree F caused relatively large errors in the data. The water temperature was impossible to control this accurately. However, aquarium type heaters were purchased and used to heat the water to several degrees above room temperature. This procedure improved the data but did not completely cure the problem. Another problem which had detrimental effects on the data was noted but never solved. For some reason, when the hot film was left in a laminar region for even a short period of time, a 'coating' apparently began to collect on the hot film and seemed to act as an insulator. When the probe was moved to a turbulent region (or shear layer) the probe would be cleansed and the readings would return to values near the original values. Obviously, it was extremely difficult to obtain data such as velocity profiles where time-averaged quantities were desired. Data such as power spectrum could

be obtained without extreme difficulty. The third problem involved the traverse mechanism. Due to physical limitations, the traverse mechanism would only move a longitudinal distance of 6.5 inches with an operational limitation of less than 5 inches (from the nozzle exit to about x/D=9).

The electronic data acquisition equipment was basically the same as that used by Chu (1987) in the air jet. These instrumentation setups plus the flow visualization setup will be described in the next section.

Instrumentation

Hot Film Anemometry

Digital data acquisition was performed with on-line processing of hot-wire and hot-film anemometers. For this purpose, DISA 56C01 anemometers operated in the constant temperature mode were used in conjunction with DISA 56C17 CTA bridges. For measurements of the instantaneous longitudinal fluctuating component, DISA 55R01 film probes were used in the water jet. An operating temperature of 40 ^{0}C (overheat of approximately 1.15) was used. Analog signals from the probes were passed through an anti-alias low pass filter. Initial runs were made with the filter set at 50 Hz. No pertinent data was observed above 20 Hz, so the filter was reset to 20 Hz. Frequency resolution was 0.078 Hz. The data were digitized with an HP-9864A A/D

board which is capable of sampling up to seven channels of data and has a maximum sampling rate of 18 microseconds on a single channel. The digital signals were processed on line with an HP-9920S minicomputer which performed all data reduction. A 15 Mbyte hard disk was used for data storage. A high resolution CRT display and a printer were available as output devices.

Calibration of the hot film probes was approximated by using the actual water jet itself at different velocities. The anemometer D.C. bridge voltage was recorded for each velocity setting as indicated by the rotometer. A King's Law calibration was utilized. This relation can be written as

$$E^2 = A + BU^{0.45} \qquad (2.2)$$

where E is the mean anemometer D.C. bridge voltage, and U is the mean velocity. A least squares method was employed to determine the calibration constants A and B.

Water Jet Flow Visualization

The primary utility of the water jet is the ability to isolate and visualize individual coherent structures. This section is intended to describe this visualization procedure.

A sheet of fairly thin transparent paper was placed on the bottom outside surface of the tank. Longitudinal (x/D) and lateral (y/D) coordinate were drawn on the paper to

enhance quantitative video analysis. Two 500 watt lamps were carefully placed so that they illuminated the tank through the paper. A standard video camera was mounted on the other side of the tank. This facilitated video pictures looking in the direction of homogeneity (z-direction).

The video pictures were recorded on a standard VHS video tape. Analysis was achieved by replaying the video tape using frame by frame and slow motion capabilities of a standard VHS video player and a Data Translation QuickCapture image processing system.

Description of Basic Flow Field Parameters

In order to insure that no unusual behavior exists in the near region of the planar water jet, data has been obtained to validate the flow field. This section will present experimental results which document the general development of the flow field.

Experimental Data Points

Experimental data which were taken included mean velocity profiles, longitudinal turbulence intensities, power spectral development, and phase correlation. The test matrix for these data are presented in Tables 1 and 2.

Flow Field Validation

This section will present basic experimental flow

TABLE 1

TEST MATRIX FOR VELOCITY PROFILES
AND TURBULENCE INTENSITIES

	Forcing Frequency			
x/D	Natural	3.5 Hz	5.3 Hz	7.0 Hz
0.25	X	X	X	X
0.5	X			
1.0	X	X	X	X
1.5	X			
2.0	X	X	X	X
3.0	X			
4.0	X	X	X	X
5.0	X			
6.0	X	X	X	X
7.0	X			
8.0	X			

TABLE 2

TEST MATRIX FOR POWER
SPECTRAL DEVELOPMENT

	Forcing Frequency			
x/D	NATURAL	3.5 Hz	5.3 Hz	7.0 Hz
0.25	X	X	X	X
1.0	X	X	X	X
2.0	X	X	X	X
4.0	X	X	X	X
6.0	X	X	X	X
8.0				X
10.0		X		X
12.0			X	
14.0				X

field data to document the general development of the planar water jet. The purpose of these data is to validate the flow field to insure that the jet behavior is similar to other planar jets found in the literature. This is necessary if the conclusions of this study are to be applied to planar jets in general.

All experimental data in this study were obtained at a Reynolds Number of 2000 where the length scale is the slot width and the velocity scale is the average exit velocity. This corresponds to an exit velocity of 0.581 ft/sec. Exit velocity was computed by taking the volume flow rate from the calibrated rotometer and dividing by the nozzle exit area.

Figures 4 and 5 present data documenting the widening of the jet and the variation of shear layer momentum thickness with longitudinal distance. Momentum thickness θ is defined as

$$\theta = \int_0^\infty (1-u/U)*(u/U)\ dy \qquad (2.3)$$

where u = local velocity in the shear layer
U = free stream velocity

Initial momentum thickness, θ, was measured to be 0.0124 inches. Initial planar jet shear development is characterized by localized increases in θ at approximately x/D=2 and x/D=4. In the similarity region the jet has been shown to widen in a linear fashion given by

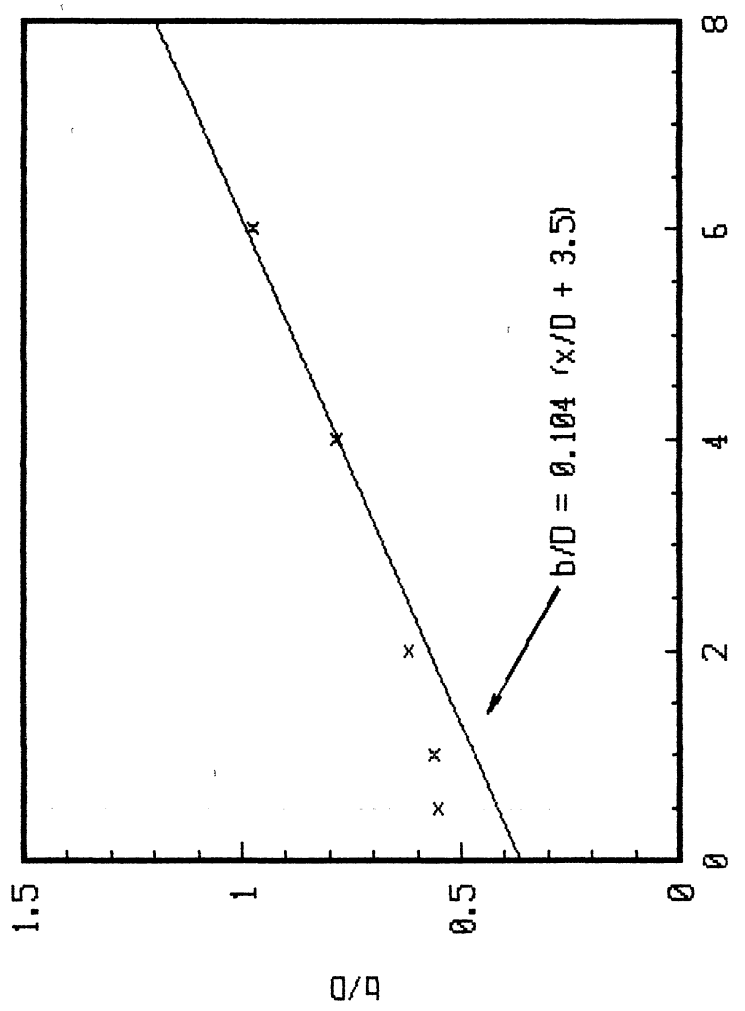

Figure 4. Natural Jet Widening

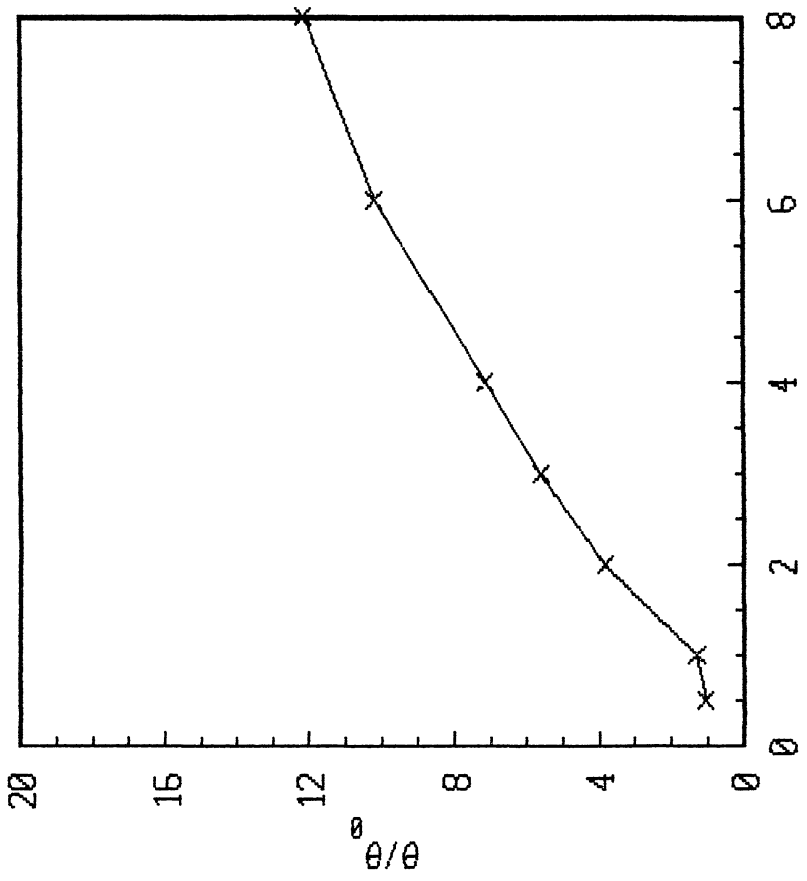

Figure 5. Natural Jet Momentum Thickness

$$b/D = k1\ (\ x/D - C1) \qquad (2.4)$$

where
- b = mean velocity half-width
- D = nozzle width
- k1 = constant (non-dimensional widening rate)
- C1 = constant (geometric virtual origin)

A straight line representing a widening rate, k1, of 0.104 and a geometric virtual origin, c1, of -3.5 is shown for reference. Since data downstream of x/D=6.0 were not available, a curve fit for the similarity region was not possible. However, the data points at x/D=4.0 and 6.0 appear to fit within the bounds of previously published values as presented in Table 3.

Mean velocity measurements were taken at the jet centerline and the velocity decay is presented as figure 6. The mean centerline velocity remained approximately equal to the nozzle exit velocity until x/D=2 and then decreased slowly until about x/D=4. A linear curve is generally fit through the data for the similarity region and can be approximated by the straight line

$$(Um/Uo)^{-2} = k2\ (x/D - C2) \qquad (2.5)$$

where
- Um = local centerline flow velocity
- Uo = max flow velocity at the nozzle exit
- k2 = non-dimensional velocity decay rate
- C2 = virtual origin

A line representing a decay rate, k2, of 0.25 and a virtual origin, c2, of -0.70 is shown for reference. Since data downstream of x/D=6.0 were not available, a curve fit for the similarity region was not possible. However, the data points at x/D=4.0 and 6.0 appear to fit within the bounds

TABLE 3

COMPARISON OF MEAN FLOW PROPERTIES FOR PLANAR JETS

Reference	Re	K1	K2	C1	C2
Flora (1969)	2 00 x 10^4 to 3 00 x 10^4 to	0 109 to 0 130	0 158 to 0 227	-15 000	2 000
van der Hegge Zınjnen (1958)	1 33 x 10^4	0 100	0 205	0 000	-1 700
Foss (1965)	5 50 x 10^4	0 085	0 257	-2 000	6 500
Kaıser (1971)	6 00 x 10^3	0 101	0 28	-2 600	0 000
Ott (1972)	1 00 x 10^4	0 097	0 228	-3 000	7 000
Jenkıns (1974)	1 45 x 10^4	0 085	0 160	-6 100	4 000
Mulej (1975)	1 60 x 10^4	0 095	0 185	-0 789	13 200
Gutmark & Wygnanskı (1976)	3 00 x 10^4	0 100	0 170	-2 000	4 700
Cervantes (1978)	1 00 x 10^4	0 083	0 240	-6 600	4 500
Chambers (1977)	6 00 x 10^3	0 100	0 190	-3 500	-3 200
Thomas (1980)	6 00 x 10^3	0 106	0 214	-3 500	-0 913
Thomas (1983)	6 00 x 10^3	0 100	0 220	-3 200	-1 600
Thomas & Brehob (1986)	1 50 x 10^4	0 086	0 253	-4 711	10 371
Prakash (1986)	7 70 x 10^3	0 104	0 180	-1 800	-0 354
CLTV (1987)	8 20 x 10^3	0 104	0 220	-3 500	-0 70
Current (1991)	2 00 x 10^3	0 104	0 250	-3 500	-0 70

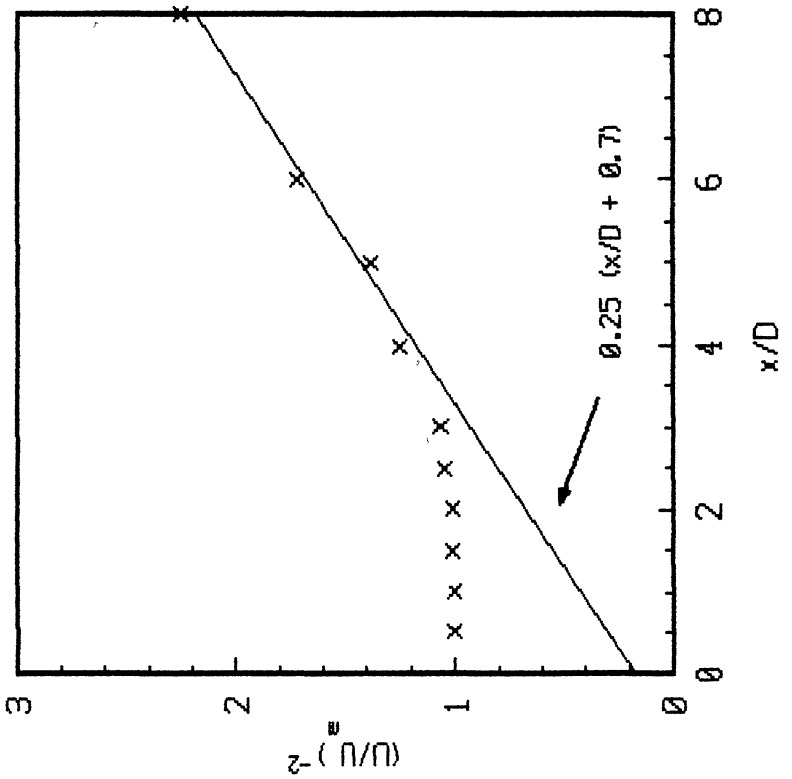

Figure 6. Mean Centerline Velocity Decay (Natural Jet)

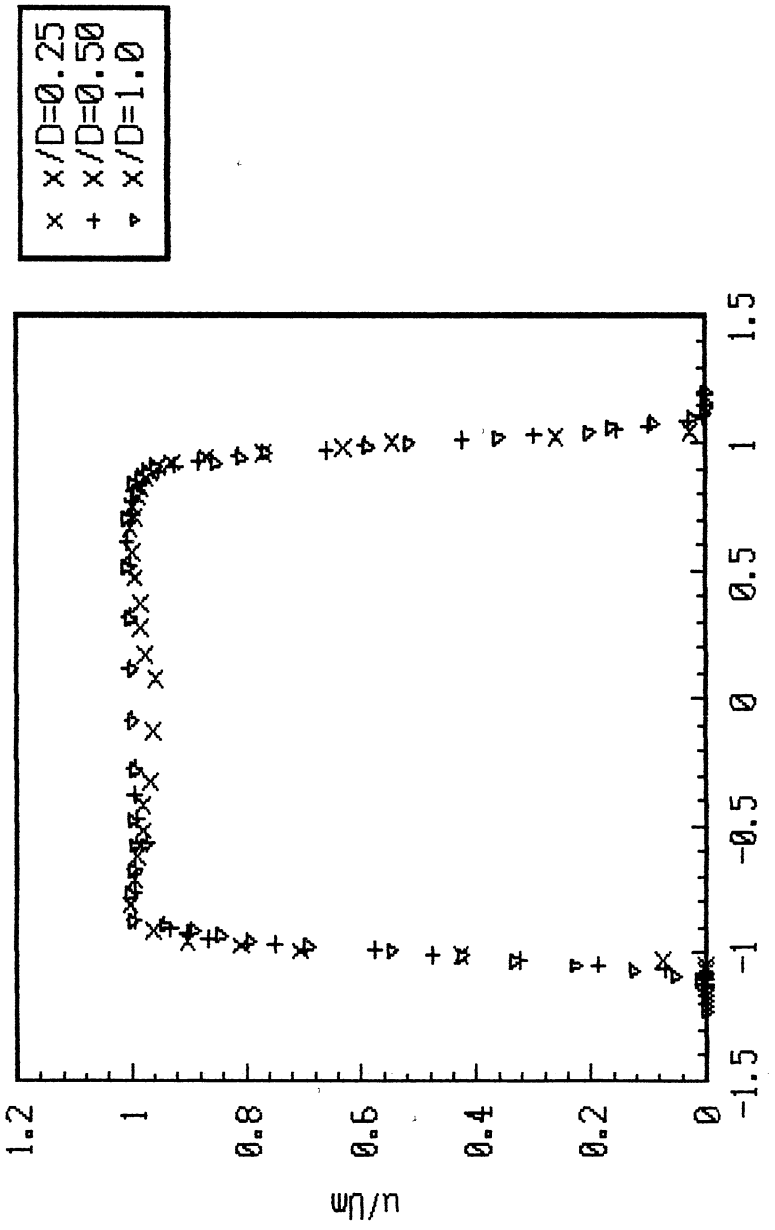

Figure 7. Mean Velocity Profiles (Natural Jet)

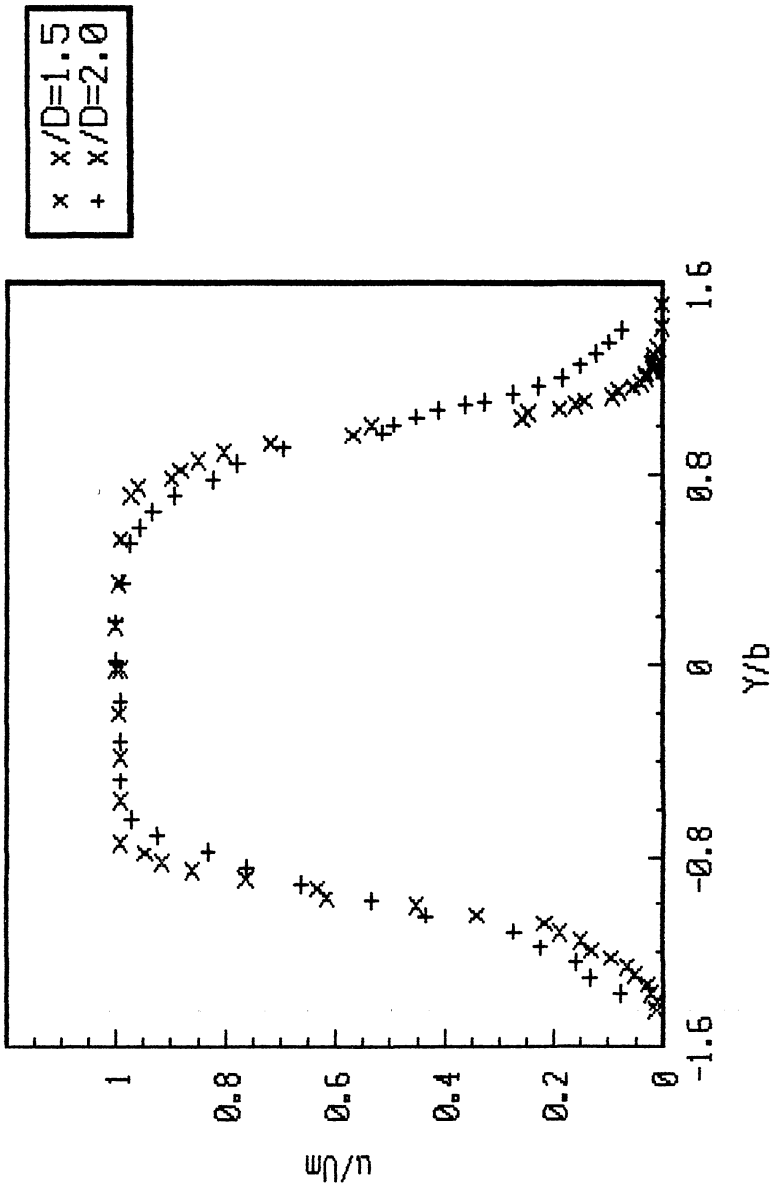

Figure 8. Mean Velocity Profiles (Natural Jet)

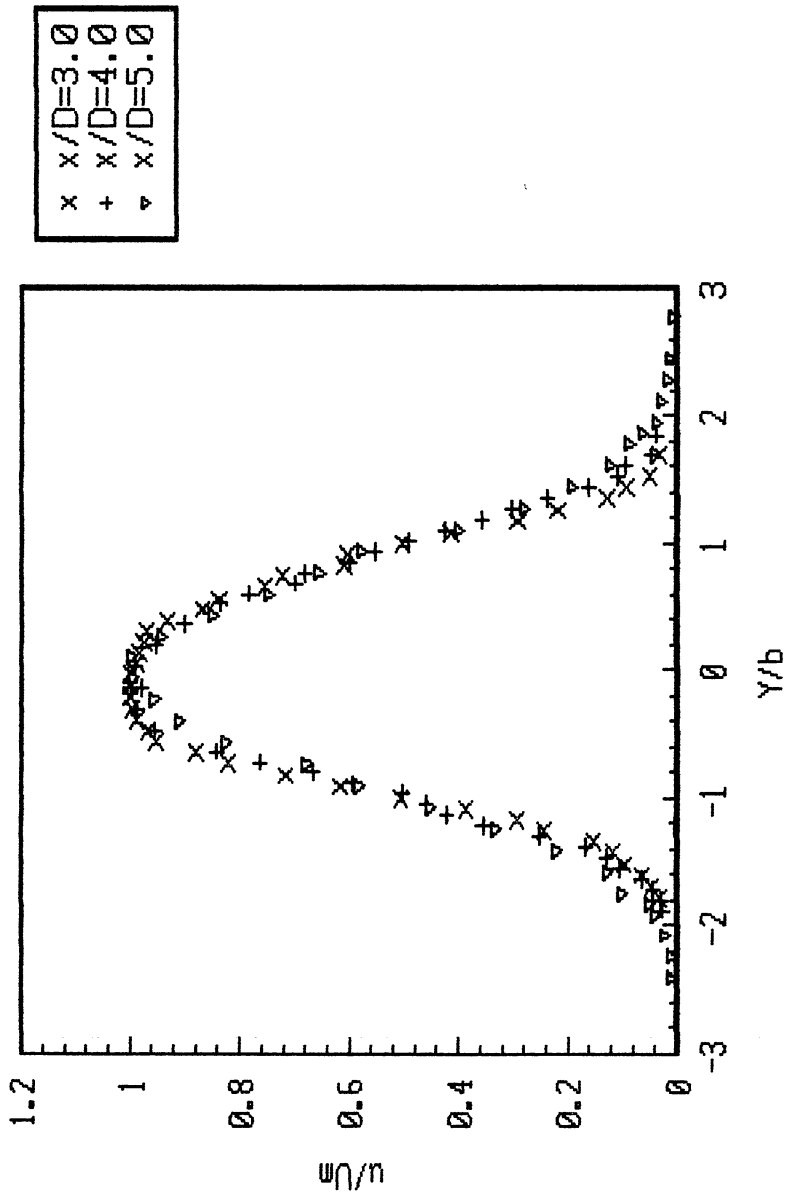

Figure 9. Mean Velocity Profiles (Natural Jet)

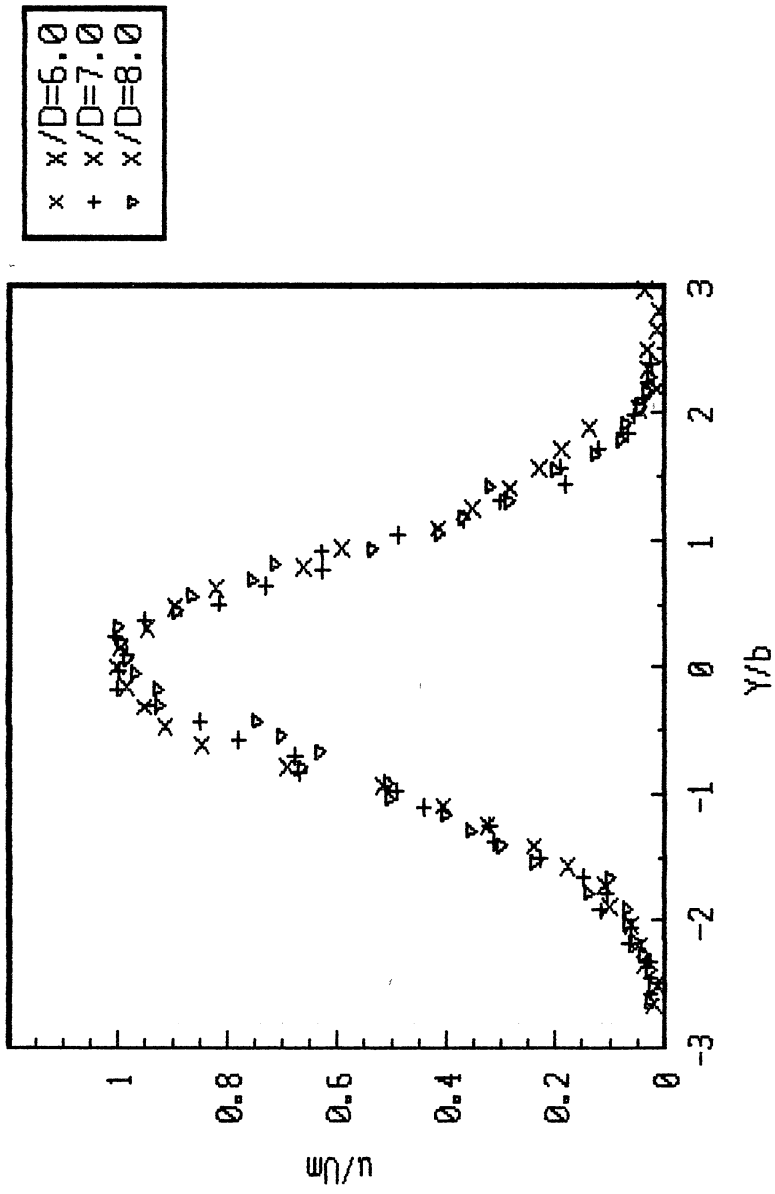

Figure 10. Mean Velocity Profiles (Natural Jet)

of previously published data (Table 3).

Mean velocity profiles are presented in figures 7 thru 10 where local velocity is normalized by the local centerline mean velocity and the lateral coordinate Y is normalized by the jet half-width b. The jet profile is initially flat except for two thin free shear layers that bound a core of irrotational fluid. An exception must be noted for flow very near the nozzle exit. A very slight dip in the flat central portion (potential core) of the profile is apparent. By x/D=0.5, the 'top hat' shaped profile is achieved. This 'top hat' type profile is characteristic of nozzles with a large contraction ratio. As x/D increases, the shear layers become larger and result in a shorter flat central portion. Between x/D of 3 to 4, the jet potential core is completely engulfed.

Longitudinal fluctuation intensity profiles were also obtained and are presented as figures 11 thru 17. These data are normalized by the local centerline mean velocity and are plotted against the lateral coordinate Y which is scaled with the local jet half-width b. Figures 11 thru 14 reveal the rapid growth of essentially symmetric peaks located at Y/b=1. This corresponds to the location of maximum mean shear du/dY. Intensity levels at the centerline are low near the nozzle exit and increase with longitudinal distance. Shear layer intensity levels diffuse toward the center with increasing longitudinal distance and the profiles take on a typical 'saddle' shape.

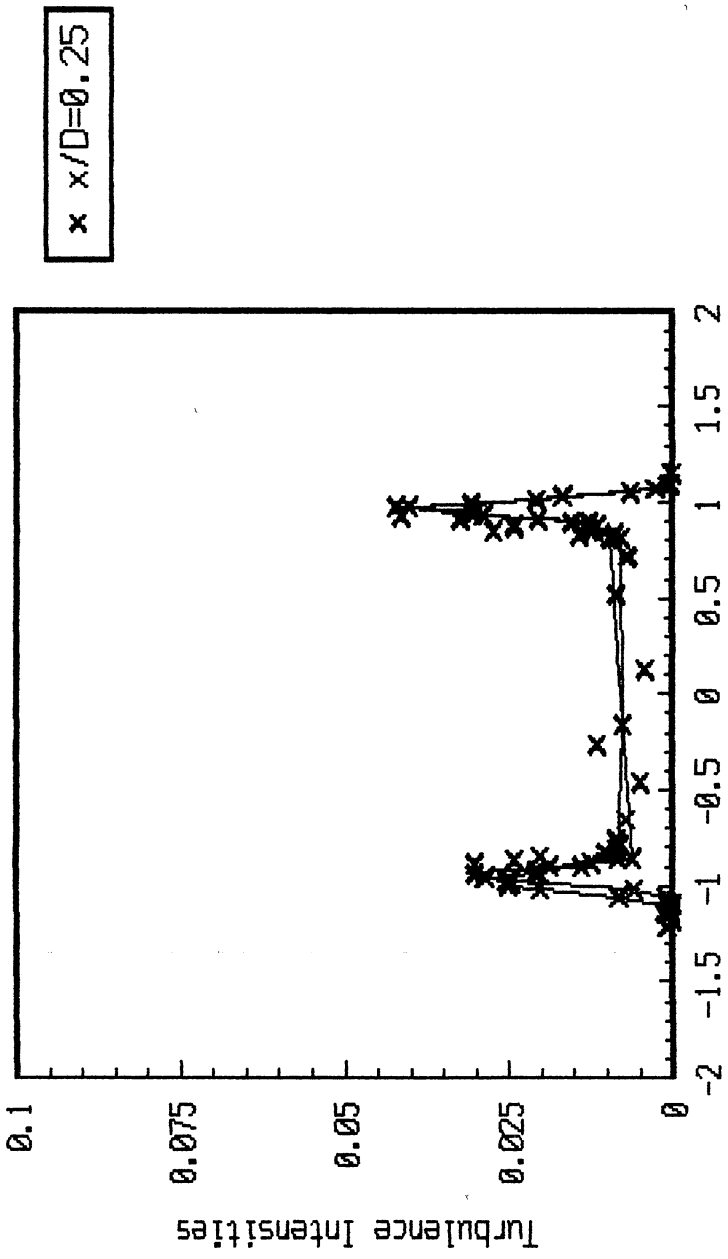

Figure 11. Longitudinal Turbulence Intensity (Natural Jet)

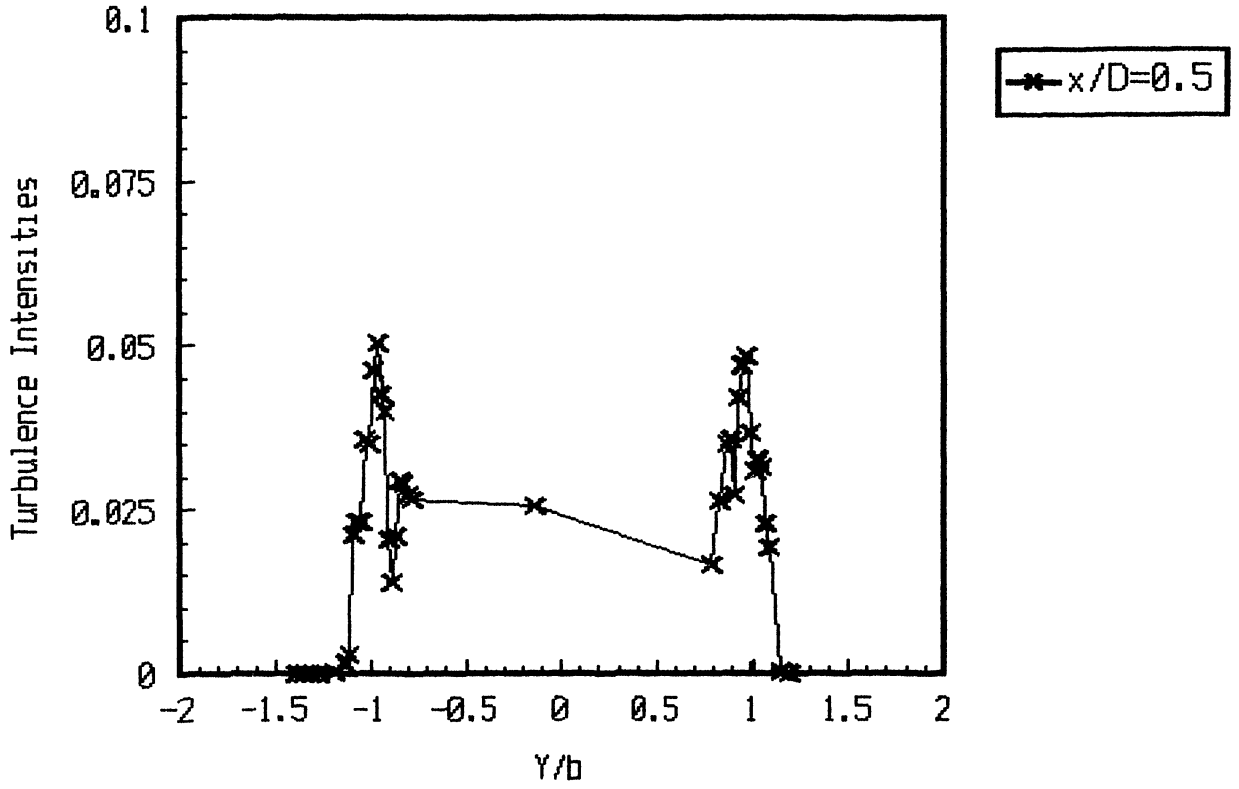

Figure 12. Longitudinal Turbulence Intensity (Natural Jet)

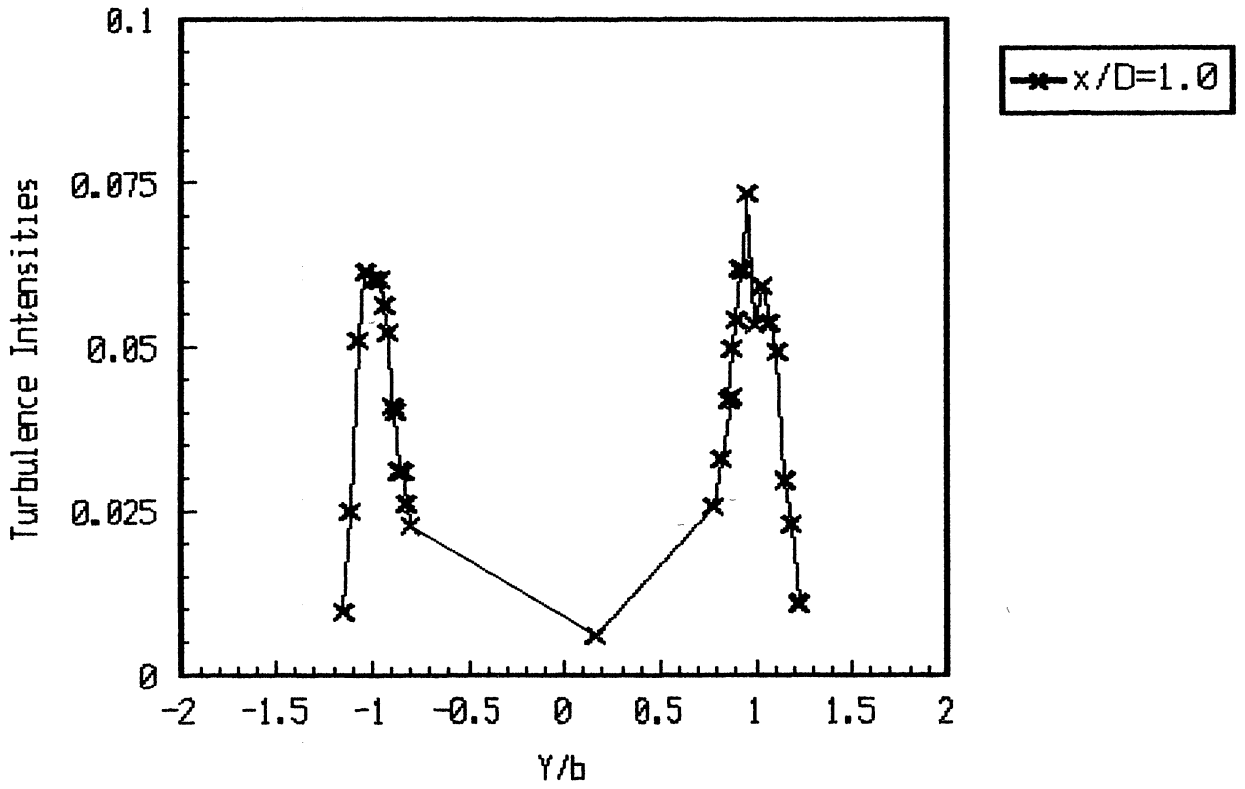

Figure 13. Longitudinal Turbulence Intensity (Natural Jet)

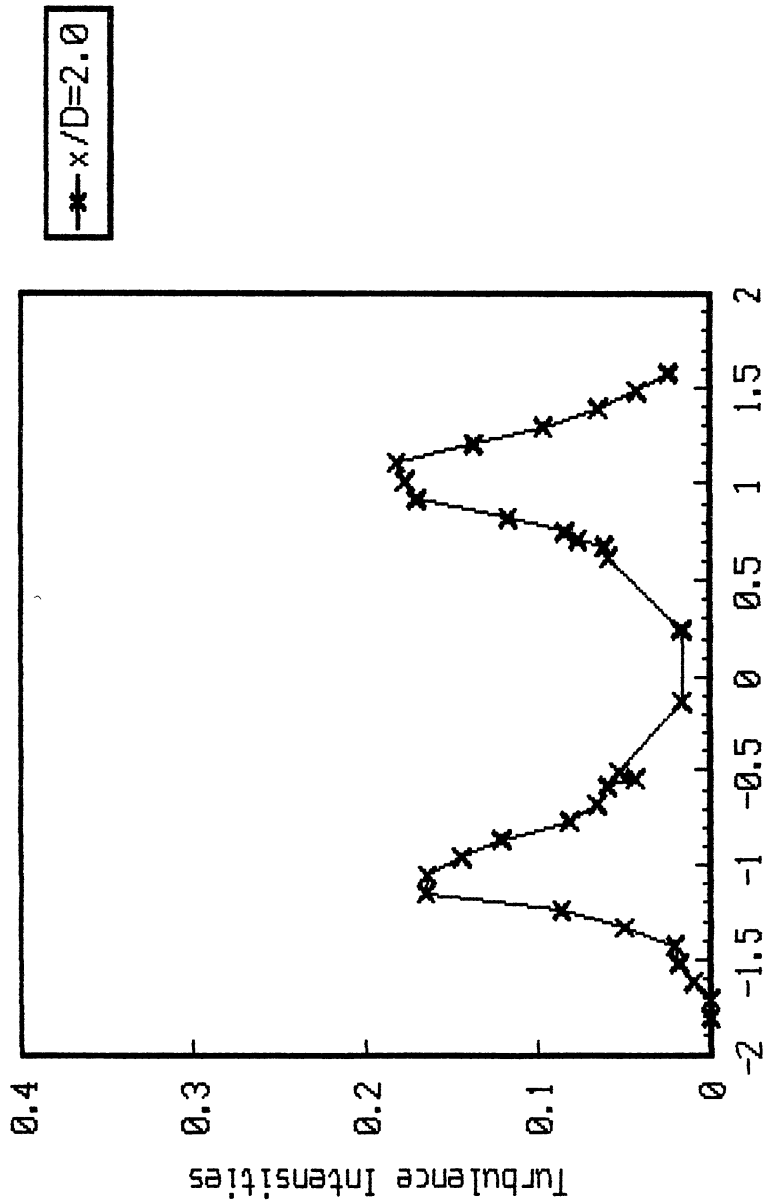

Figure 14. Longitudinal Turbulence Intensity (Natural Jet)

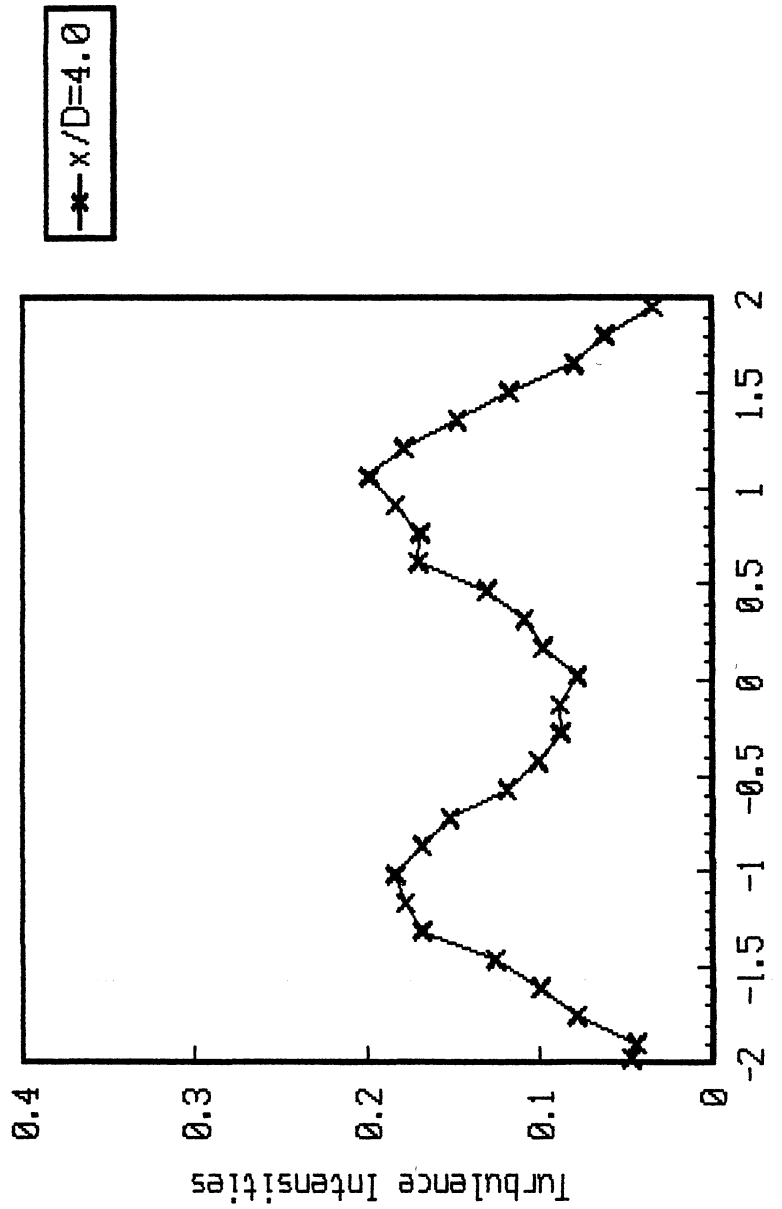

Figure 15. Longitudinal Turbulence Intensity (Natural Jet)

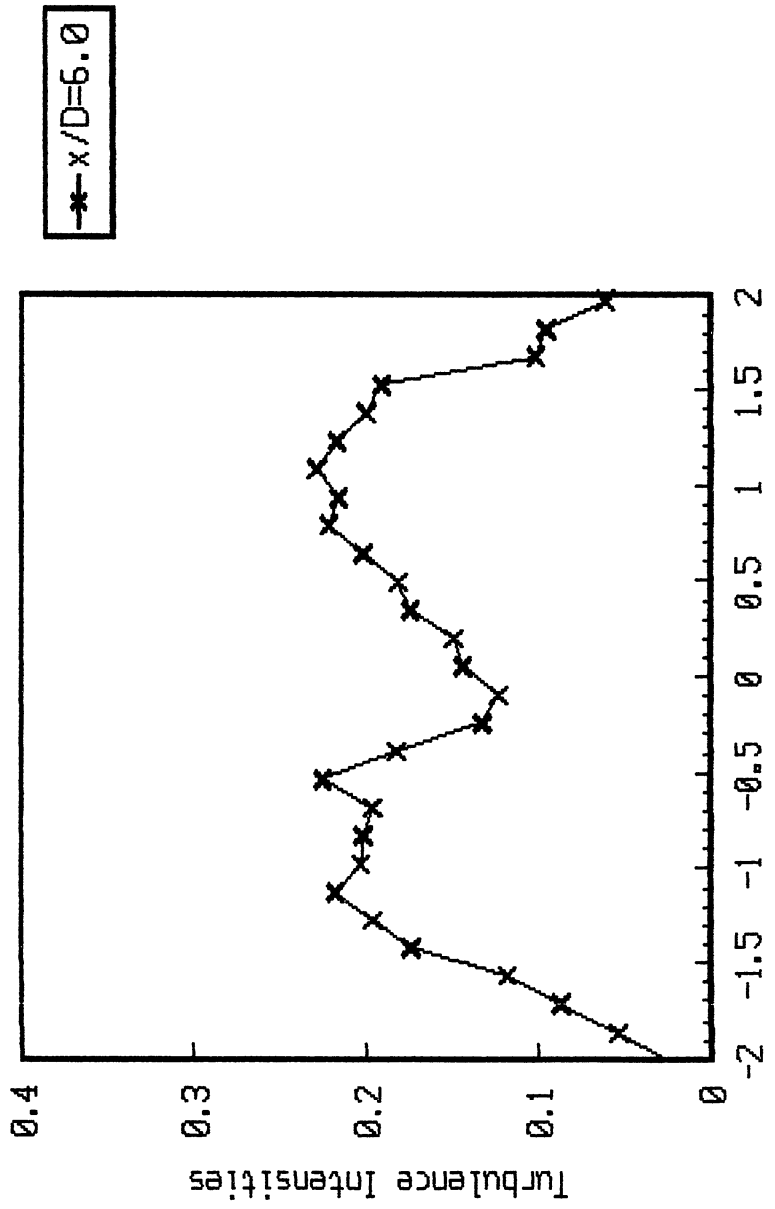

Figure 16. Longitudinal Turbulence Intensity (Natural Jet)

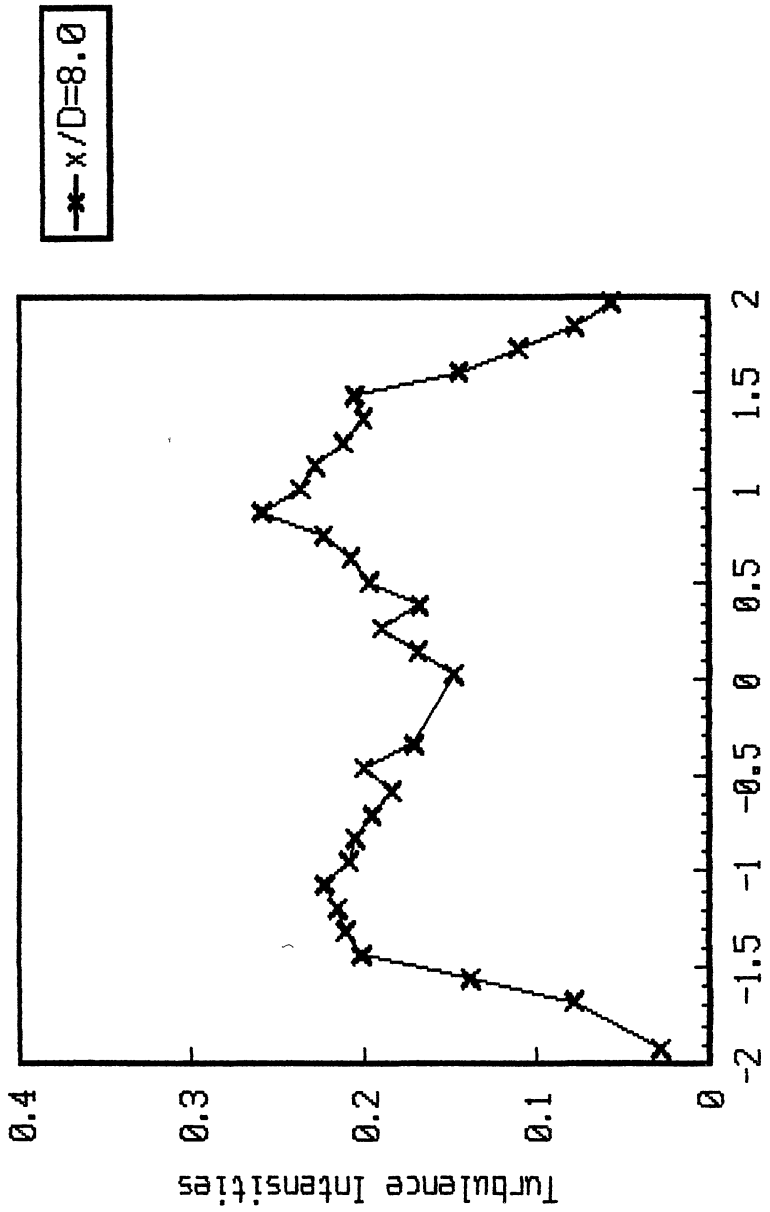

Figure 17. Longitudinal Turbulence Intensity (Natural Jet)

The Effects of Fixed Frequency Excitation On Basic Flow Parameters

Acoustic excitation is often used to organize the initial instability wave in free shear layer transition studies. This facilitates the documentation of the downstream evolution of the instability wave. There continues to be some debate as to whether or not the physics of transition in the artificially excited flow is essentially similar to the corresponding natural flow. Hussain (1980) notes that all flows are excited by background laboratory disturbances. Obviously, the amplitude of the applied excitation is extremely important. In the work to be reported, excitation was applied upstream of the nozzle exit to introduce a symmetric longitudinal perturbation into the flow field.

As described in an earlier Section, a fixed frequency excitation from an eccentric disc rotating in contact with a rubber membrane upstream of the nozzle exit was used to excite an instability at forcing frequencies of 3fc (5.3 HZ and $St=f\theta/U=0.23$) and 4fc (7 HZ, St=0.30) where fc is the jet column mode frequency (passage frequency of structures at the end of the potential core) of 1.75 HZ (St=0.07). The 7.0 HZ frequency is slightly below the shear layer most unstable frequency of 7.8 (ST=0.33) as estimated by a linear stability analysis. Total longitudinal turbulence intensity (defined as the rms longitudinal velocity

fluctuation divided by the local mean centerline velocity) at the nozzle exit was measured to be 0.0148 for 7 Hz and 0.0140 for 5.3 HZ as compared to 0.0119 for the natural flow. The maximum increase of 0.3% of the mean exit velocity is fairly large and effectively dominated the structure formation and evolution (Hussain 1986).

Measurements were performed to determine what effect the excitation had on the basic development of the jet flow. Shear layer turbulence intensity profiles comparing natural and excited conditions for various longitudinal locations are presented as figures 18 thru 22. Figure 18 shows that excitation at 7 HZ and 5.3 HZ significantly increases the turbulence intensity at x/D=0.5. The difference decreases until at x/D=2 the excited and natural conditions are virtually identical (Fig 20). However, the center intensity level continues to be higher for the forced cases as far downstream as x/D=6 (Fig 22). A comparison of the curves in figures 16 and 17 reveals that the turbulence intensity profiles have similar profiles. This implies that the profiles are approaching self-similar behavior by x/D=8. However, it is a general characteristic of the jet flows that mean flow quantities exhibit self-similar behavior before the turbulence quantities do. Thus complete similarity would not be expected until much further downstream.

The effect of forcing on the jet widening rate is presented as Fig 23. Very little difference is noted out

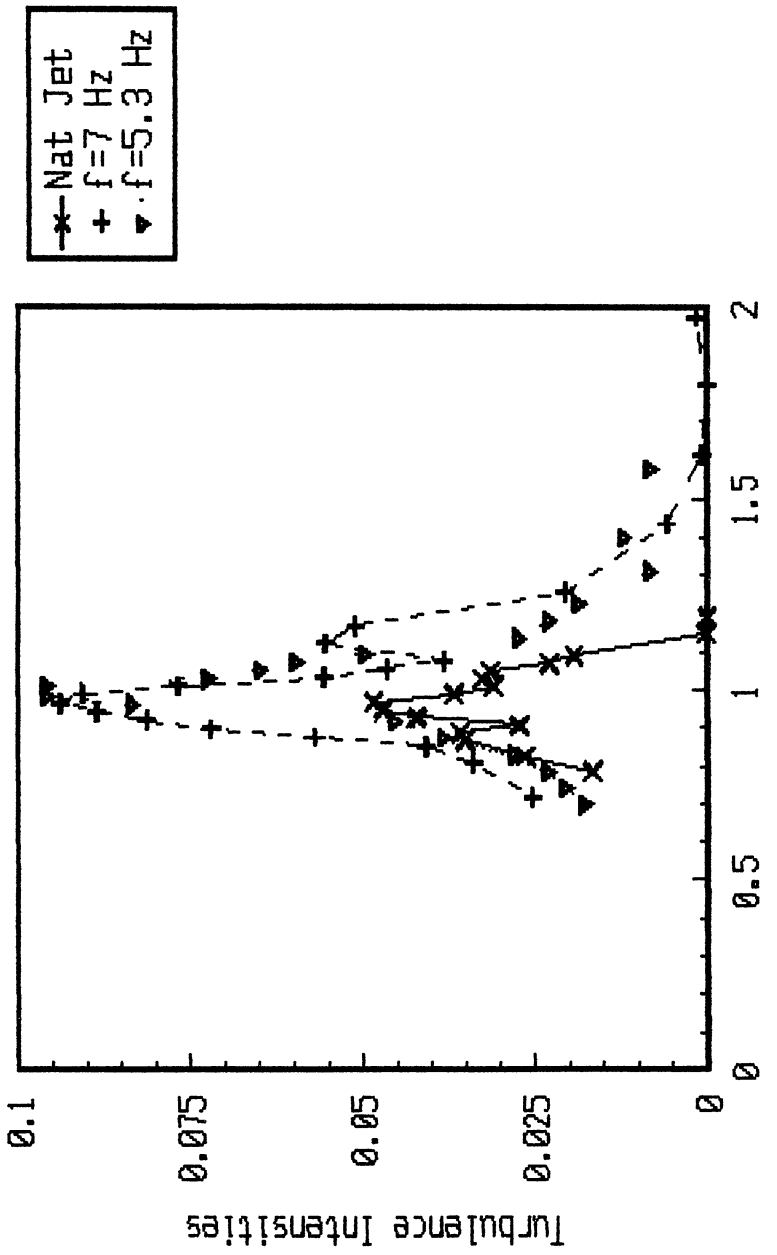

Figure 18. Effect of External Forcing on Turbulence Intensities, x/D=0.5

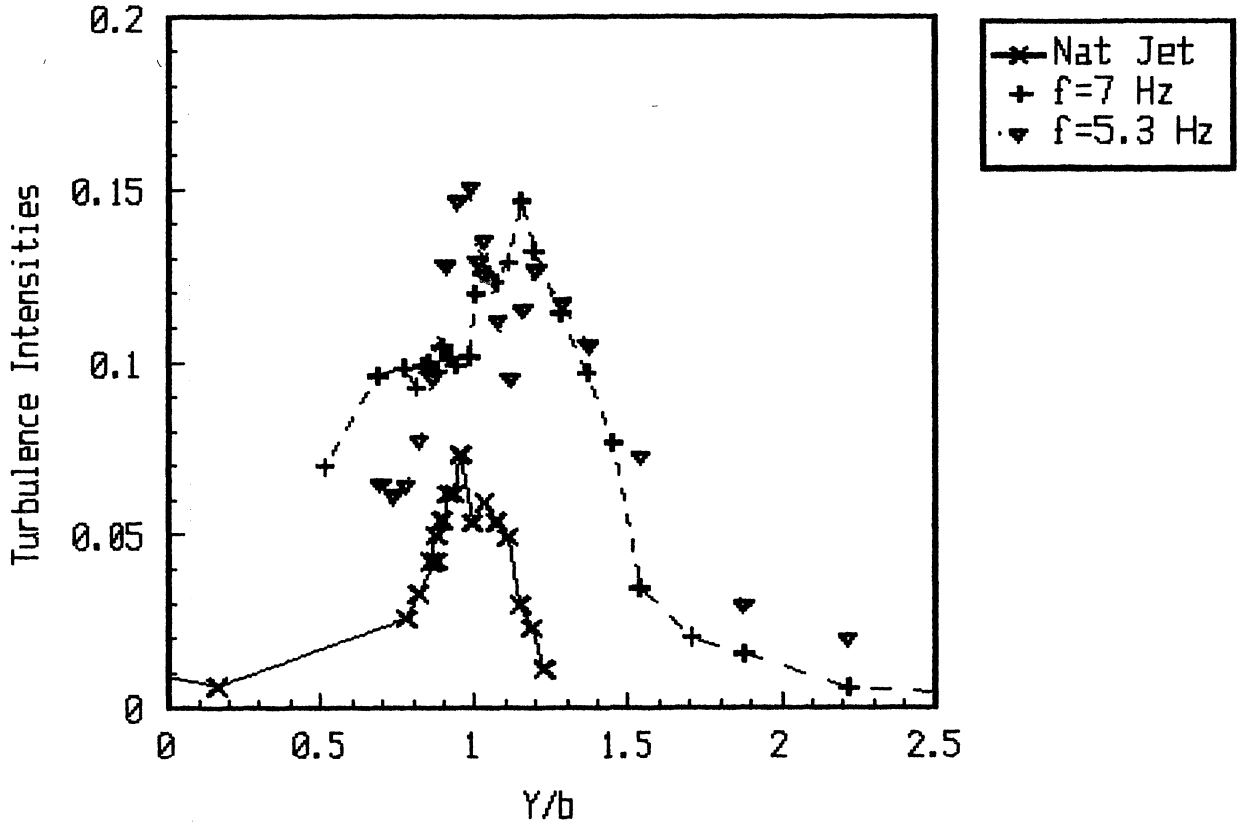

Figure 19. Effect of External Forcing on Turbulence Intensities, x/D=1.0

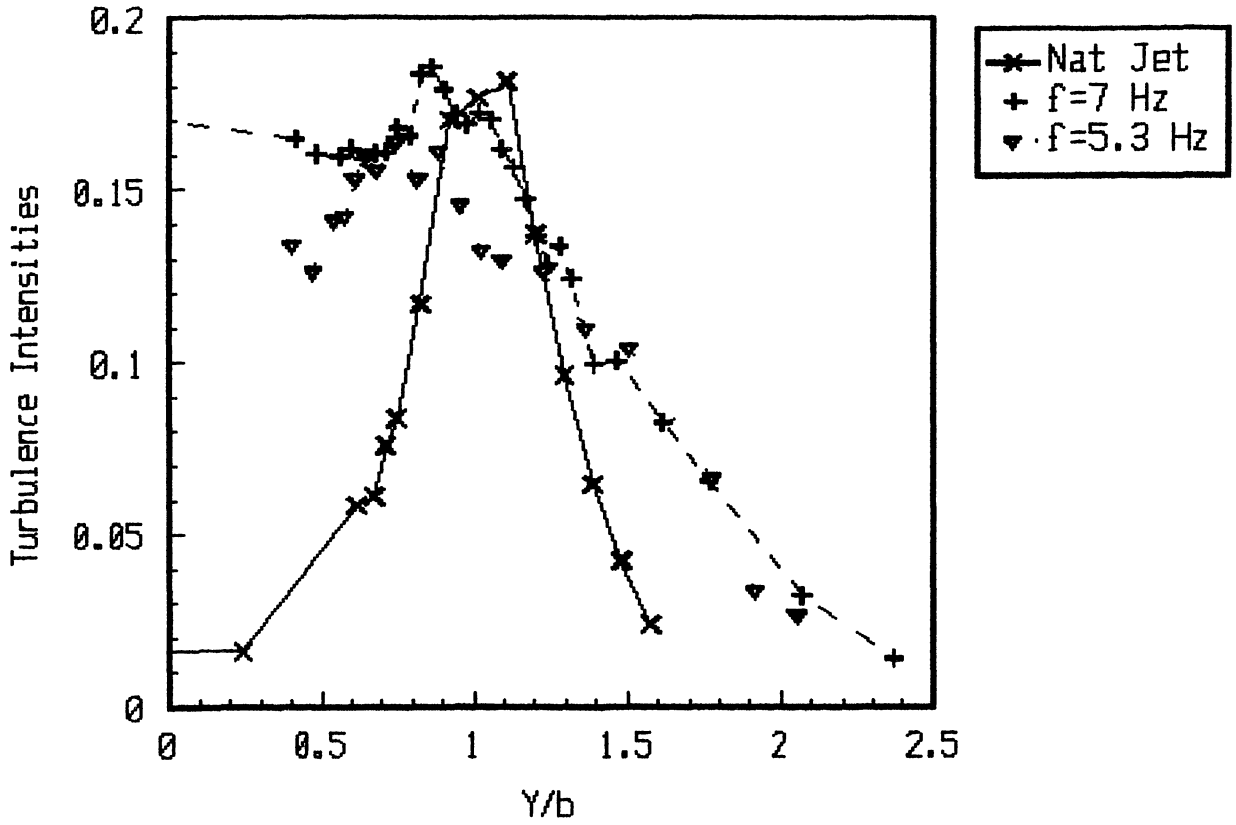

Figure 20. Effect of External Forcing on Turbulence Intensities, x/D=2.0

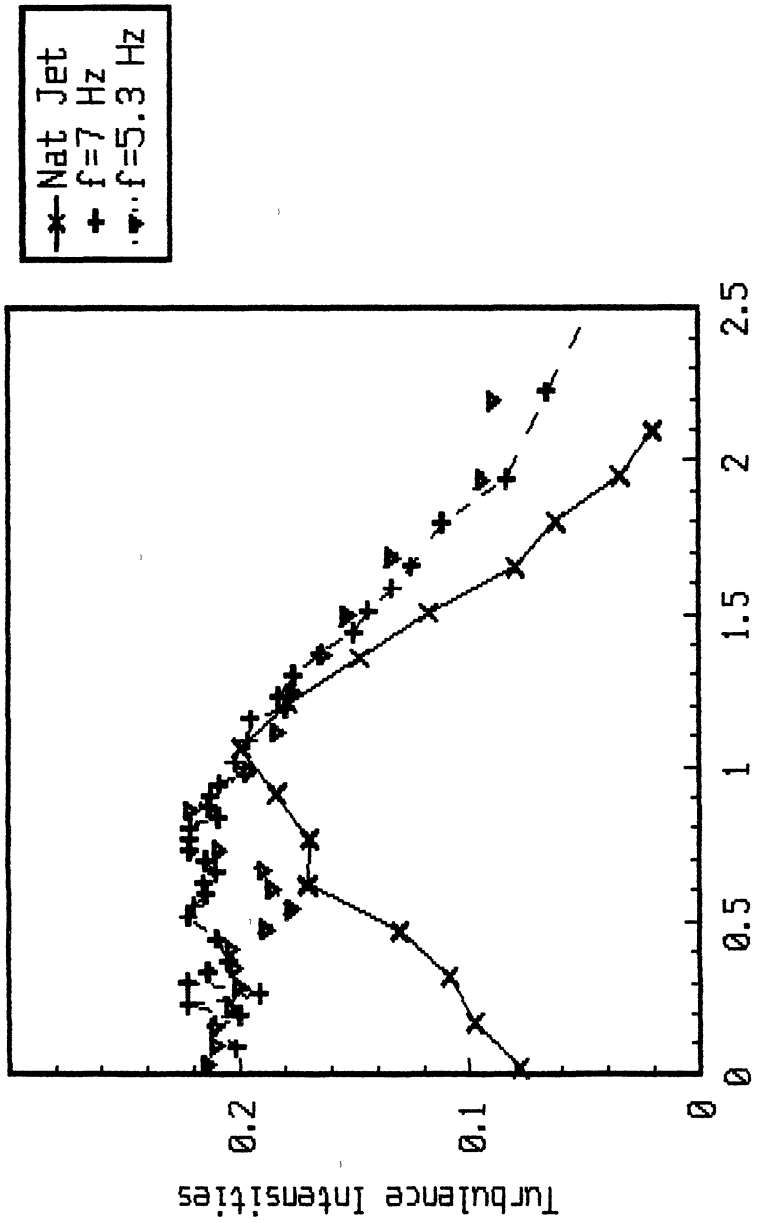

Figure 21. Effect of External Forcing on Turbulence Intensities, x/D=4.0

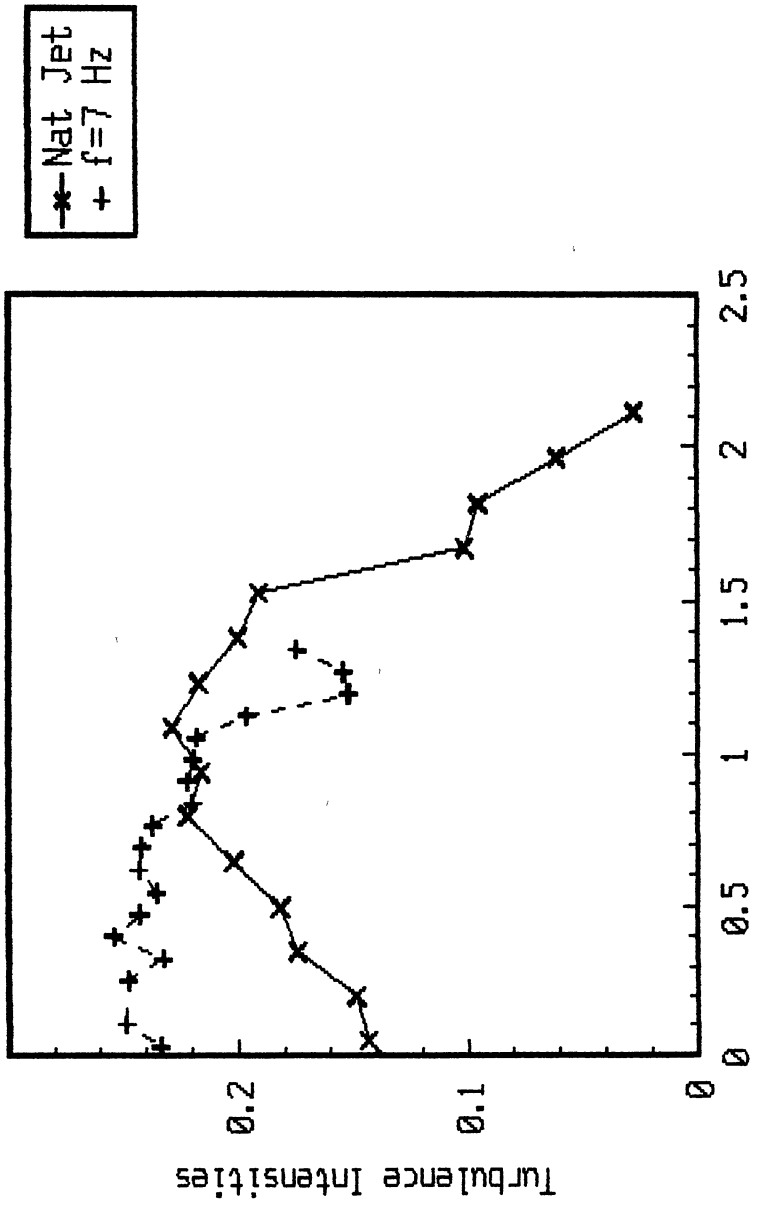

Figure 22. Effect of External Forcing on Turbulence Intensities, x/D=6.0

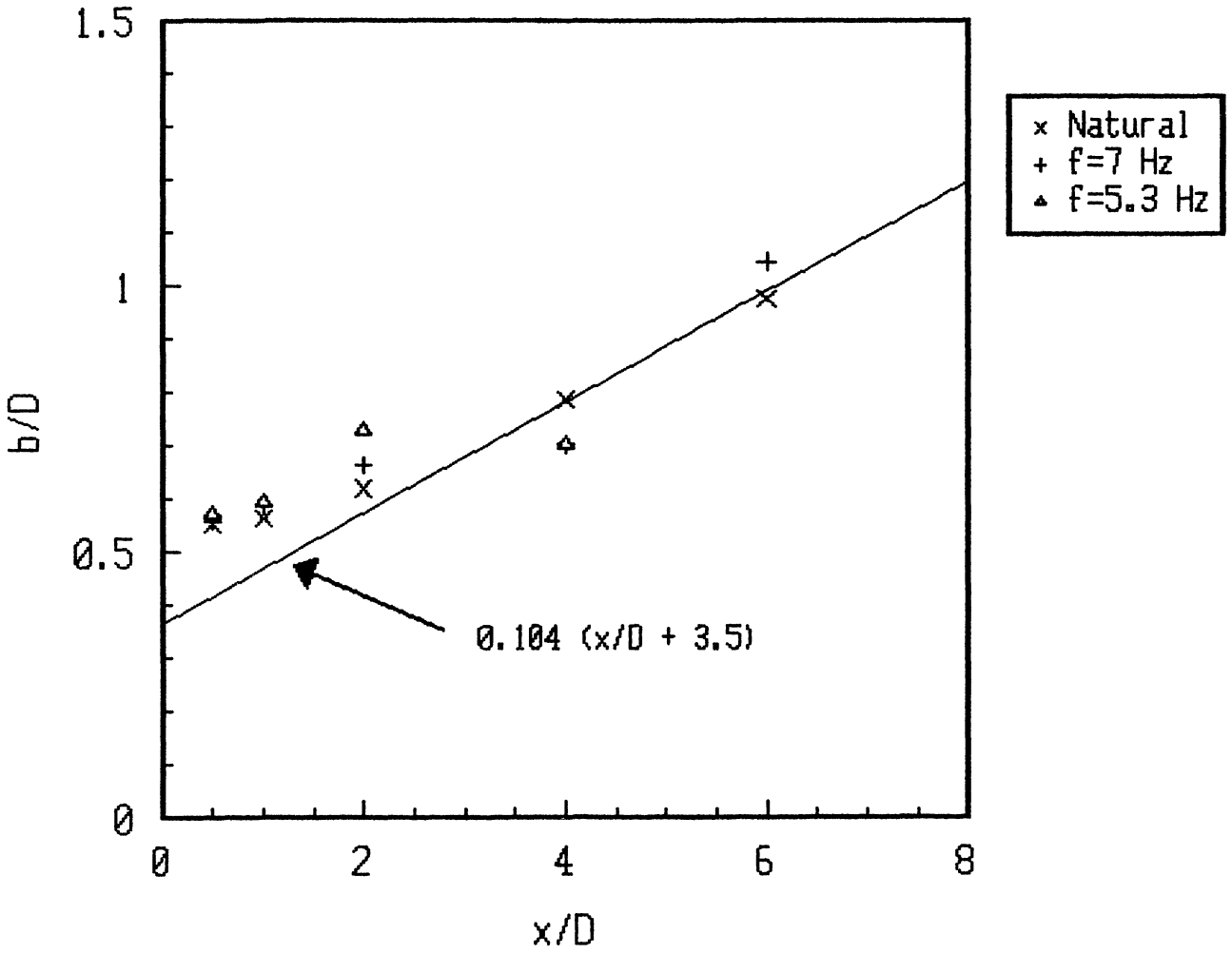

Figure 23. Effect of Forcing Frequency on the Jet Widening

as far as x/D=4. However, at x/D=6, the 7 HZ case begins to show a significant increase. Based on data from repetitive runs, the accuracy of these values is expected to be on the order of +5%. A similar trend is noted for the momentum thickness as presented in Fig 24. Essentially constant momentum thickness exists for both the natural and 3.5 HZ cases until x/D=1. For 7 and 5.3 HZ, a significant increase is measured after x/D=0.5. By x/D=6, momentum thickness is significantly greater for the 5.3 HZ case than even the 7 HZ case and almost twice as large as the natural jet. Mean centerline velocity decay with increasing longitudinal position is presented as Fig 25. No change is noted for any initial condition until x/D>2 and no significant decrement occurs until x/D>4. All three cases exhibit similar patterns.

In the following sections, power spectral measurements at the jet centerline and in the shear layer are presented.

Power Spectrum Development

The spectral evolution of longitudinal fluctuations in the water jet is presented in this section. For the spectral measurements to be reported, a standard 'hot-film' probe was used in the constant-temperature mode. The hot-film signals were passed through anti-alias filters and then digitized by an HP-98640A analog/digital conversion board. Standard digital FFT techniques were used to

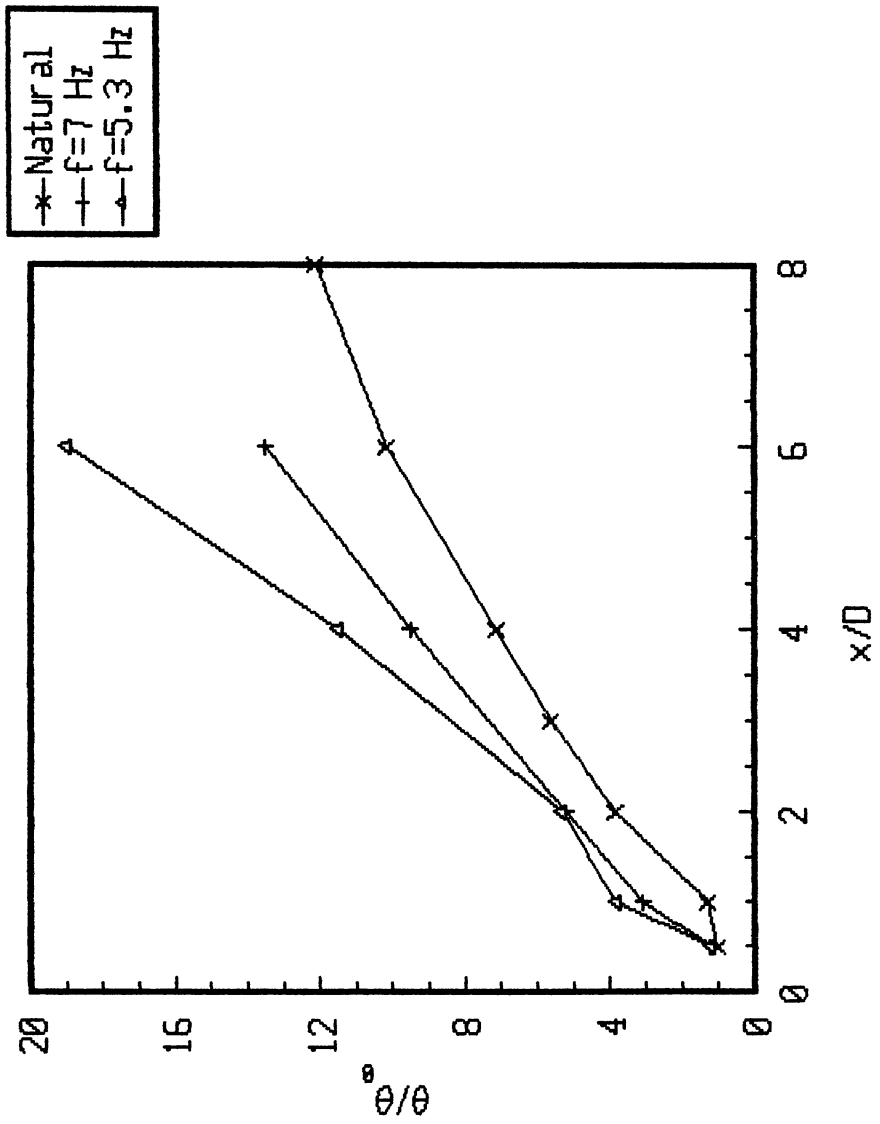

Figure 24. Effect of Forcing Frequency on Momentum Thickness

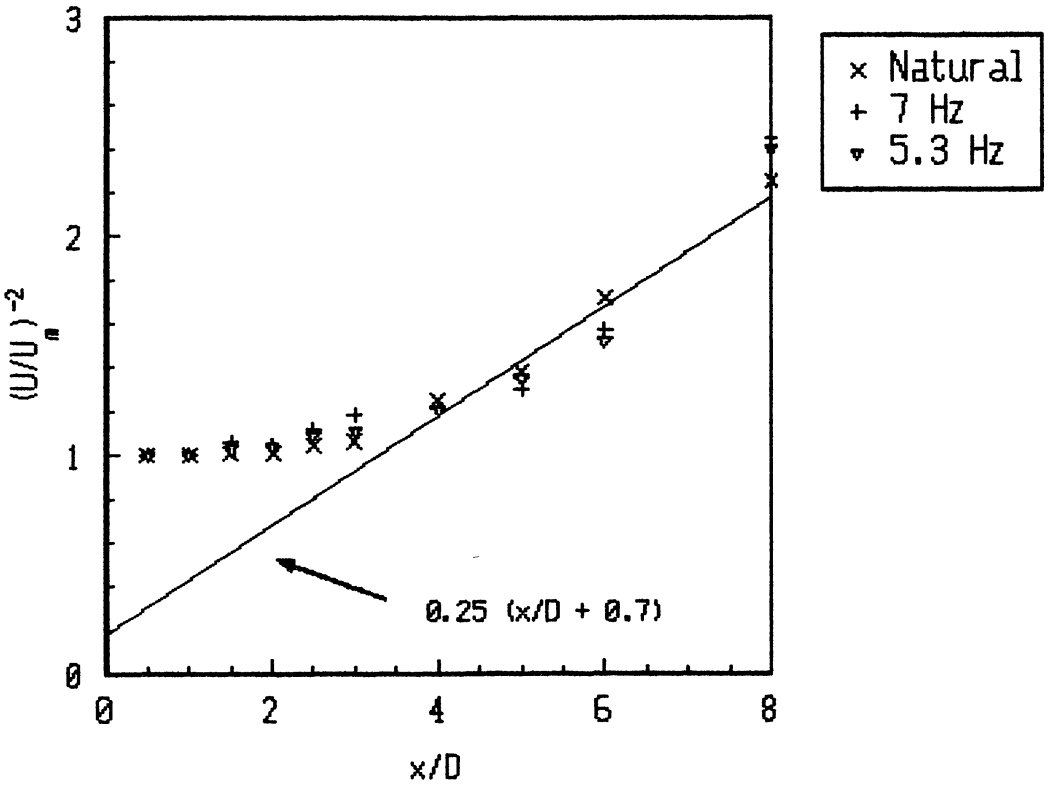

Figure 25. Effect of Forcing on Mean Centerline Velocity Decay

compute the power spectra with smooth spectral estimates obtained by ensemble averaging 200 samples. Frequency resolution ranged between approximately 0.1 Hz at a Nyquist frequency of 0.1 kHz and 0.04 Hz at a Nyquist frequency of 0.04 kHz. Each sample contained 2048 data points. The power spectra were measured at selected streamwise locations throughout the developing jet shear layers along a longitudinal line where $U/U_M=0.6$.

Initial streamwise development of the water jet shear layer spectra for the initial conditions under consideration are presented in the following sections.

Natural Jet. Figure 26 presents the initial streamwise spectral development of the natural water jet. A low frequency mode of approximately fc/4=0.47 Hz (where fc=1.75 Hz) was observed to have a much larger amplitude at x/D=0.25 than the largest peak located at the shear layer most unstable frequency plus fc/4 (fu+fc/4=8.3 Hz). An additional peak was located at 4.8 Hz which is (fu/2 + fc/2) suggesting that the subharmonic may be amplitude modulated at the frequency fc/2. For the water jet with no external forces, fc=1.75 Hz which corresponds to a Strouhal number $fc\theta/U=0.07$ (based on momentum thickness and mean exit velocity U/2). This structured passage frequency was determined from longitudinal power spectra obtained near x/D=4. It should be noted that the subharmonic of fu was observed to be suppressed. Amplitudes of this shear layer

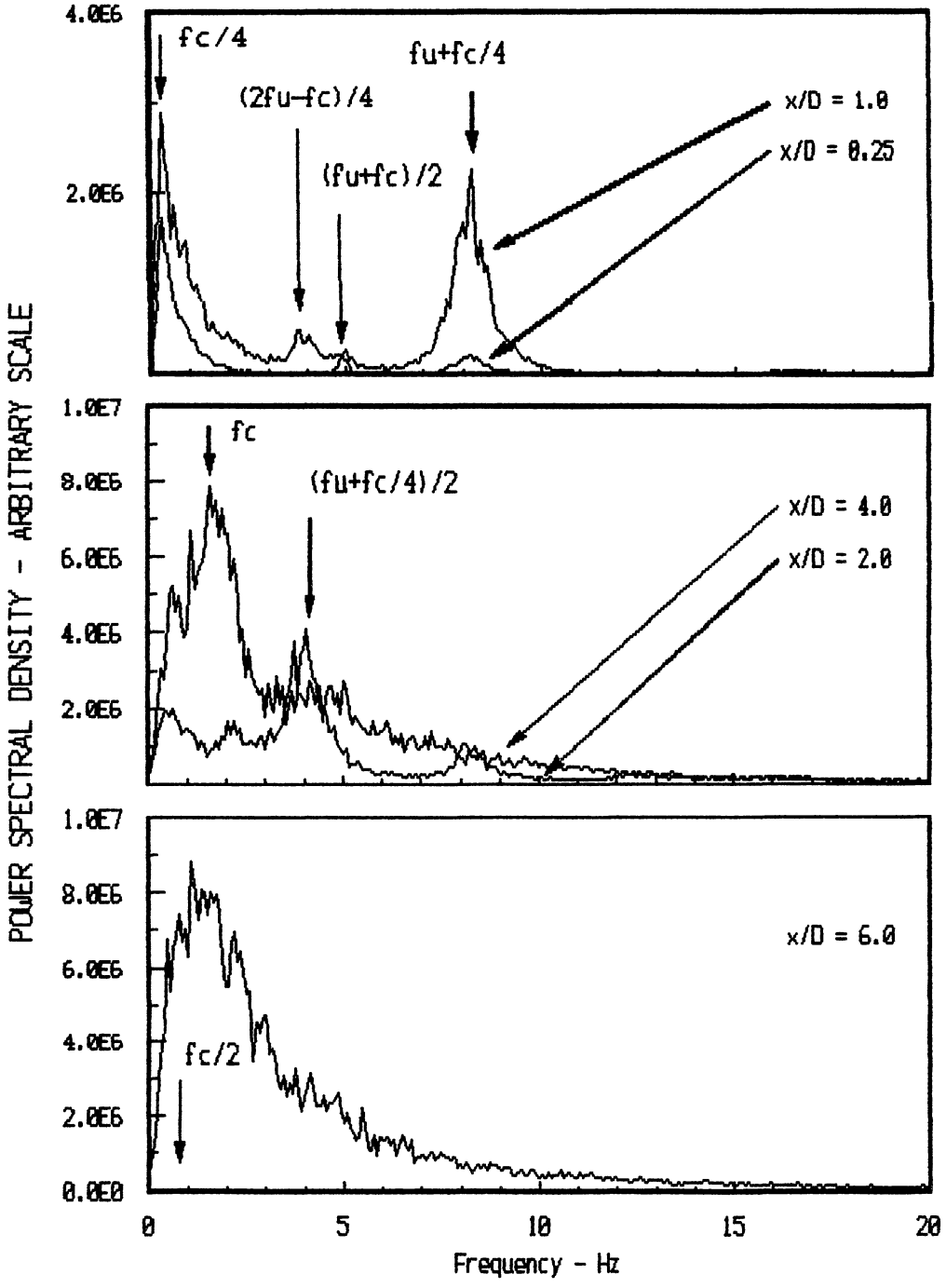

Figure 26. Spectral Development, Natural Jet

most unstable frequency fu+fc/4 grows until at x/D=1 it overtakes the fc/4 mode. At this longitudinal location the subharmonic is still suppressed and the (fu+fc)/2 mode has decayed. A new subharmonic sideband at (2fu-fc)/4 = 3.8 Hz shows limited growth but rapidly decays and is not noticeable by x/D = 2. By x/D=2 the frequencies fu+fc/4 and fc/4 have decayed and the subharmonic frequency (fu+fc/4)/2 has become prominent. This indicates that substantial nonlinear modal interactions have begun. An additional frequency near the jet column mode (fu/4 or fc + fc/4) is also apparent. The jet column mode fc has become dominant by x/D = 4. A very broad peak centered between fc and fc/2 developed by x/D=6.0.

Excitement at 7 Hz. Spectral evolution of longitudinal velocity fluctuation in the jet shear layer with an initial boundary condition influenced by excitation at 7 Hz is presented in this section. Figures 27 and 28 present the early spectral development and as was the case for the natural jet, a low frequency mode of 0.47 Hz exists near the nozzle exit. This is very close to one fourth of the jet column mode, i.e fc/4. A large amplitude peak was observed at fe with a very small peak near the natural jet most unstable frequency fu = 7.8 Hz. The excitation frequency dominates out past x/D>2 but unlike the natural jet, the subharmonic begins to develop into a prominent mode but completely disappears by x/d=4. Development of

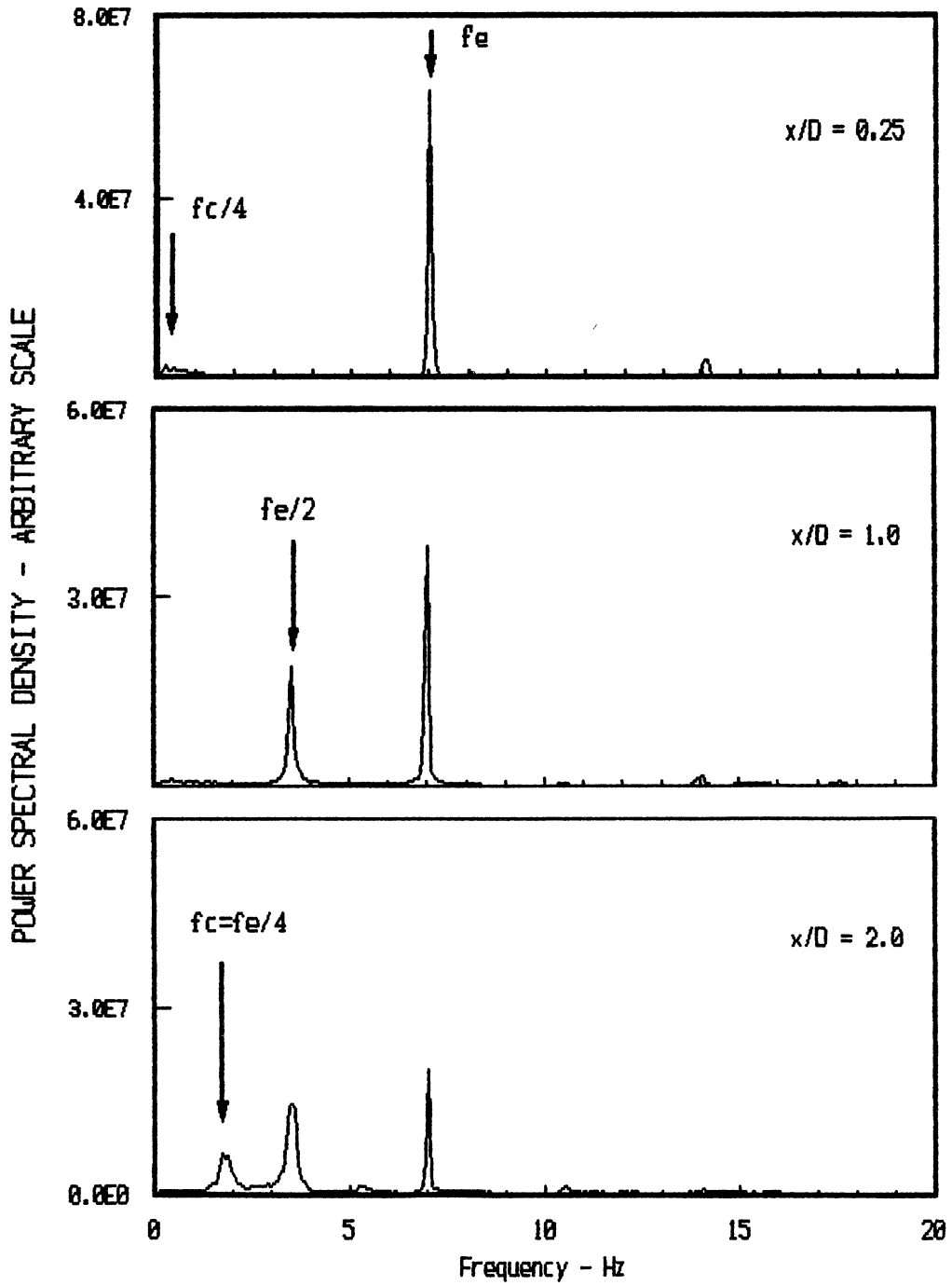

Figure 27. Spectral Development
(Forcing Frequency = 7 Hz)

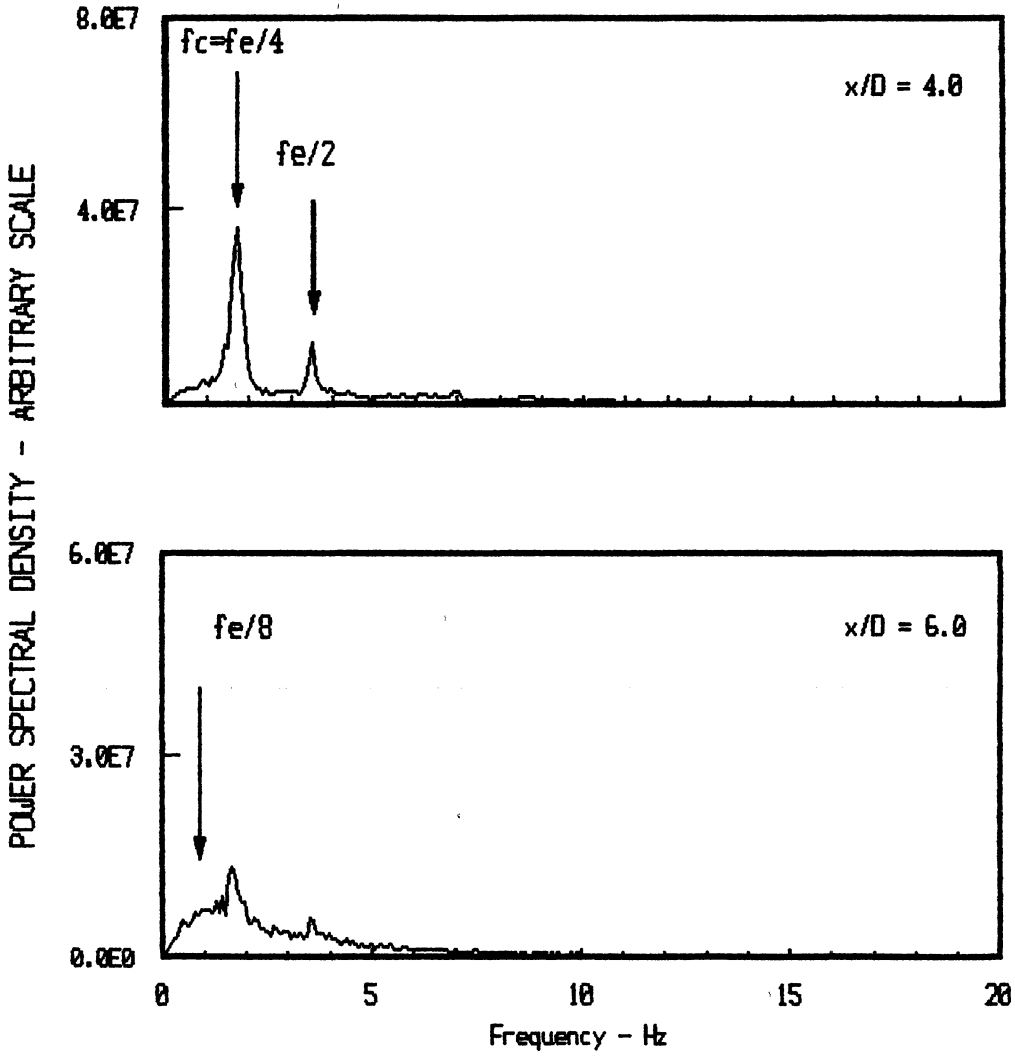

Figure 28. Spectral Development
(Forcing Frequency = 7 Hz)

the subharmonic and suppression of the low frequency mode seems to be characteristic of a tuned jet. by x/D=2, a second subharmonic (which corresponds to the jet column mode) begins to develop and the harmonic becomes saturated and begins to decay. By x/D=4, the harmonic has almost disappeared, the first subharmonic fe/2 has become saturated and is decaying, and the second subharmonic fe/4 is dominant. Perhaps it should be noted again that the jet column mode fc=1.75 Hz is equal to the second subharmonic fc/4. Thus, $fe = (fc)2^n$ where n for this jet is 2 (if n is an even number the jet is called a tuned jet and typically exhibits strong growth patterns for the subharmonic frequencies). By x/D=6, fe/4 has also saturated and the growth of a broad band of frequencies centered at fe/8 have begun to grow.

Excitation at 5.3 Hz. The spectral evolution of longitudinal velocity fluctuation in the jet shear layer under the influence of excitation at 5.3 Hz is presented in this section. Excitation at this frequency suppressed the natural jet column mode fc and produces a new excited jet column mode frequency of fe/2=2.65 Hz. Early spectral development is similar to the previous cases and is presented as Figures 29 and 30. The dominant spectral mode is fe = 5.3 Hz with low amplitude peaks at fu+fc/4 = 8.3 Hz and 2fe = 10.6 Hz and a broad band low frequency mode centered from about 0.55 Hz to 0.625 Hz (fc/3). By x/D =

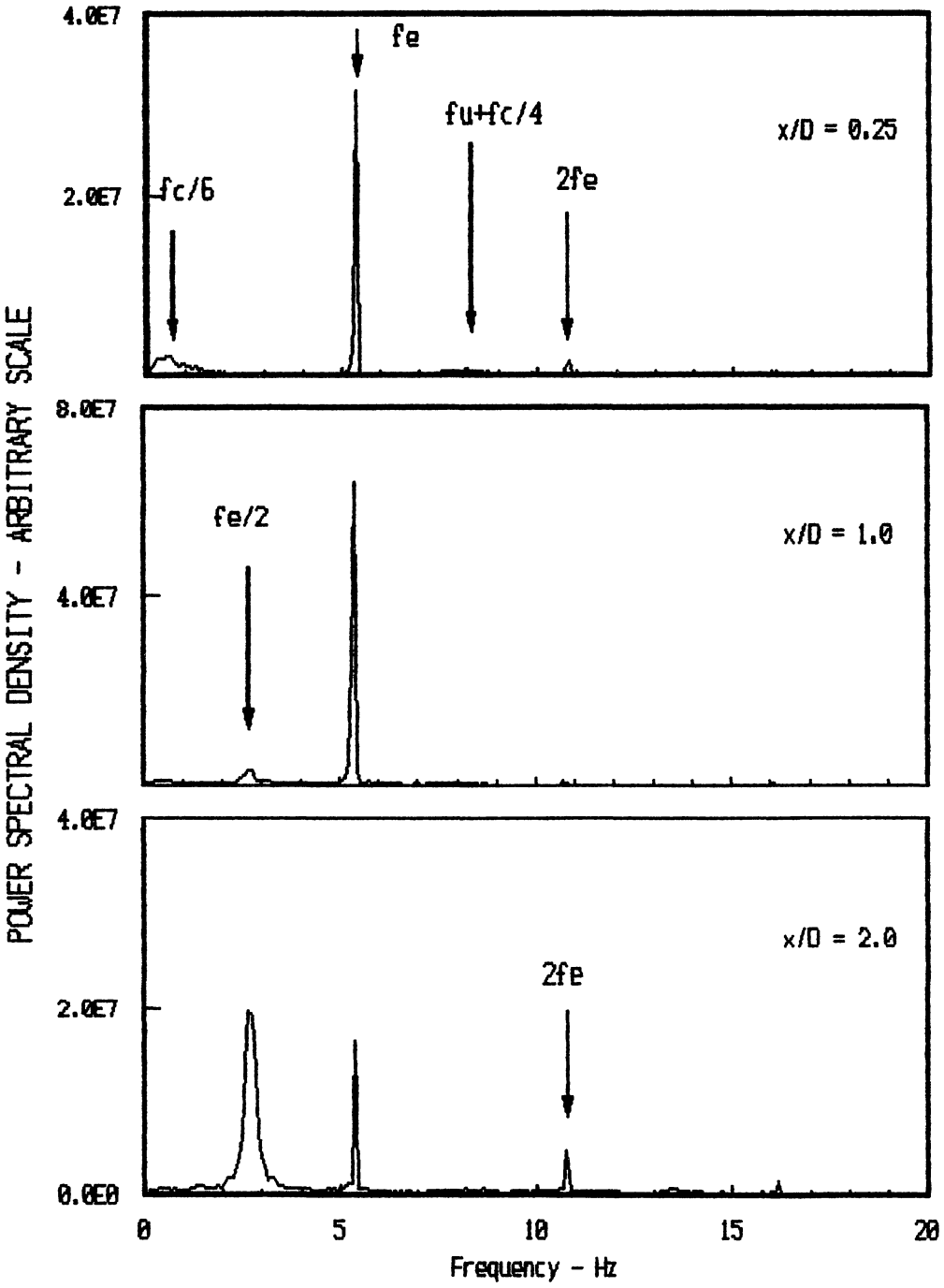

Figure 29. Spectral Development
(Forcing Frequency = 5.3 Hz)

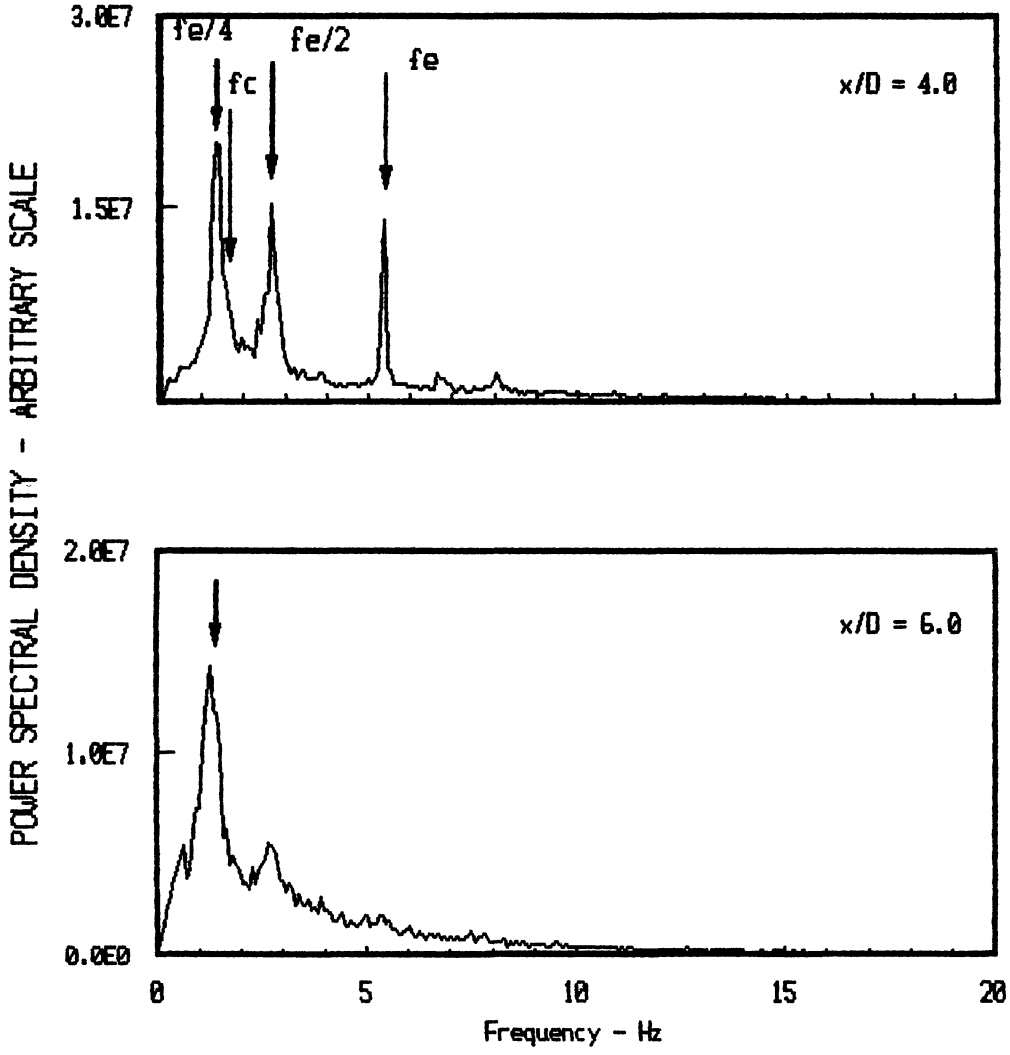

Figure 30. Spectral Development
(Forcing Frequency = 5.3 Hz)

1, the subharmonic fe/2 begins to grow but the excitation frequency is still dominant and the low frequency mode (fc/3) is detectable. For x/D > 2, the first subharmonic becomes dominant and the harmonic fe begins to decay. However, near the end of the potential core (x/D=4), the second subharmonic has begun to grow and is beginning to dominate. Both the harmonic and subharmonic modes are still very evident. As stated earlier, the natural jet column mode (fc=1.75 Hz) noted for the other cases does not exist but is approximately centered between the first and second harmonic. The third harmonic begins to grow and is detectable by x/D = 6.

Conclusion

Based on the data presented in this chapter, it is concluded that the planar water jet exhibits behavior which is in general agreement with that observed by other researchers. No unreasonable or unexpected results are indicated. Therefore, the experimental data to be presented in the next chapter are expected to be common to all planar jet flow field facilities.

CHAPTER III

MEASUREMENTS AND ANALYSIS OF VORTICAL PATHS AND INTERACTIONS

This section presents the results of a flow visualization study regarding coherent structure movements in the developing region of a planar jet. The discussion will center around three critical issues. First, where does the jet become turbulent? Second, what are the typical (and some 'nontypical') types of vortex interactions and are they periodic? Third, does the coherent structure motion become chaotic. If the motion does become chaotic, where does this occur and is there any relationship to the location where the jet becomes turbulent?

In order to isolate the dominant flow mechanisms present in the initial roll-up and eventual pairing of the coherent structures, low level mechanical excitation was introduced upstream of the nozzle exit as described in Chapter II. Video tape data was taken which utilized a dye injection method to cause the coherent structures to become visible and distinguishable. Insight was obtained regarding the physical initiation, subsequent interactions, and periodicity of these structures. Data were recorded

with the camera pointing in the direction of coherent structure homogeneity (defined as the z-direction in Chapter I). As described in Chapter II, a Reynolds number of 2000 was chosen for this study and forcing was set at 7.0 Hz, and 5.3 Hz. The jet column mode frequency fc for the natural jet was 1.75 Hz. Strouhal numbers ($fe\theta/U$) were 0.30 for external forcing at fe=7 Hz and 0.23 for the forcing at fe=5.3 Hz.

As evidenced by video tape data, vortex formation occurred at approximately the same time and location in each shear layer. For longitudinal locations as far downstream as x/D=6 or 7, subsequent vortex motions and interactions exhibited approximate spatial and temporal similarity. Thus, data has been analyzed for only one shear layer.

Onset of Turbulence

Turbulent fluid motion might be defined as an irregular condition of flow in which the various quantities demonstrate a random variation with time and space coordinates such that statistically average values can be obtained (Hinze, 1975). It is obvious from power spectra that the flow for this water jet was not turbulent near the nozzle exit. The question arises: at what approximate longitudinal location does the flow become fully turbulent? Two approaches were used in an attempt to answer this question. Fully turbulent flow was defined for flow

visualization to be the location where the two-dimensional dye structures were no longer distinguishable. For the statistical analysis using hot wire anemometry, fully turbulent flow is related to the small-scale eddie transition. These will be described in the following paragraphs.

First, the longitudinal location where the coherent structures lost their two-dimensional nature was identified using the flow visualization data. For forcing at fe=7 Hz, the structures were strongly two-dimensional until the second pairing. This occurred at an 'average' location of x/D=5.5 which is a substantial distance downstream from the end of the potential core. As discussed in Chapter II, the end of the potential core is located by noting a decrease in the mean centerline velocity. This appears to occur between x/D=2.5 and 3 (see Fig 24). Since the fe=5.3 Hz case quickly became less organized, identification of the 'exact' location where the two-dimensional structures broke down was more difficult. However, it appeared that this event usually occurred somewhere between x/D=4 and 6. Thus, for either flow condition, the 'observed' location where distinct two-dimensional coherent structures were no longer evident was associated with a pairing mechanism and occurred well past the end of the potential core.

Second, the magnitude of the roll-off exponent in the velocity spectrum was used as an indicator of the small-scale onset (Jimenez, 1979 and Ho & Huang, 1982). In order

to understand the implications of this approach, a brief review of certain aspects of isotropic turbulence theory is required (see Hinze, 1975 for detailed explanations).

Isotropic turbulence is the simplest type of turbulence where no preference for any specific direction occurs. Also, a minimum number of quantities and relations are required to describe its structure and behavior. As the turbulence grows to its full development, the larger eddies produce smaller eddies which in turn produce smaller eddies, etc. This occurs through inertial interaction and results in an energy cascade from the larger to the smaller eddies. The wavelength range of the energy spectrum where the eddies make the main contribution to the total kinetic energy of turbulence is called the energy-containing eddies. This is a low (but not the lowest) wavelength range and is the range where the energy spectrum shows its maximum. If the Reynolds number is sufficiently high, the next higher wavelength range contains eddies that obtain energy from larger eddies at the same rate as they transfer energy to smaller eddies. Thus, these eddies are in statistical equilibrium with each other. Since the inertial transfer of energy is the dominating factor, this range is called the 'inertial subrange'. The highest wavelength range is associated with the smallest eddies and provides the main contribution to the total dissipation.

From the Kolmogoroff spectrum law, a special relationship exists in the inertial sublayer between the

energy spectrum and the wavenumber. If the turbulent flow field has a constant mean velocity which is large as compared to the turbulence velocities, the spectrum law can be written in terms of frequency instead of wavenumber. Then the wavenumber K is related to the frequency by $K^b = c\ f^b$ where c is a constant. Kolmogoroff's spectrum law becomes

$$E = a\ f^{\,b} \qquad (3.1)$$

where: E - power spectral density

f - frequency

a - constant

b - roll-off exponent

When the exponent b reaches a value of -1.67, the flow is considered to be turbulent.

There was some concern about the applicability of this theory to the present data. This theory is based on isotropic turbulence at high Reynolds numbers. If the Reynolds number is too low, the inertial subrange may not exist. The energy-containing range and the dissipation range may simply meet in continuous (or discontinuous) lines. At x/D=6, the natural jet Reynolds number (based on mean centerline velocity and single shear layer momentum thickness) was calculated to be 275. This is below the bottom limit of Re=750 for a mixing layer (see the review article by Ho and Huerre, 1984). However, It was decided that if the slope of the three-dimensional spectrum was

constant at approximately -1.67 for a decade of frequency, the jet would be assumed to be fully turbulent at that x/D location.

For the excited and natural jet cases, the energy spectrum is plotted on a log-log scale and presented as figures 31, 32 and 33. A representative slope for the inertial subrange and dissipation range was approximated using equation 3.1. Data is presented for longitudinal locations of x/D=4 and 6. For every case, the exponent b in equation 3.1 was found to have a value of approximately -1.7 at x/D=6. The slope was nearly constant for a fairly large frequency range, indicating that the flow was fully turbulent by this location. At x/D=4, a value of b= -1.3 for the 7 Hz and natural jet and -1.1 for the 5.3 Hz case represent average slopes, indicating that fully turbulent flow did not exist at x/D=4.

Both the visual observation and the analysis indicate that the jet is not fully turbulent at x/D=4 but has become fully turbulent by x/D=6. Thus, the fully turbulent condition occurs well beyond the end of the potential core. This is in general agreement with the results published by Sato (1960).

Coherent Vortical Motions

The phenomenon of initial roll-up and formation of 'eddies' in free shear layer flows is well documented. While great care was taken in this study to visually

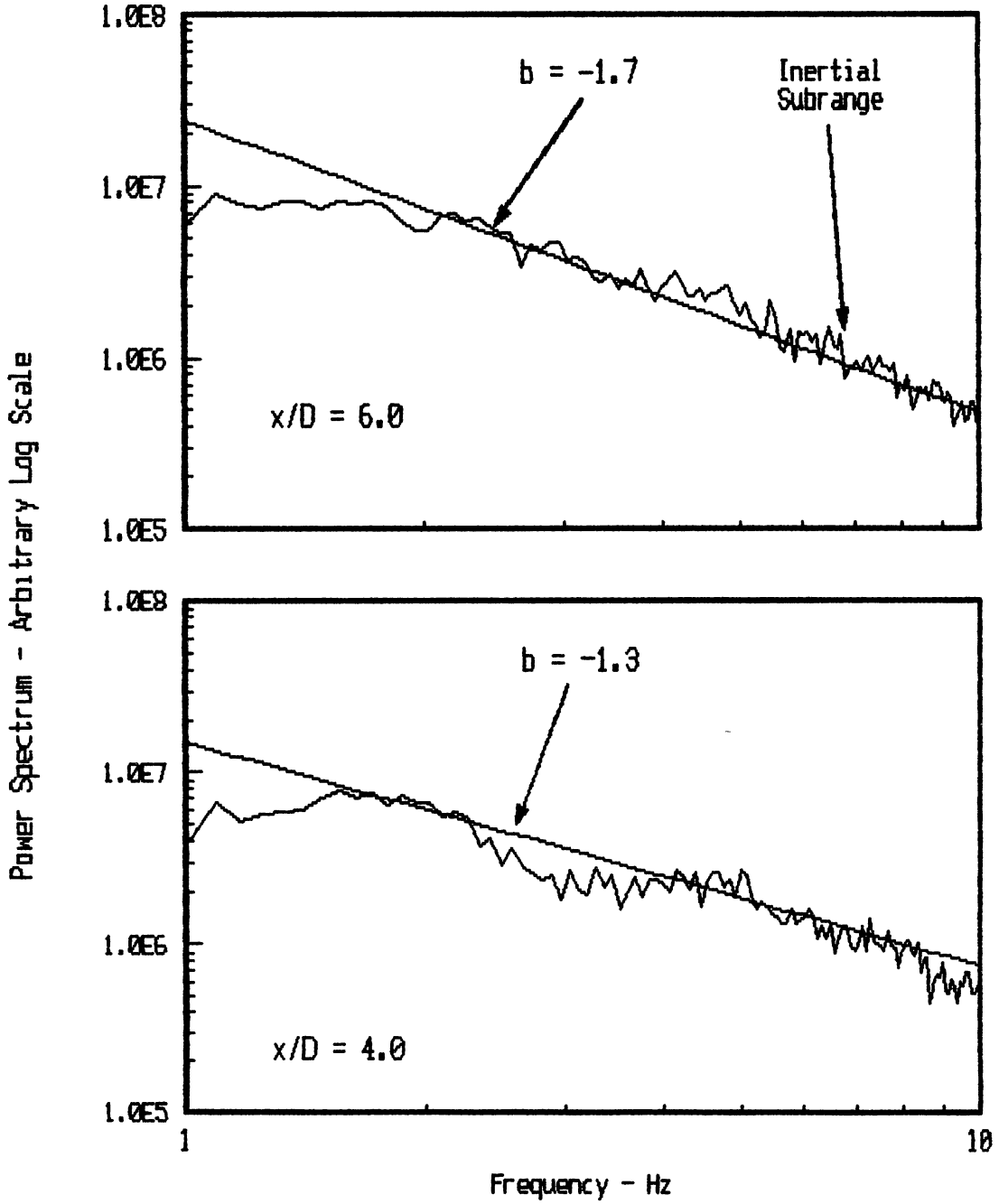

Figure 31. Slope of the Inertial Subrange, Nat Jet

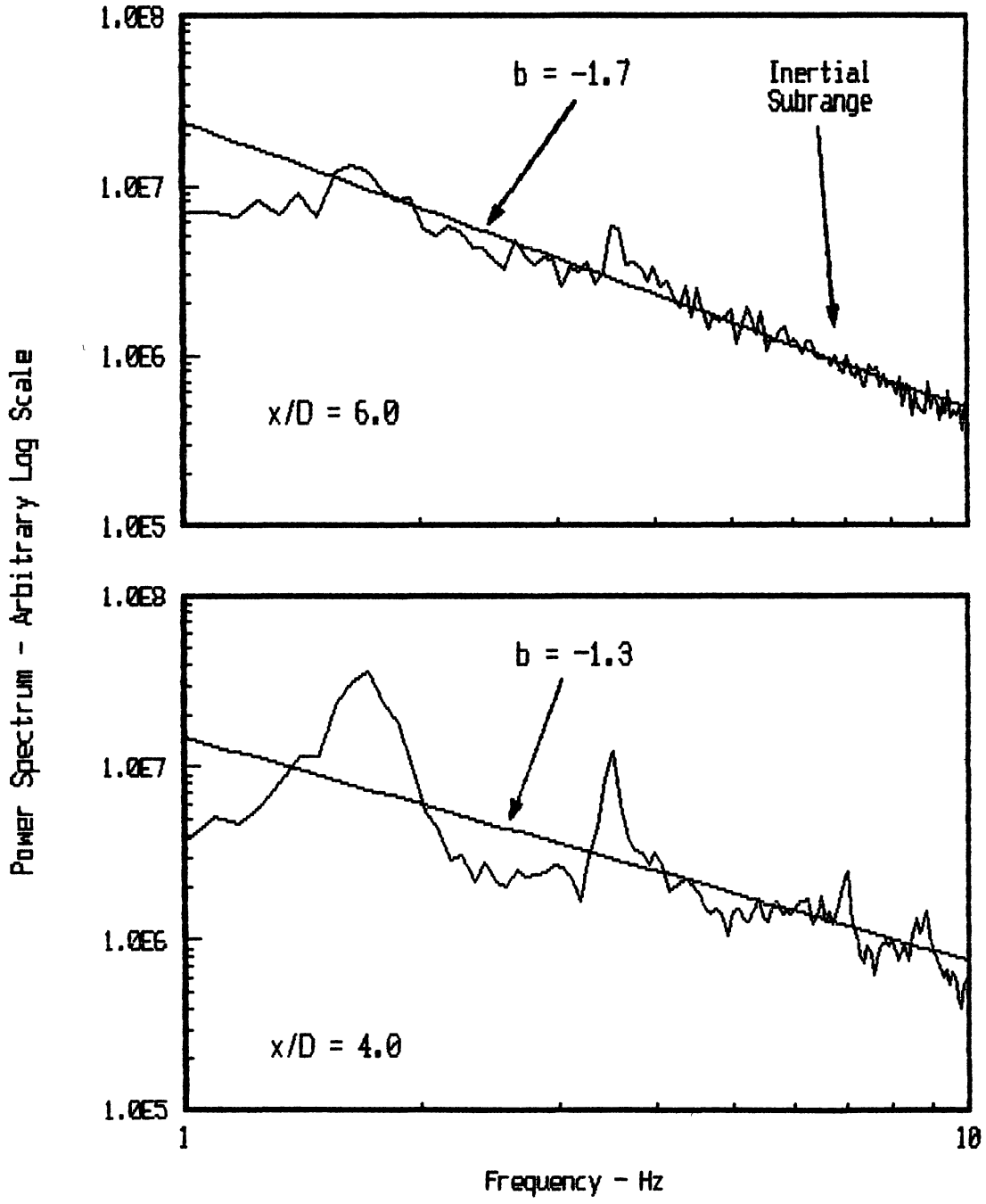

Figure 32. Slope of the Inertial Subrange, f=7 Hz

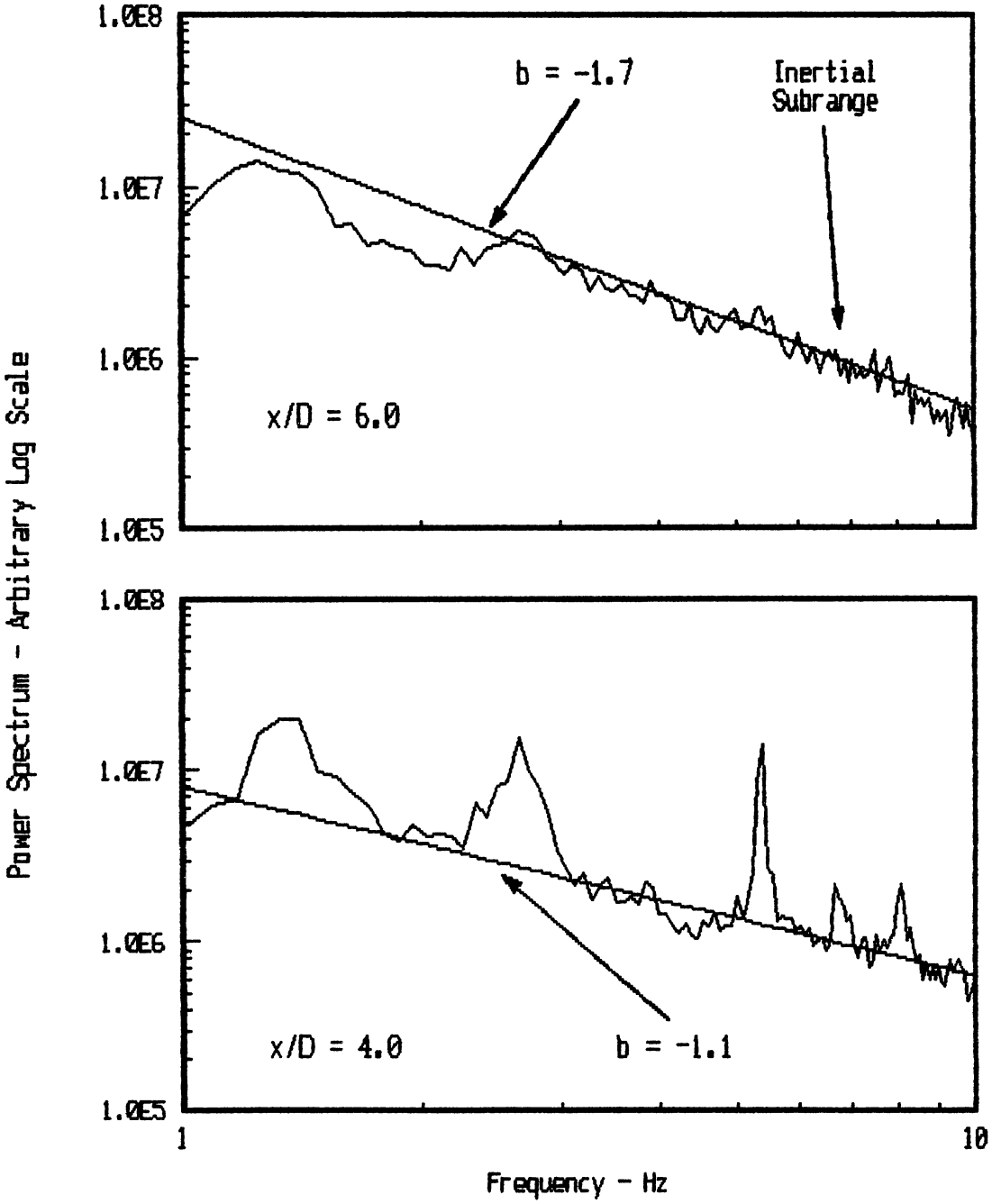

Figure 33. Slope of the Inertial Subrange, f=5.3 Hz

represent the vortices as accurately as possible, many difficulties are inherent in this type of analysis. First, some caution is obviously warranted in assuming a quantitative relationship between the visualized structure using dye injection and vorticity. The dye image is actually a streakline and is different from a pathline or a streamline if the flow is not steady state. Hama (1962) concludes that vortices cannot be positively identified based only on the rollup of the streakline. He states that it is likely that streakline rollup will behave similar to a vortex but that the concentration of dye does not constitute sufficient criterion to identify a vortex (see Hussain, 1983). In spite of this fundamental difficulty in interpolating flow visualization data, numerous researchers have made direct association between visualized dye structures and vortices (see Rockwell, 1972; Rockwell and Niccolls, 1972; Brown and Roshko, 1974; Browand and Troutt, 1985; Fiedler and Mensing, 1985; and Monkewitz, 1988). Lasheras and Choi (1988) suggest that the visualized structure must infer some concentration of vorticity, and as such are valid indications of the formation and movements of vortical structures. Additional difficulties are confronted in determining the instant of initial roll-up and the instant of pairing completion. Location of initial roll-up was determined by identifying a coherent structure and viewing the video tape backward in time until the first noticeable instance of rotation occurred.

Complete pairing was identified as the location where only one structure was distinguishable or where the structure was rotating as a single entity.

Differences between the developing planar jet and any other form of free shear layer flow are substantial and should be noted. The jet consists of two mixing layers which interact with each other and thus disrupt the long term mixing layer type development. It has been shown (Thomas & Chu, 1989) that the interaction of these layers creates a resonance effect which alters the layers essentially from the nozzle exit. The fundamental difference between a shear layer and a jet is the existence of a second length scale (the width or diameter of the nozzle) for the jet. An axisymmetric jet is also substantially different from a planar jet in that a single vortex is formed in the near region which is of course an annular vortex. The developing planar jet consists of cylindrical structures (vortices) which have positive rotation in one shear layer and negative in the other. In all physical experimental setups, these structures are not infinite but must end. Usually flow field confining plates are placed at the ends of a planar jet and the vortex ends as it interacts with the boundary layer.

Despite these differences, vortex pairing (or merging) mechanisms similar to those in mixing layers were observed in this study. Few incomplete pairings (mergings which include a portion of a vortex that had been torn apart or

shredded) were observed. This seems to agree with Monkewitz (1988) who found that in a mixing layer, 'shredding' occurs so infrequently that it is impossible to map out by conditional sampling techniques. Limited mergings similar to 'collective interactions' were observed in the jet where four vortices pair simultaneously. As will be described in following sections, the actual pairing usually consists in the downstream vortex moving slightly outward into the quiescent flow and slowing down. This vortex tracking analysis confirms that the vortex not only slows down but often actually comes to a virtual stop. An upstream vortex then moves inward into the high energy core flow and accelerates. Usually the vortices merge as the inner vortex passes the outer vortex. Although occasionally the inner vortex is accelerated past the outer vortex and continues downstream without pairing.

The most frequently observed types of vortex interactions are discussed in the following sections. These analyses were accomplished by viewing a section of the video tape data, frame by frame, and tracking each vortex from formation to approximately x/D=8.0. About 30 seconds of data was studied for each flow condition, which resulted in the tracking of about 200 vortices in each shear layer. Since, as stated in the introduction to this chapter, the shear layers exhibited approximate spatial and temporal symmetry up to a longitudinal position of at least

x/D = 6, vortex movements and interactions to be reported are analyzed in only one shear layer.

Forcing at 7 Hz

For this forcing frequency, the typical formation, motion, and interaction of coherent structures is summarized below.

roll-up -- occurred at about x/D=1.0

first pairing -- consisted of two vortical structures merging at about x/D=2.5

second pairing -- consisted of two structures (each of which were made up of two vortices which had already paired) merging at about x/D=5.5

As stated earlier, this was a highly organized (as compared to other forcing frequencies) flow field. However, this most common mode of structure interactions was observed for only about 60% of the time. Perhaps this interaction mode can be best understood by an examination of the 'vortex tracking' plot presented as figure 34 and the video sequence in figures 35 and 36. Vortex v1 forms and is convected downstream at 0.19 Uo (Uo is the mean jet velocity at the nozzle exit). Vortex v2 forms, moves inward toward the jet centerline and is convected downstream at 0.38 Uo until it pairs with v1 near x/D=2.5. The resulting structure is convected downstream to 0.23 Uo.

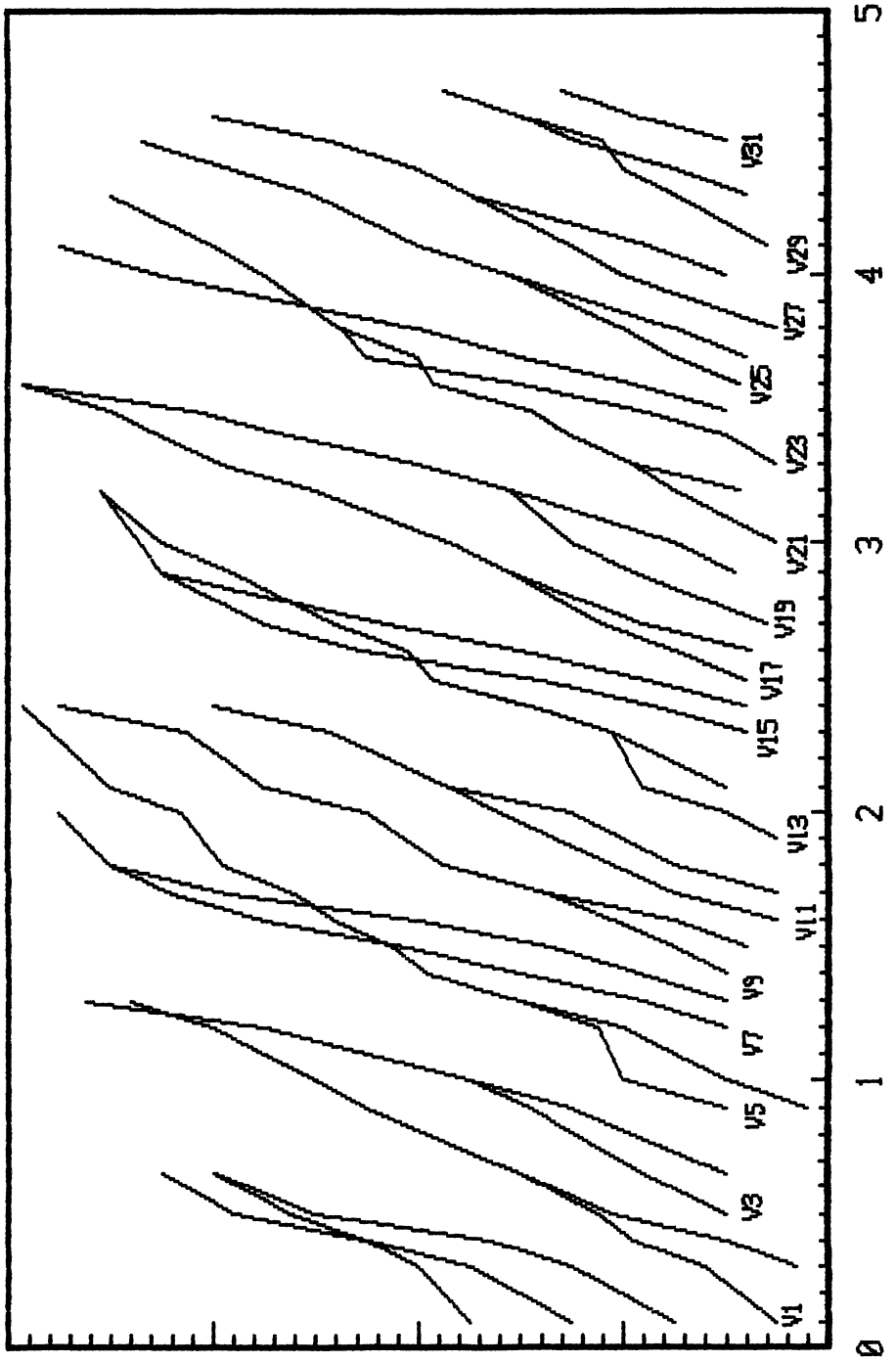

Figure 34. Vortex Trajectories, f=7 Hz

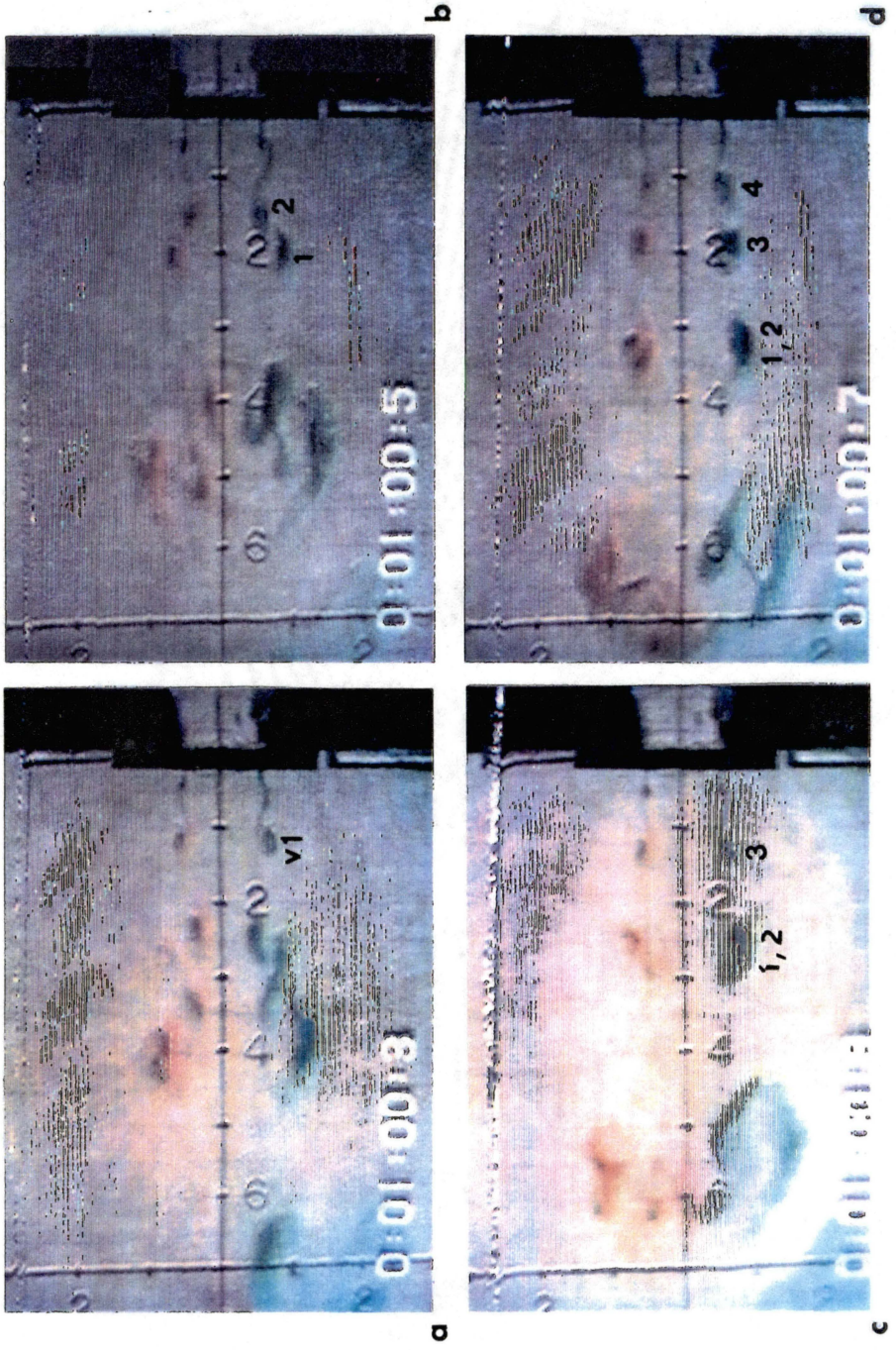

Figure **35.** Video Sequence of Vortex Trajectories, f=7 Hz

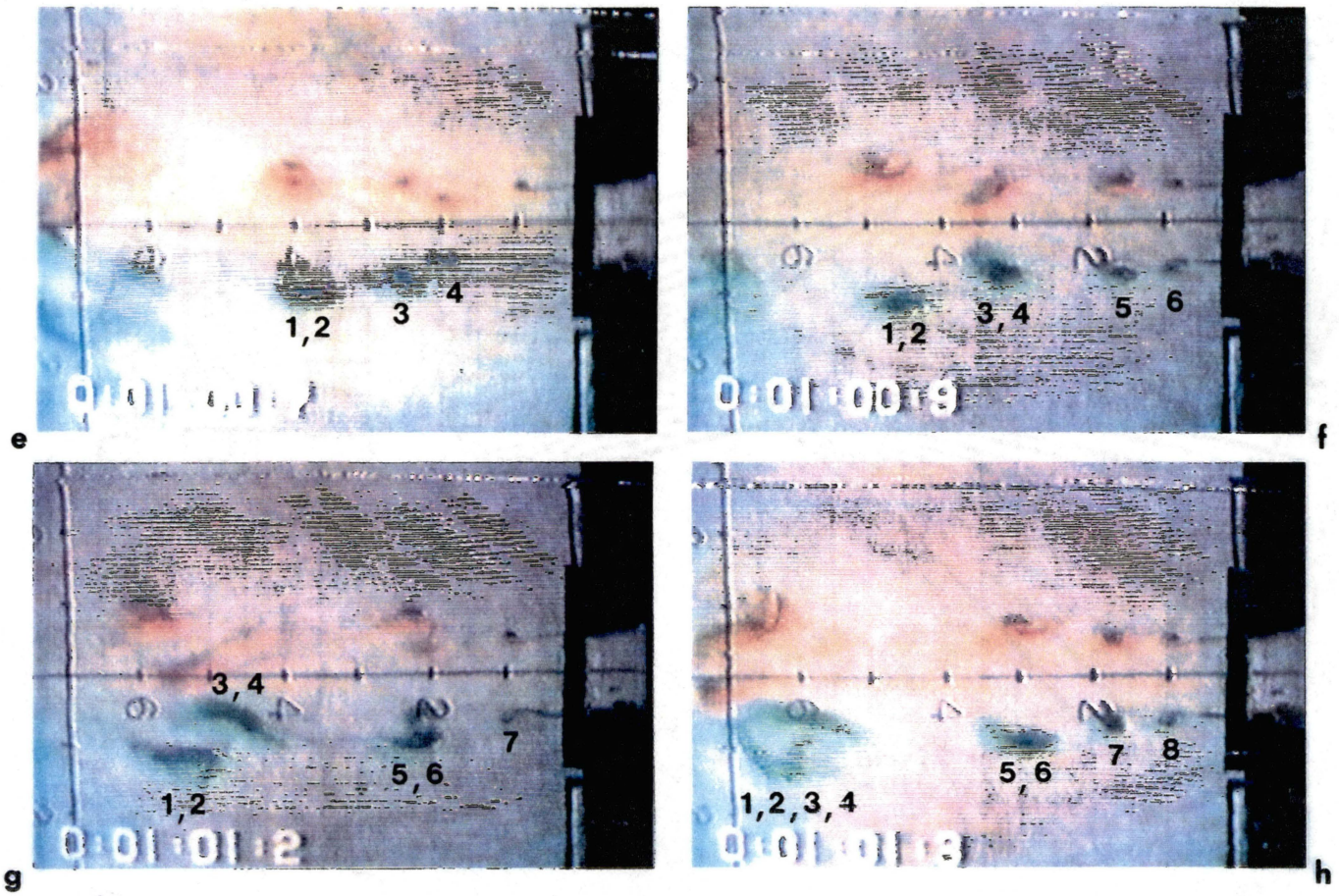

Figure 36. Video Sequence of Vortex Trajectories, f=7 Hz

Vortices v3 (at 0.2 Uo) and v4 (at 0.31 Uo) pair atx/D=3.0, move inward and are convected downstream at 0.42 Uo. The resulting structures pair at about x/D=6.0. This pattern also exists for the vortex groups (v17,v18,v19,v20) and (v25,v26,v27,v28).

Numerous other interaction modes were observed to occur for short periods of time. Two fairly common 'minor' modes will be noted. One resulted from a phenomenon (which occurred less than 15% of the time) in which vortex pairing was inhibited. The vortices still formed at about x/D=1.0 but no pairing was observed until well beyond the end of the potential core. Vortex v24 is an example of this mode. The second mode occurred less than 5% of the time and consisted of two vortices pairing between x/D=1.5 and x/D=3.0; but, the following two vortices do not pair until about x/D=6.5. These two vortices then quickly merge with the previously paired structure (see vortex groups v5,v6,v7,v8 and v13,v14,v15,v16).

The average convective velocity between x/D=1.0 and x/D=2.0 displayed a wide variance. Some vortices moved as slowly as 0.04 ft/sec (0.07 Uo) while others moved as fast as 0.58 ft/sec (1.0 Uo). The faster velocity usually was associated with the following vortex as it moved inward into the potential flow just prior to pairing. This lateral movement is shown on figure 37 for the vortex group (v5,v6,v7,v8). Vortex v5 is formed, moves outward and slows down to a velocity of 0.07 Uo. Vortex v6 is formed

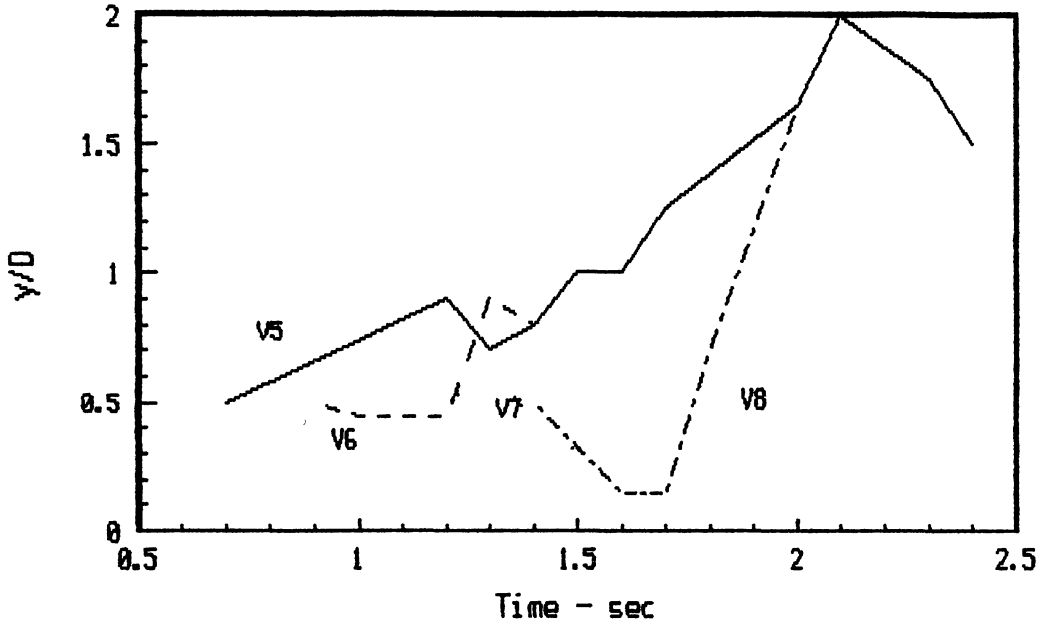

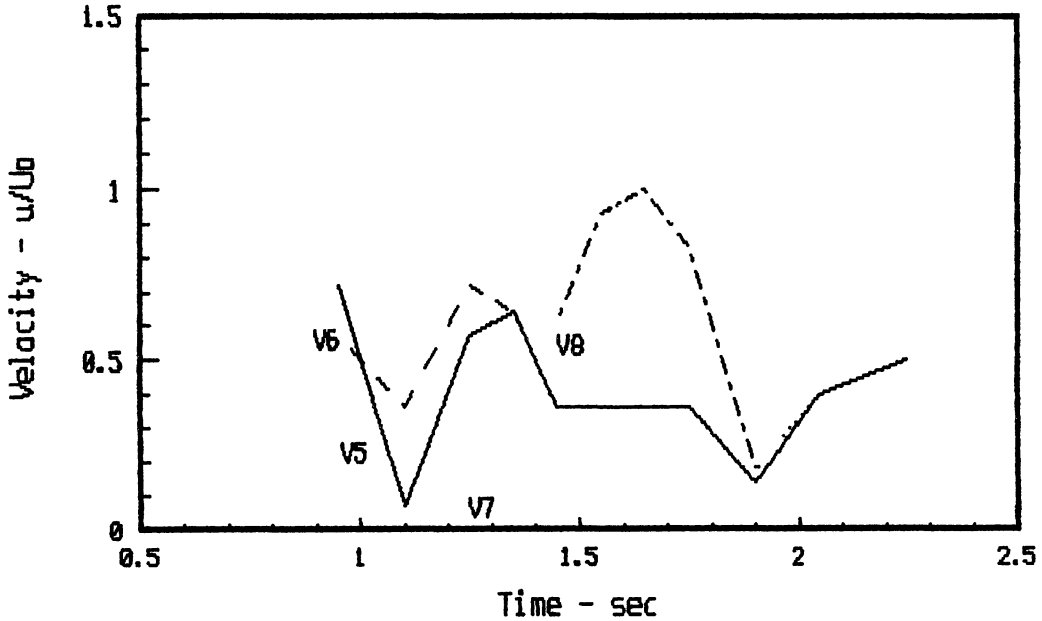

Figure 37. Lateral Vortex Trajectories and Longitudinal Convective Velocities, f=7 Hz

and moves inward and accelerates to 0.71 Uo. Vortices v7 and v8 both move inward and accelerates to velocities near Uo. Vortex v7 finally overtakes v6 at about x/D=6.5 and they pair.

It is generally accepted that the vortical structures are convected downstream at about 60% of the local centerline velocity. This study shows that an averaging process does not allow for complete understanding of physics involved. Some vortices form and move very slowly while others are convected downstream near (or perhaps even slightly above) the local centerline velocity. The large velocity difference seems to be mainly the result of a simple Biot-Savort relationship between the vortices.

Usually, initial vortex roll-up could be identified as early as x/D=1.0. However, some vortices could be identified as early as x/D=3.0.

Forcing at 5.3 Hz

For this forcing frequency, there was one major mode which was observed for approximately 90% of the vortices. This mode was:

roll-up -- occurred at about x/D = 0.5 to 0.75

first pairing -- consisted of two vortical structures merging between x/D = 2.5 and 4.5

second pairing -- no second pairing was observed until at least x/D=5.5. The

make-up of this pairing (if it was observed) varied significantly. Generally, it consisted of either a paired structure plus a single vortex or a simultaneous merging of a paired structure and two vortices.

A 'vortex tracking' plot is presented as figure 38 to illustrate this major modes as well as other modes. As stated earlier, this was originally thought to be an untuned jet and without careful examination the flow field has the appearance of being almost random. The total number of distinct dye images form at a rate slightly above 10 Hz. This might be associated with the harmonic of the forcing frequency (fe=5.3 Hz). Unfortunately, a comparison with the spectral analysis (figure 29) reveals that near the nozzle exit, the harmonic ($f \approx 10$ Hz) is not significant. Close examination of the dye structures resulted in an understanding that approximately every other dye structure never demonstrated any rotation. Since rotation is a fundamental characteristic of vortices, it was concluded that these structures were not vortices. Approximately one-half of the nonrotating dye structures were easily explained. They formed very early ($x/D \leq 0.5$) but remained only a 'bulge' in the 'tail' of the preceding vortex. By $x/D=1$, the vortex had engulfed the nonrotating structure.

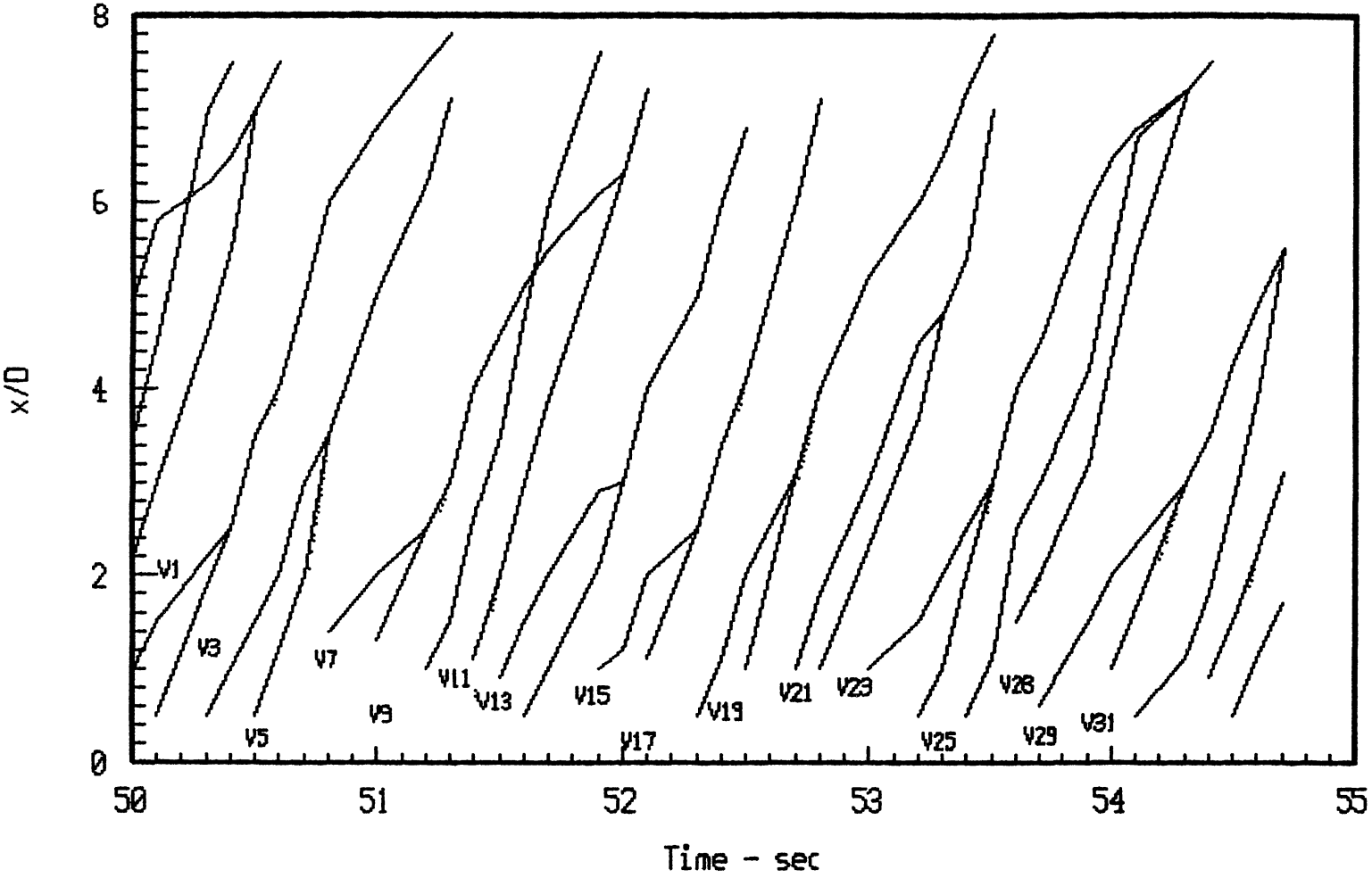

Figure 38. Vortex Trajectories, f=5.3 Hz

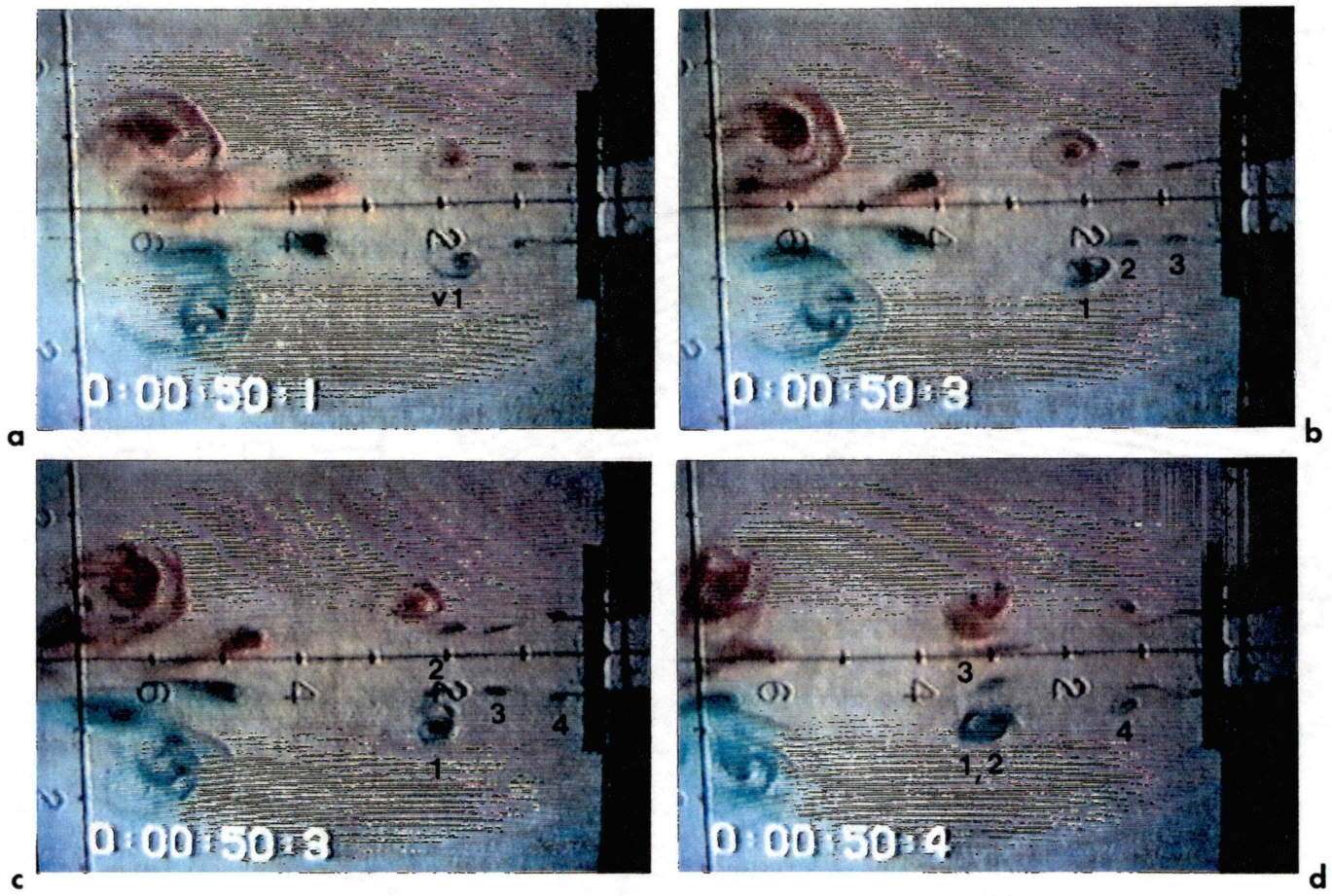

Figure **39.** Video Sequence of Vortex Trajectories, f= 5.3 Hz

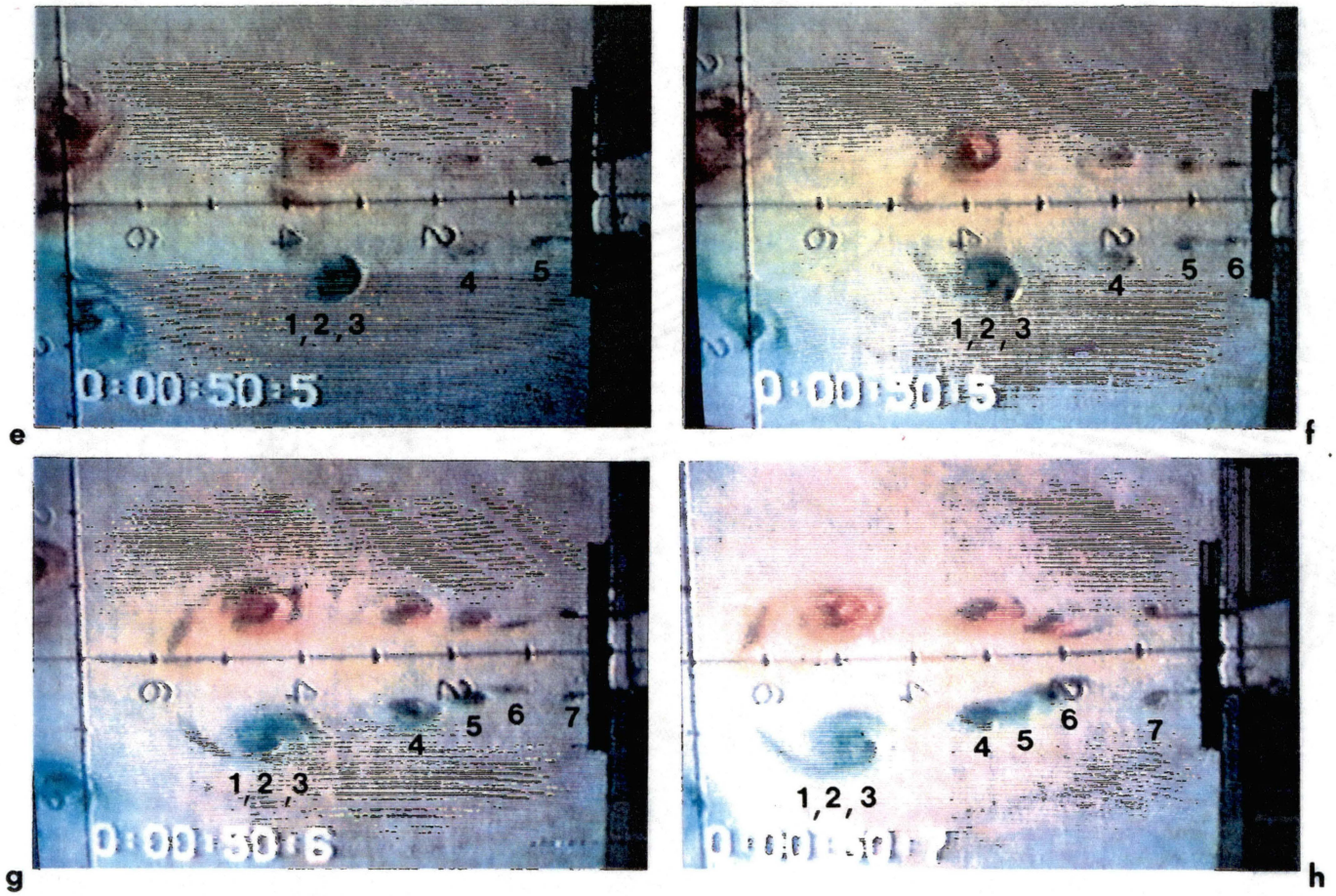

Figure **40.** Video Sequence of Vortex Trajectories, f=5.3 Hz

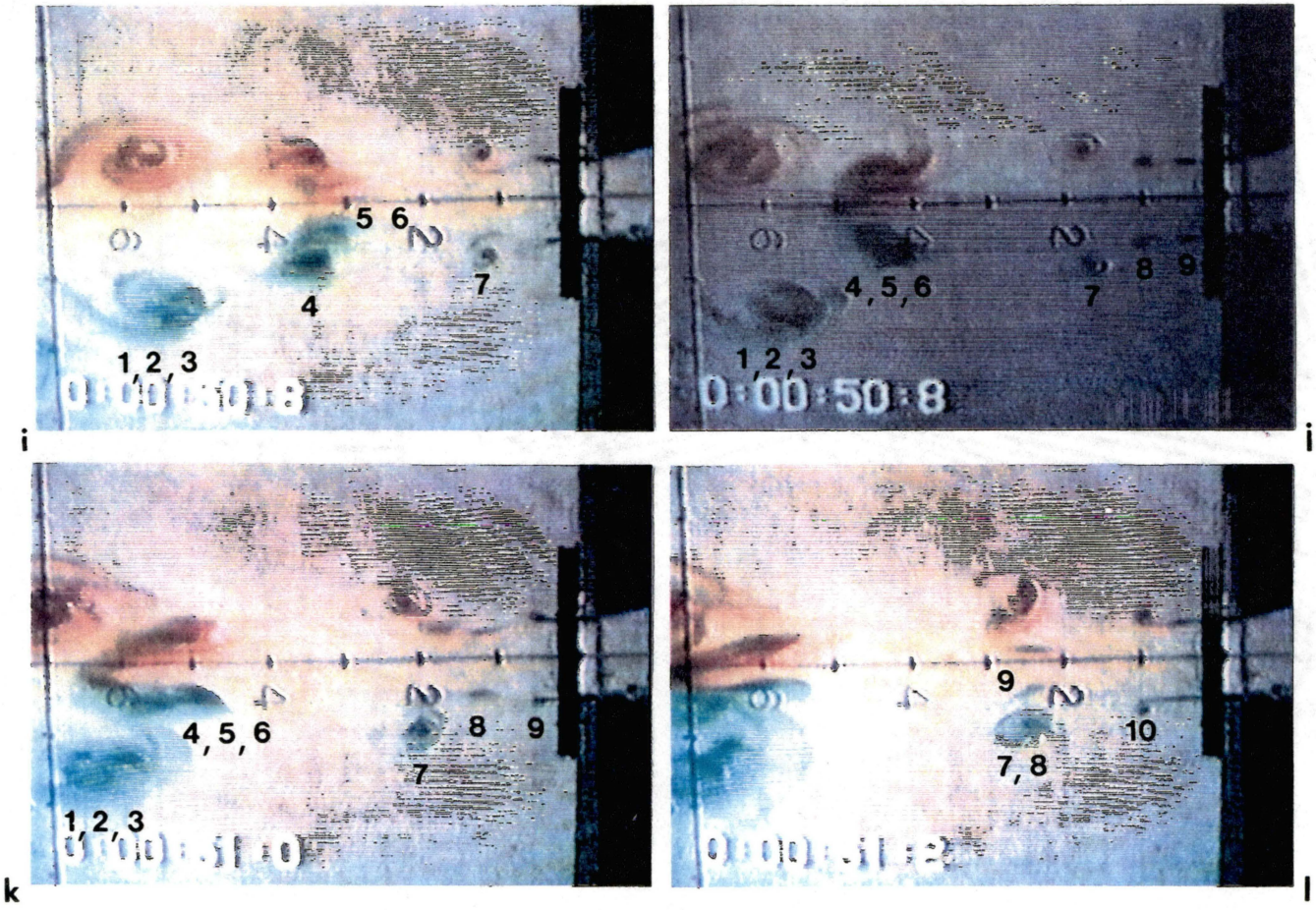

Figure **41.** Video Sequence of Vortex Trajectories, f=5.3 Hz

Thus, it was concluded that the 'bulge' was a part of the immature vortex. The other 'half' of the nonrotating structures were much more difficult to understand. These structures formed and became distinct and separate structures (see the dashed lines on figure 38 labeled as v3,v6,v9,v12,v17,v20,v25,etc.). Inclusion of these structures and the vortex structures, results in an average structure formation rate near the shear layer most unstable frequency of 7.8 Hz. Thus, these streakline concentrations seem to be related to the shear layer most unstable frequency but are not coherent vorticity-bearing fluid (Hussian, 1983). Understanding of which structures were vortices, revealed a highly repetitive pairing mechanism. This mode is demonstrated by the vortex group (v1,v2) in figure 38. Vortex v1 forms near x/D=1.0, moves slightly outward and is convected downstream at 0.21 Uo. Vortex v2 forms near x/D=0.5, moves slightly inward and is convected downstream at 0.28 Uo. These vortices pair between w/D=2.0 and 2.5. A similar pattern exists for vortex groups (v4,v5), (v7,v8), (v13,v14), (v15,v16), etc. The location of pairing varied widely from x/D=2.5 to 4.5 or later. Even though this pairing mechanism was dominant, the vortex motion and especially the pairing location appeared to be random. Video pictures (figures 39, 40 and 41) illustrate the vortex motion for vortices v1, v2, v4, v5, v7, and v8. Note that the structures v3, v6, and v9 do not display any rotation.

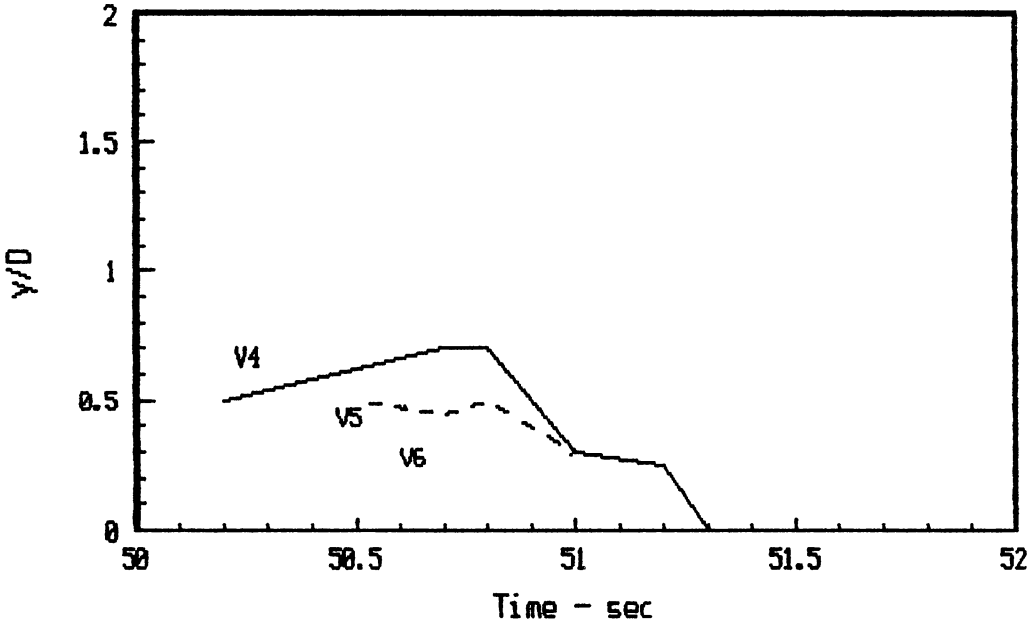

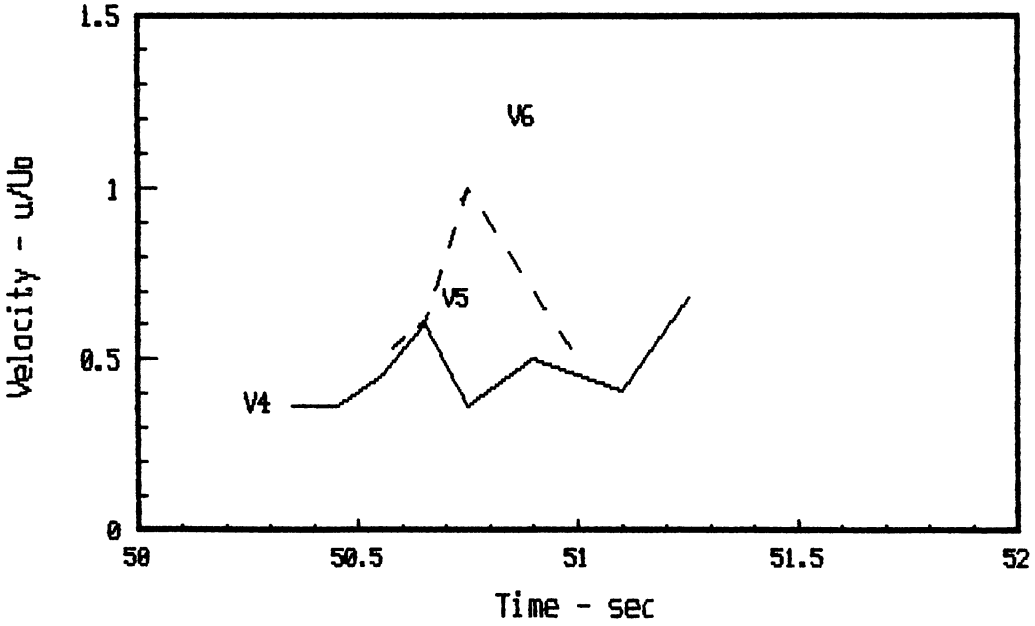

Figure 42. Lateral Vortex Trajectories and Longitudinal Convective Velocities, f=5.3 Hz

Other modes which were observed (for less than 3% of the time each) included single vortices which did not pair until at least x/D>6 (vortex v10), two vortices which would pair with several preceding structures simultaneously (vortex 27) and a single vortex which paired with a previously paired structure (vortices v11 and v32). The location of initial vortex formation appeared to be even more scattered than for the 7 Hz case. Vortices were first observable between x/D=0.5 and 1.0.

Initial convective velocities and subsequent lateral movements were similar to the 7 Hz case. Figure 42 (for the vortex group v4,v5) supports the general trend of convective velocities increasing for trailing vortices as they move inward into the potential core.

Comparison of the flow field when it is Forced at 7 Hz and at 5.3 Hz

The 7 Hz (fe=7 Hz) mode produced a tuned jet which encouraged development of the subharmonic frequency. This was evidenced by the pairing of two vortices (development of the first subharmonic) and the subsequent pairing of two paired structures (development of the second subharmonic fe/4=fc). Thus, the dominant feature of this mode was the pairing of only two structures at a time. However, no purely periodic modes were discovered and mode switching appeared to be random.

The 5.3 Hz (fe=5.3 Hz) mode was expected to produce an untuned jet which was expected to suppress subharmonic development. However, as evidenced by the spectral data (figure 30), both the first and second subharmonics formed. The natural jet column mode frequency did not develop. The nonrotating dye structures give testimony that the shear layer was forced to rollup at a frequency substantially different from the natural jet most unstable frequency. Nevertheless, as in the 7 Hz case, no purely periodic modes could be found to exist and mode switching appeared to be random.

Chaotic Motion of the Vortical Structures

One of the initial intentions of this study was to identify the patterns of vortex motion for various forcing frequencies. It seems logical that these patterns should exist. The flow field is governed by the deterministic Navier-Stokes equations. It appears that the near region flow could be modeled by the two-dimensional and perhaps even inviscid equation. Great care was taken to provide a 'clean' flow field. Many hours were spent watching the flow and examining the video tape. Alas, no purely periodic modes. This posed an interesting although perplexing question. Since the flow is governed by a set of deterministic, nonlinear equations and has carefully controlled, periodic initial conditions, why is the

resulting flow not periodic? The answer must lie in fairly recent studies in the area of 'chaos'.

As is presented in section 1.2.2, even very simple non-linear equations such as the logistic equation, will exhibit chaotic behavior under certain conditions. Unfortunately, the problem of establishing the existence of chaos is much more difficult for experimental data than for theoretical equations. Moon (1987) suggests several indicators of chaos. Four of these are well suited for the present data.

1) Power Spectra
2) Fractal Dimension
3) Estimation based on the Feigenbaum number
4) Lyapunov Exponent

Each one of these indicators will be examined in detail to establish the existence of chaotic motion in the planar jet. The approximate longitudinal location where chaos begins will also be identified.

Theoretical Background

The classic Navier-Stokes equations are the governing set of equations for the planar jet flow field (and most other fluid phenomenon).

$$\frac{\partial V}{\partial t} + V \cdot \nabla V = \Delta P - \nu \nabla^2 V \qquad (3.2)$$

where V is the velocity vector

P is the pressure

ν is the kinetic viscosity

Since this study used water (a Newtonian fluid) as the working medium, the viscous term is linear. The non-linearity lies in the convection term $V \cdot \nabla V$. This is the term that for certain initial and boundary conditions may lead to chaotic behavior.

Experimental Data

Data were obtained directly from the video tape for both the 5.3 Hz and the 7 Hz cases. The natural jet case was not used because the rollup and subsequent motion of the structures were extremely difficult to quantify. Also, the forced cases represented the most orderly flow and the least likely to become chaotic. A line perpendicular to the flow was placed on the monitor at a specific x/D location. The time at which each vortex (in a single shear layer) passed the line was recorded. The video recorder records 30 frames per second, so the time resolution is 1/30 second. Passage of the vortex was assumed to be the time interval before the vortex center passed the x/D location. Approximately 700 data points were taken. These were fed into a computer program to obtain a new data set containing the time intervals between vortex passages. This last data set was used to compute Poincare maps, the fractal dimension, bifurcation maps and the Lyapunov exponent. Data are obtained for x/D locations from 0.075

to 2.5 for the 5.3 Hz condition and from 0.075 to 2.75 for the 7 Hz condition.

Poincare Sections

As described in section 1.2.2, a Poincare section is a sequence of points in phase space generated by the penetration of a continuous evolution trajectory through a specified plane in the space. Examination of the resulting pattern in the phase plane allows differentiation between periodic and nonperiodic motion.

For the current data, Poincare sections (more specifically, first return graphs) are plotted by obtaining 3-dimensional histograms for each x/D location. The horizontal axis is the time interval (t_n) between a vortex and the preceding vortex. The vertical axis is the time interval (t_{n+1}) between the vortex and the following vortex. These axes are normalized by multiplication of the forcing frequency, (i.e. t_n f_e). The third dimension is the number of times each combination occurred. The bifurcation parameter is obviously x/D. These data are contour plotted and presented as figures 43 through 51 for 7 Hz and 54 through 60 for 5.3 Hz. Due to the video 'shutter' speed and the difficulty in locating the center of the vortex, the accuracy of the data (t_n) is estimated to be plus or minus 0.017 seconds.

Figure 43 shows that for the 7 Hz case the data is almost periodic near the nozzle exit. There is some

scattering of the data well outside of estimated accuracy. The section is symmetric about a 45 degree line indicating an invertable map. As shown by figures 44 through 46, the flow remains almost periodic until x/D = 1.125 where a additional broadening of the point occurs. A bifurcation occurs somewhere between x/D = 1.25 and 1.375 (figures 47 and 48) but the pattern remains symmetric indicating the map is still invertable. However, the Poincare section at x/D = 1.375 appears to be the intersection of a torus with the plane. Thus the motion has become quasiperiodic (actually biperiodic) with two competing frequencies whose ratio is rational. It appears that this conclusion should have some strong implications regarding vortex motion in the jet. These implications are unclear and should be the topic of future studies. A slow developing nonsymmetric point begins to develop by x/D = 1.75 (figure 49) indicating the map has become noninvertable. This results in a second bifurcation by x/D = 2.25 (figure 50). The nearly complete quadratic map, as will be seen in the 5.3 Hz case, never develops. By x/D = 2.5 the pattern (figure 51) has some resemblance to the Henon Map as presented by Shaw (1984). The bifurcation diagram (figure 52) shows two clear bifurcations. This diagram was generated by producing a three-dimensional histogram of the time intervals between vortex passage versus x/D location. Since the total number of occurrences for any time interval becomes diluted as bifurcations occur, the histogram was

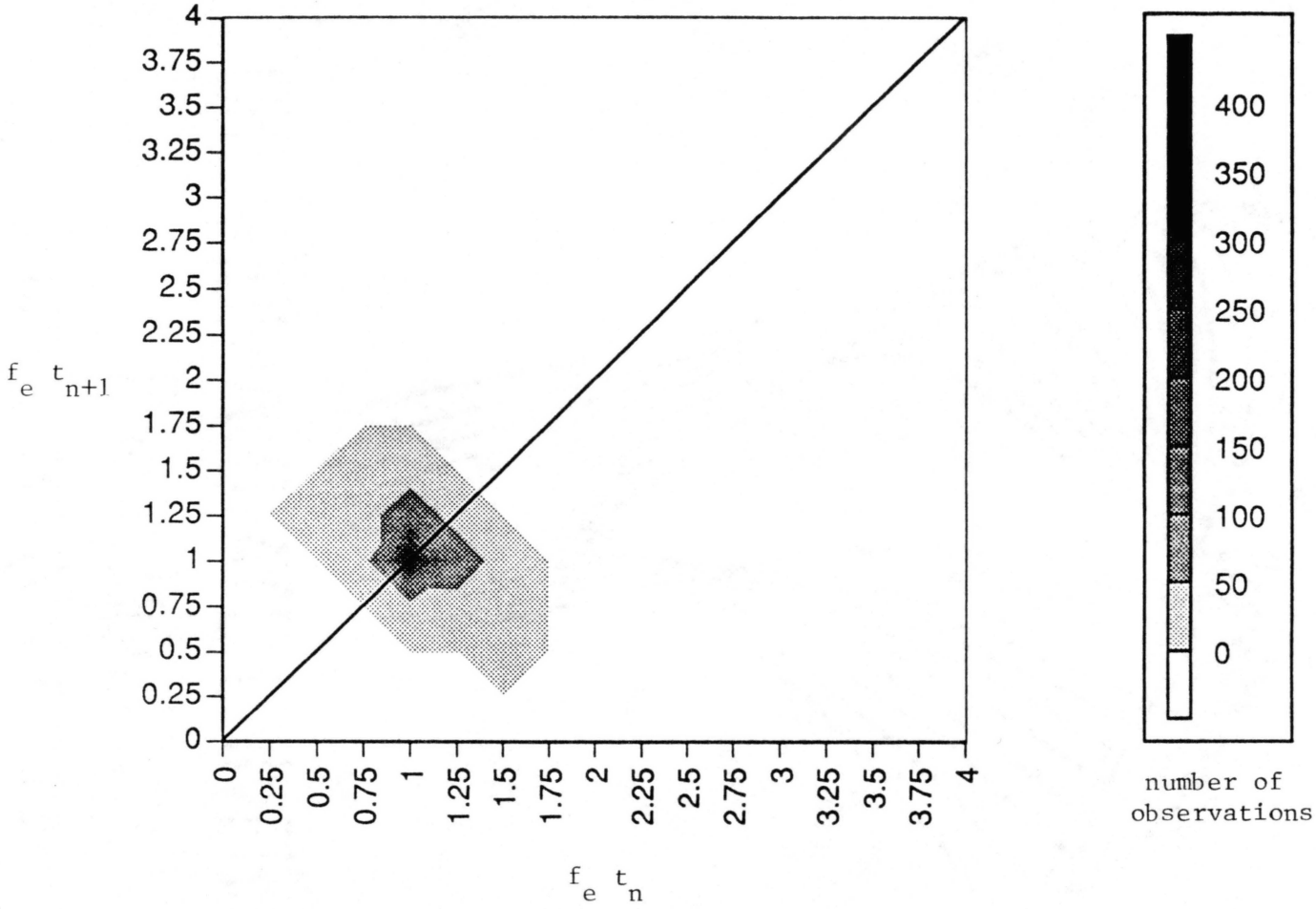

Figure 43. Poincare Section, f=7 Hz, x/D=0.75

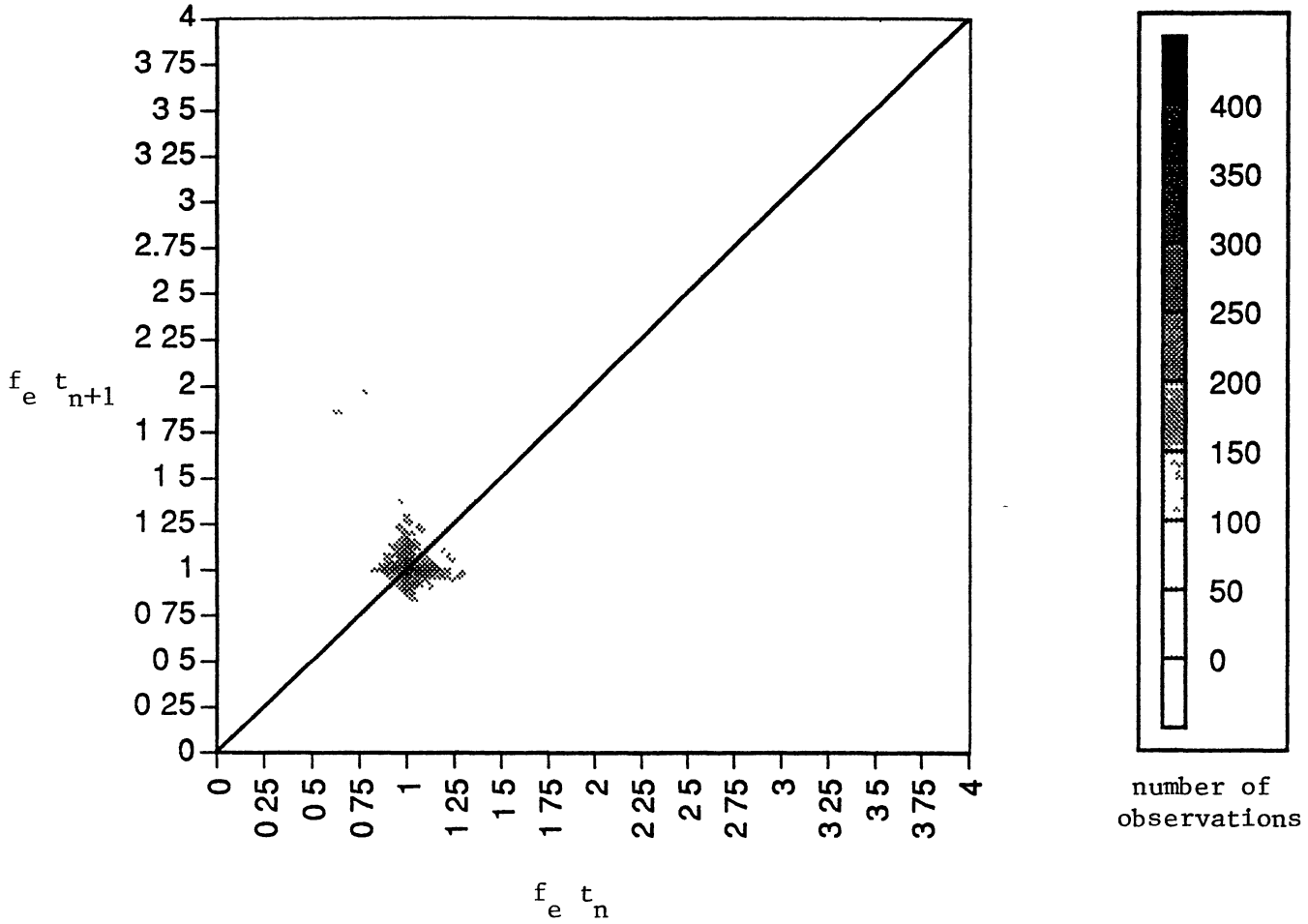

Figure 44. Poincare Section, f=7 Hz, x/D=0.875

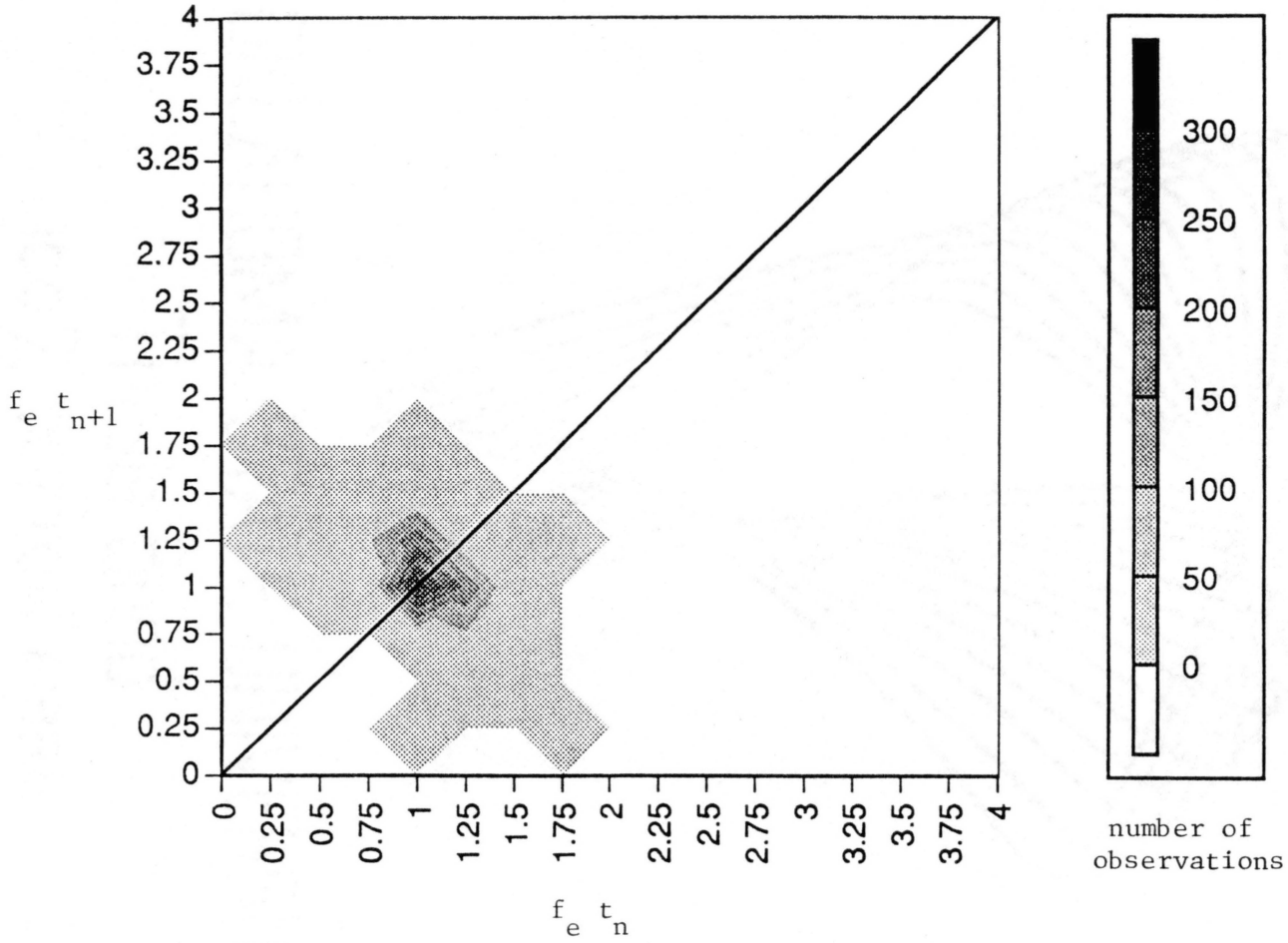

Figure 45. Poincare Section, f=7 Hz, x/D=1.0

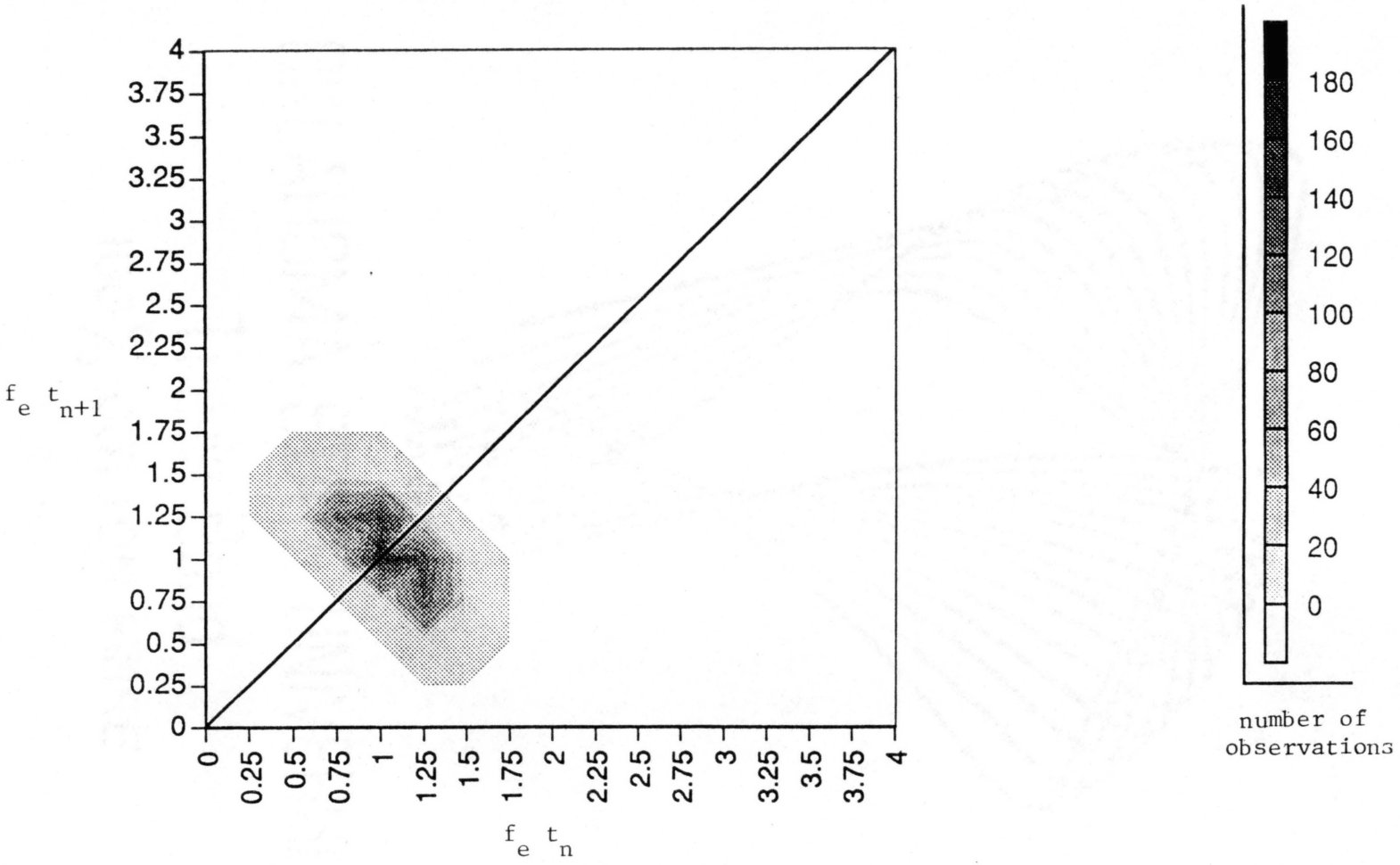

Figure 46. Poincare Section, f=7 Hz, x/D=1.125

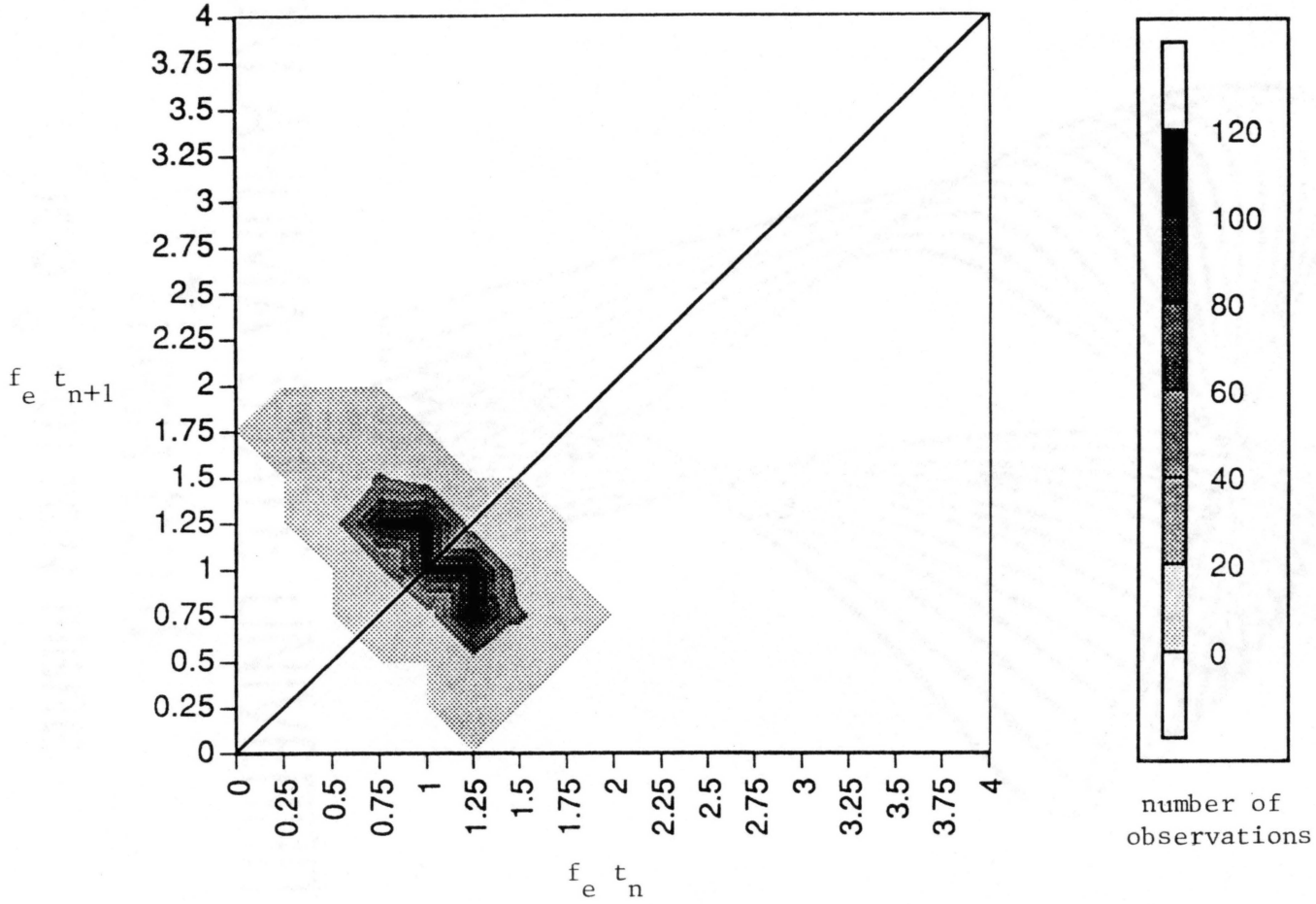

Figure 47. Poincare Section, f=7 Hz, x/D=1.25

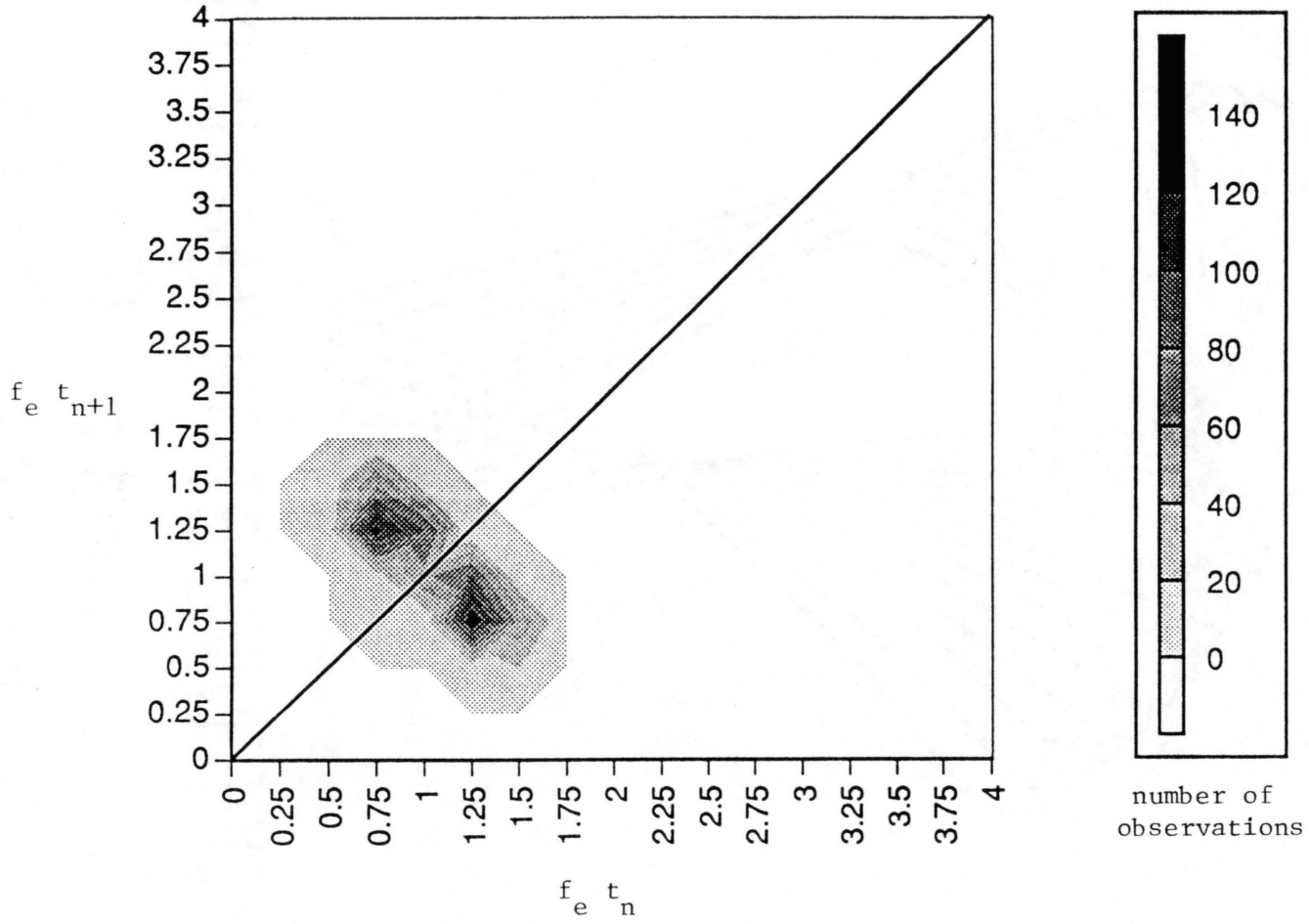

Figure 48. Poincare Section, f=7 Hz, x/D=1.375

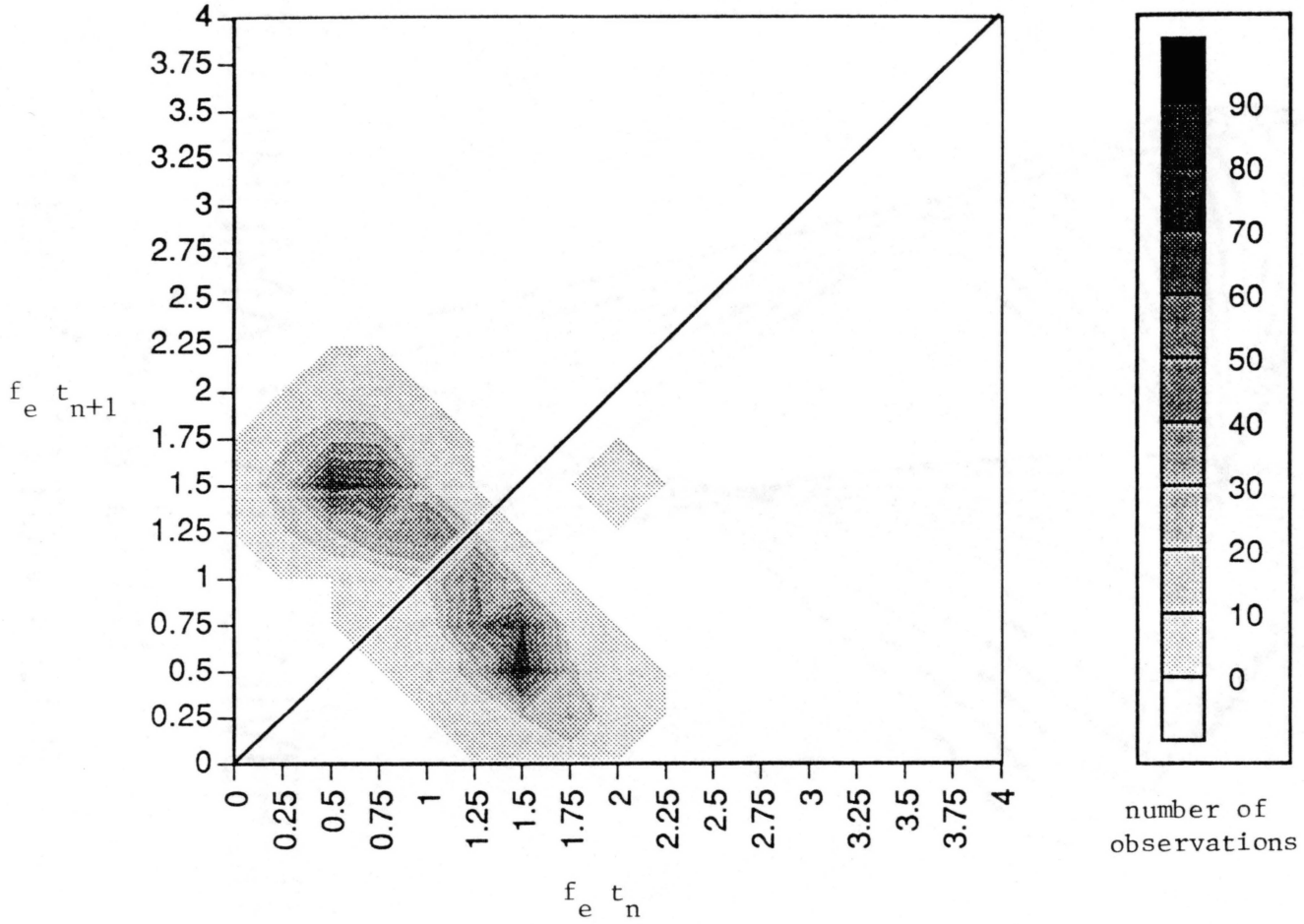

Figure 49. Poincare Section, f=7 Hz, x/D=1.75

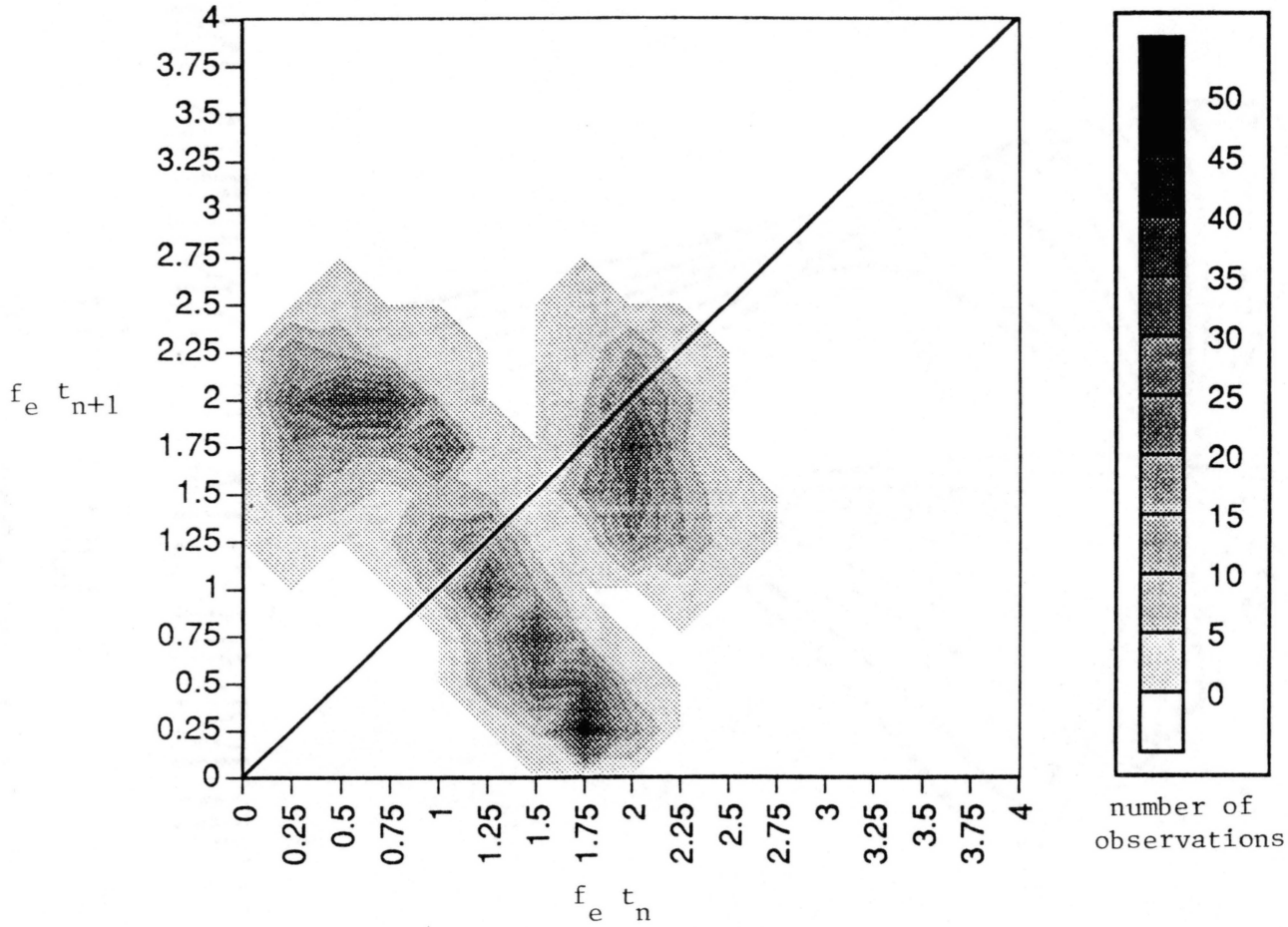

Figure 50. Poincare Section, f=7 Hz, x/D=2.25

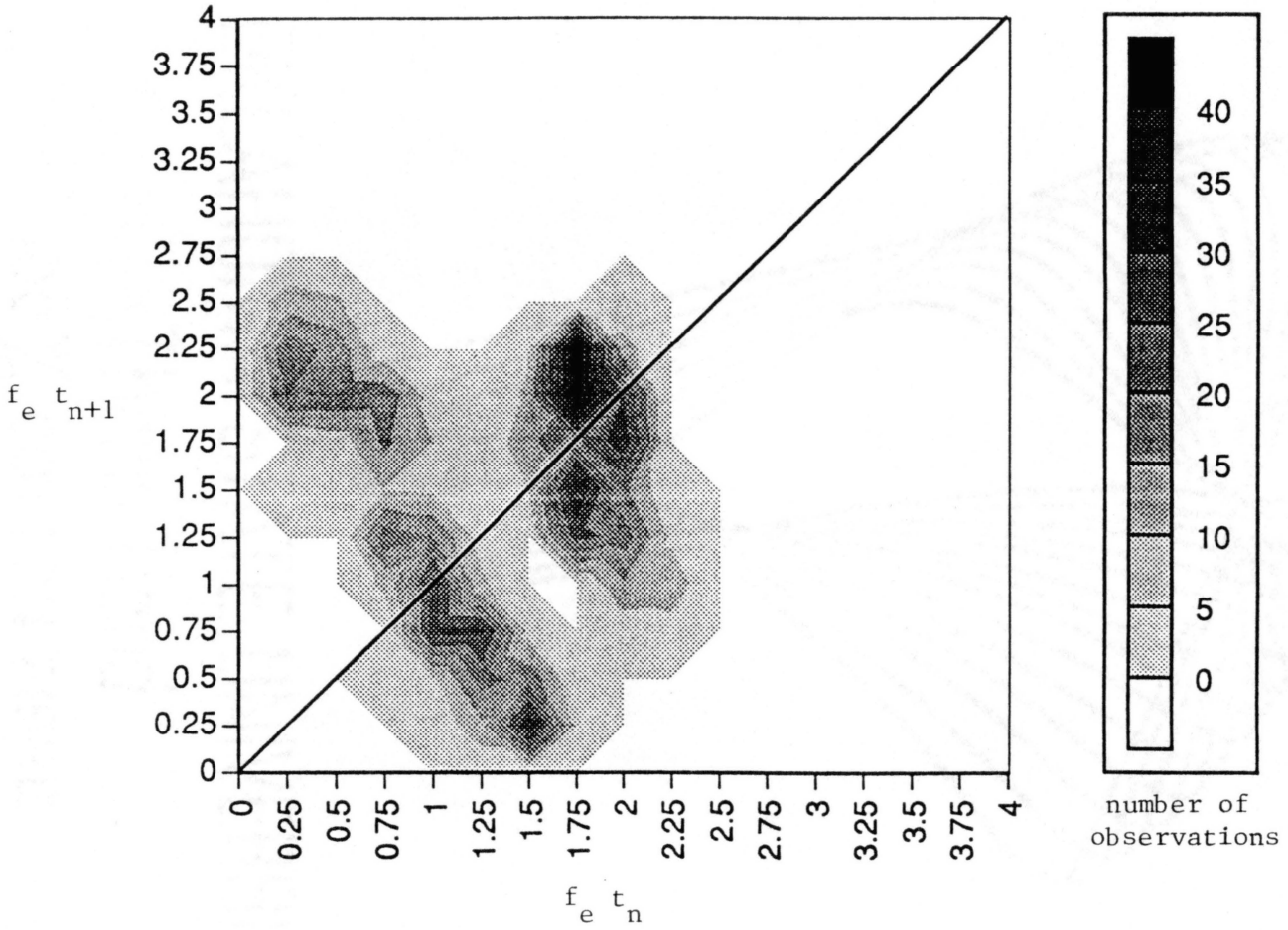

Figure 51. Poincare Section, f=7 Hz, x/D=2.5

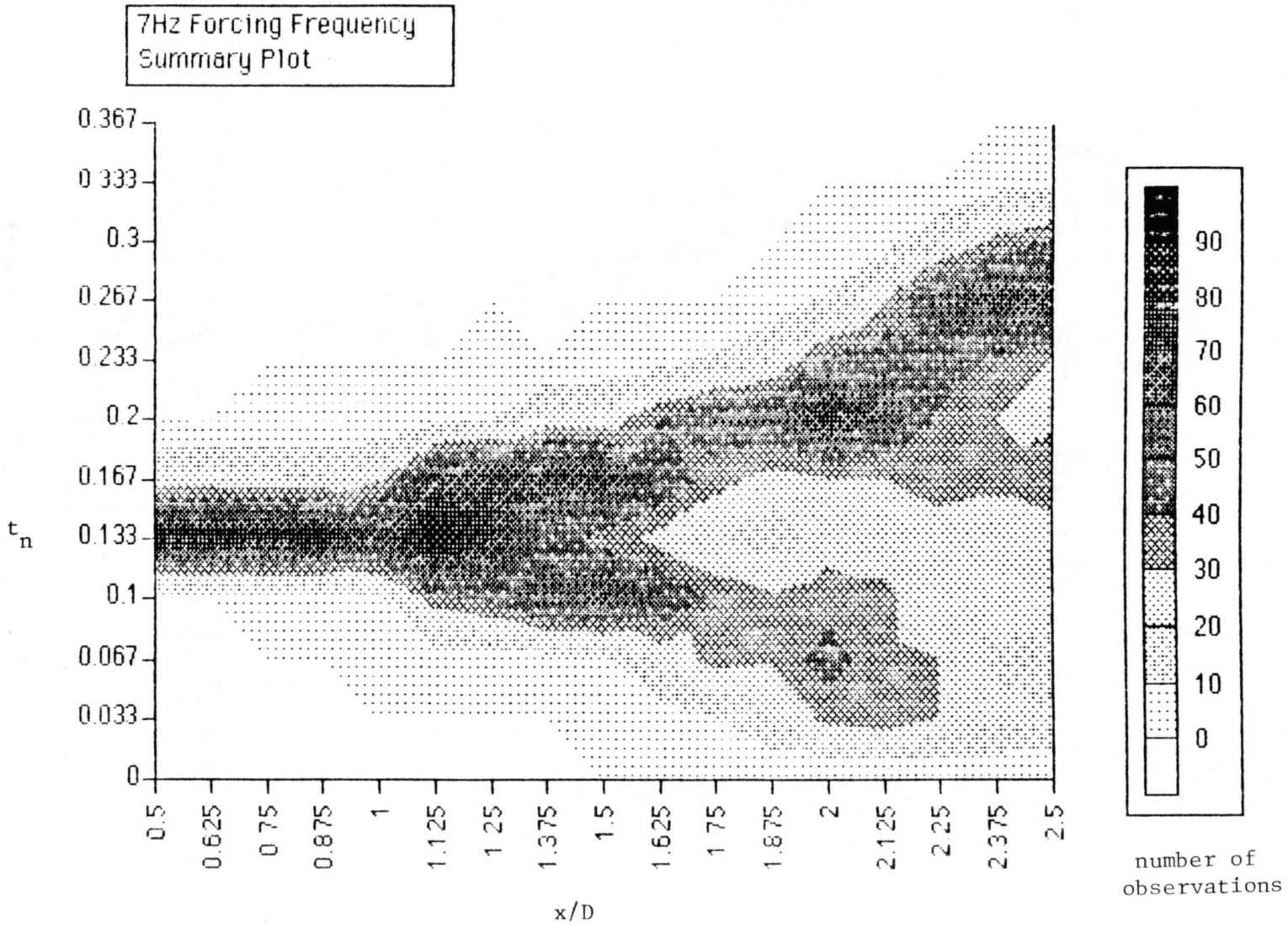

Figure 52. Bifurcation Diagram, f=7 Hz

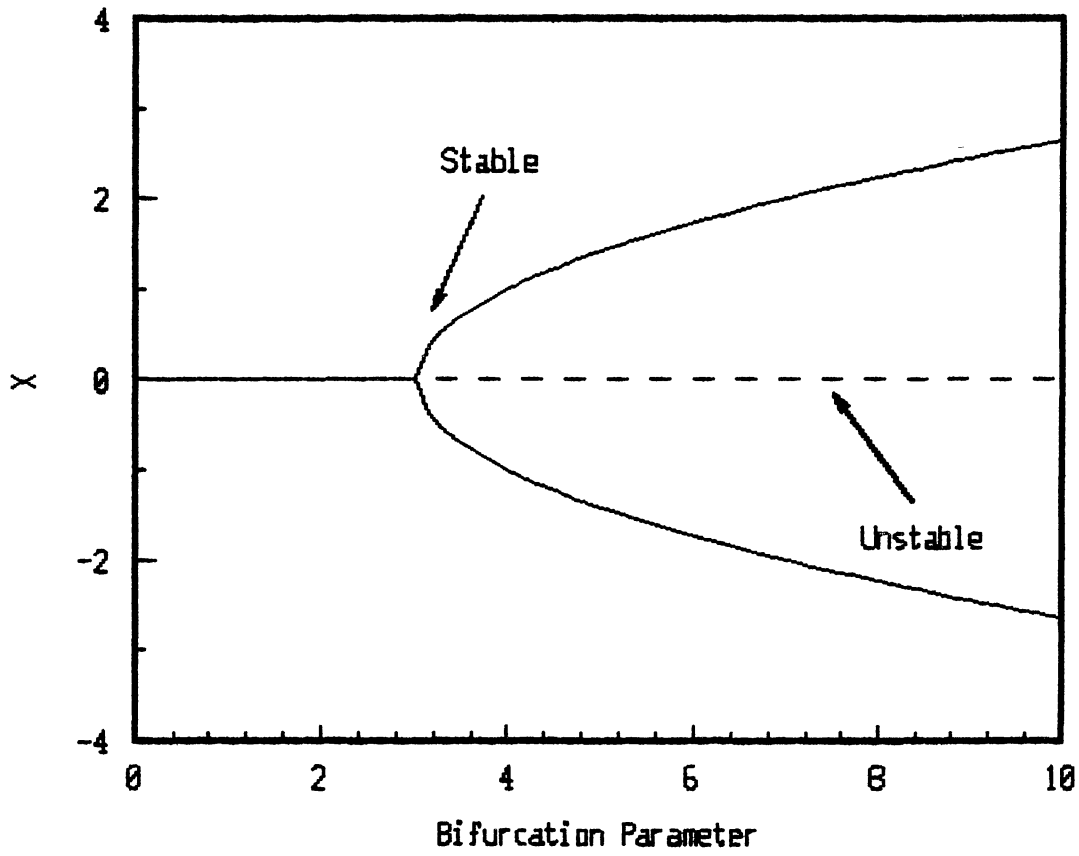

Figure 53. Schematic of a Pitchfork Bifurcation

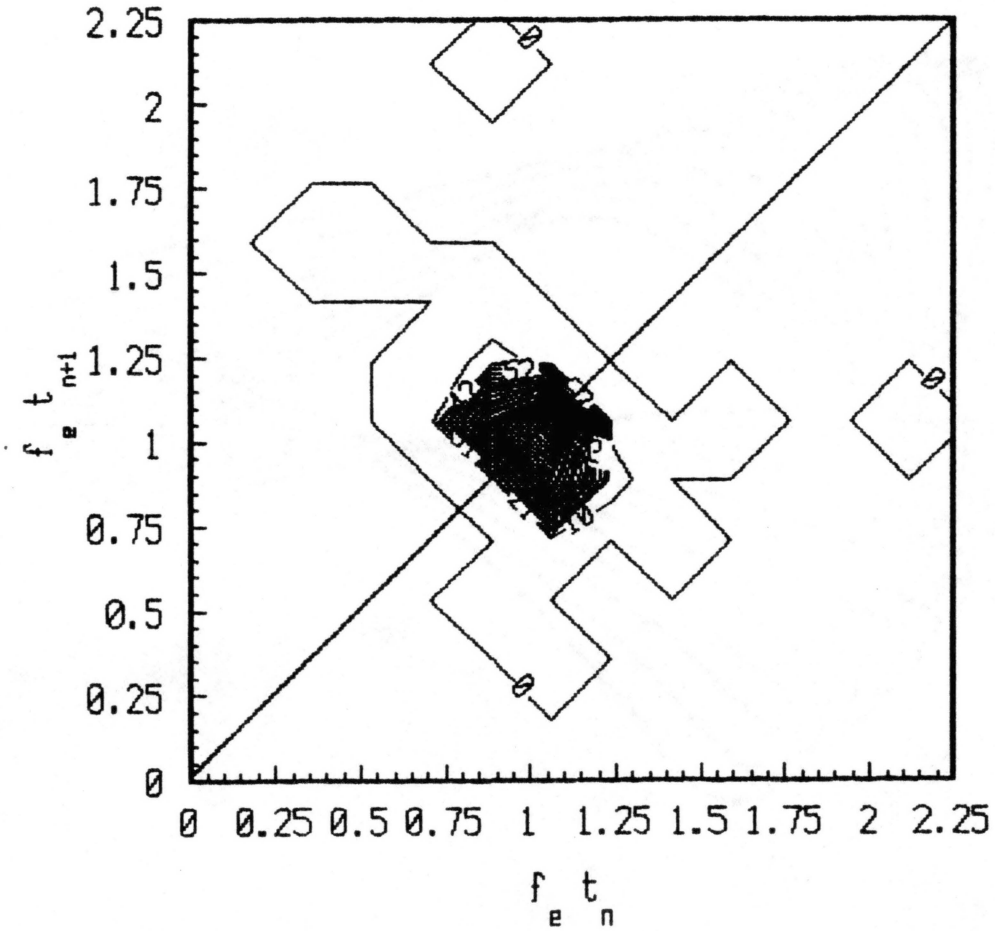

Figure 54. Poincare Section, f=5.3 Hz, x/D=0.75

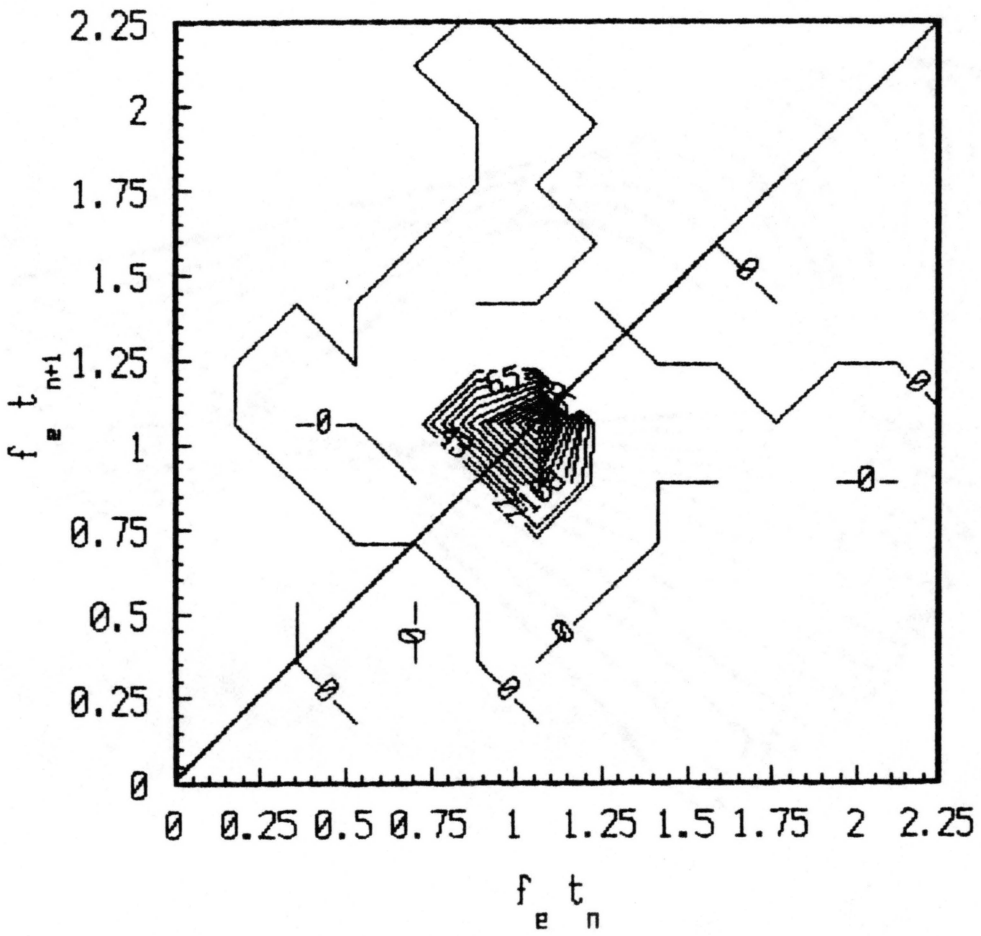

Figure 55. Poincare Section, f=5.3 Hz, x/D=0.875

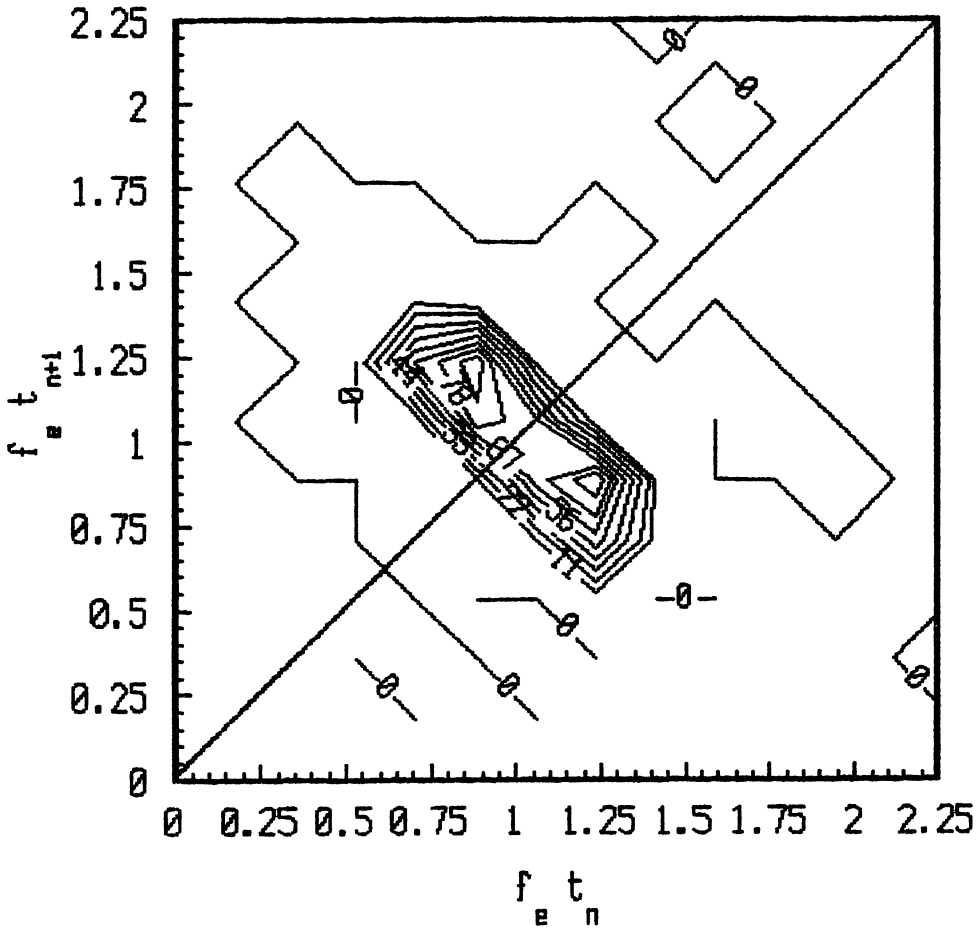

Figure 56. Poincare Section, f=5.3 Hz, x/D=1.25

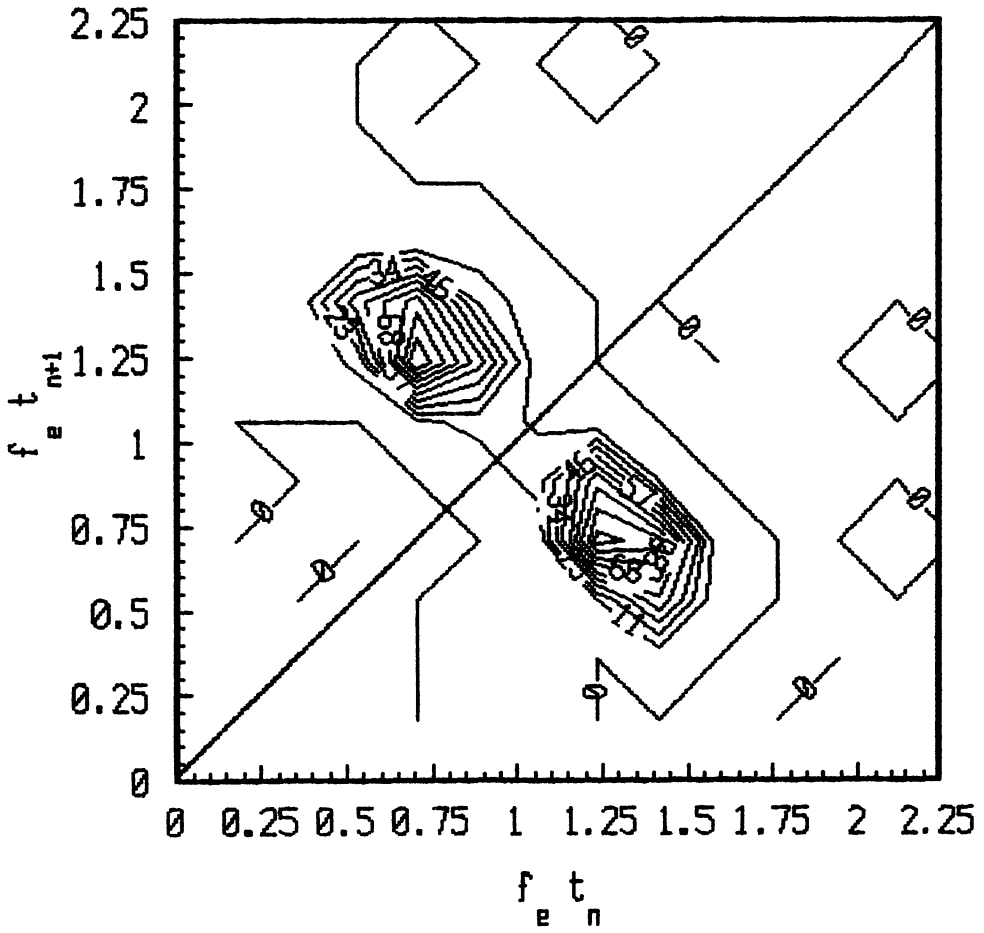

Figure 57. Poincare Section, f=5.3 Hz, x/D=1.50

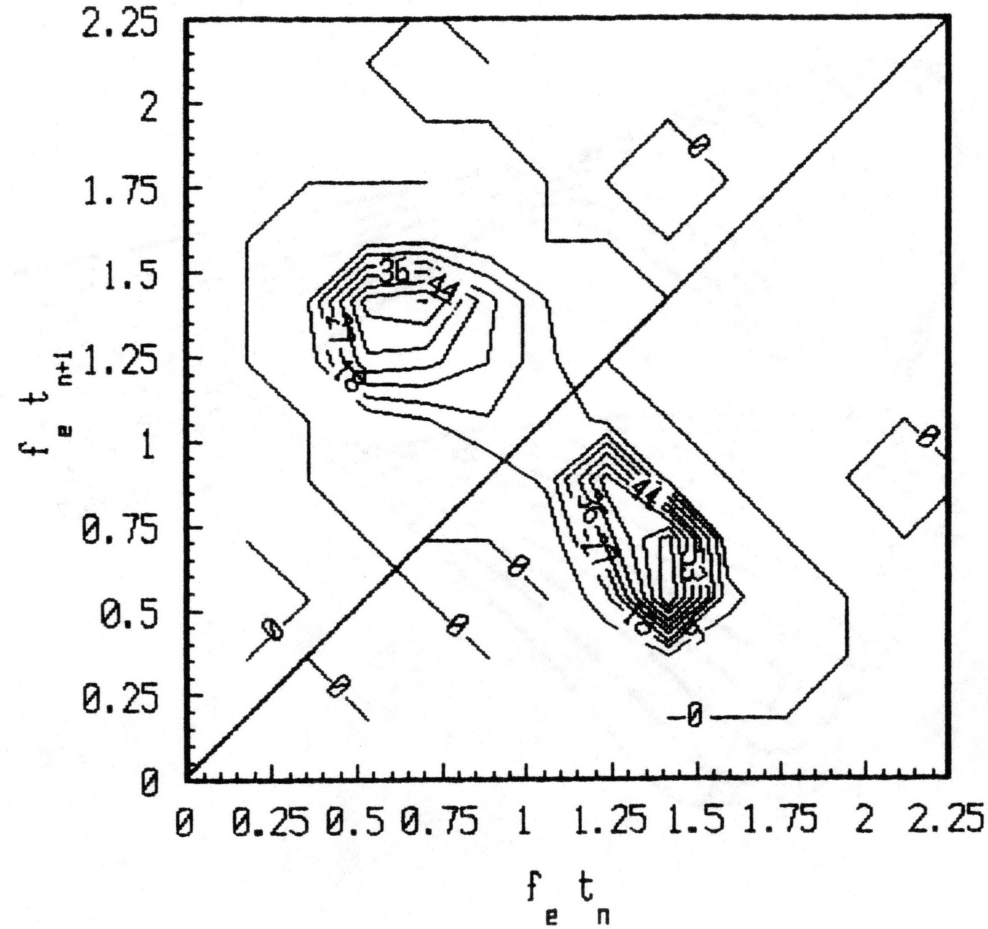

Figure 58. Poincare Section, f=5.3 Hz, x/D=1.75

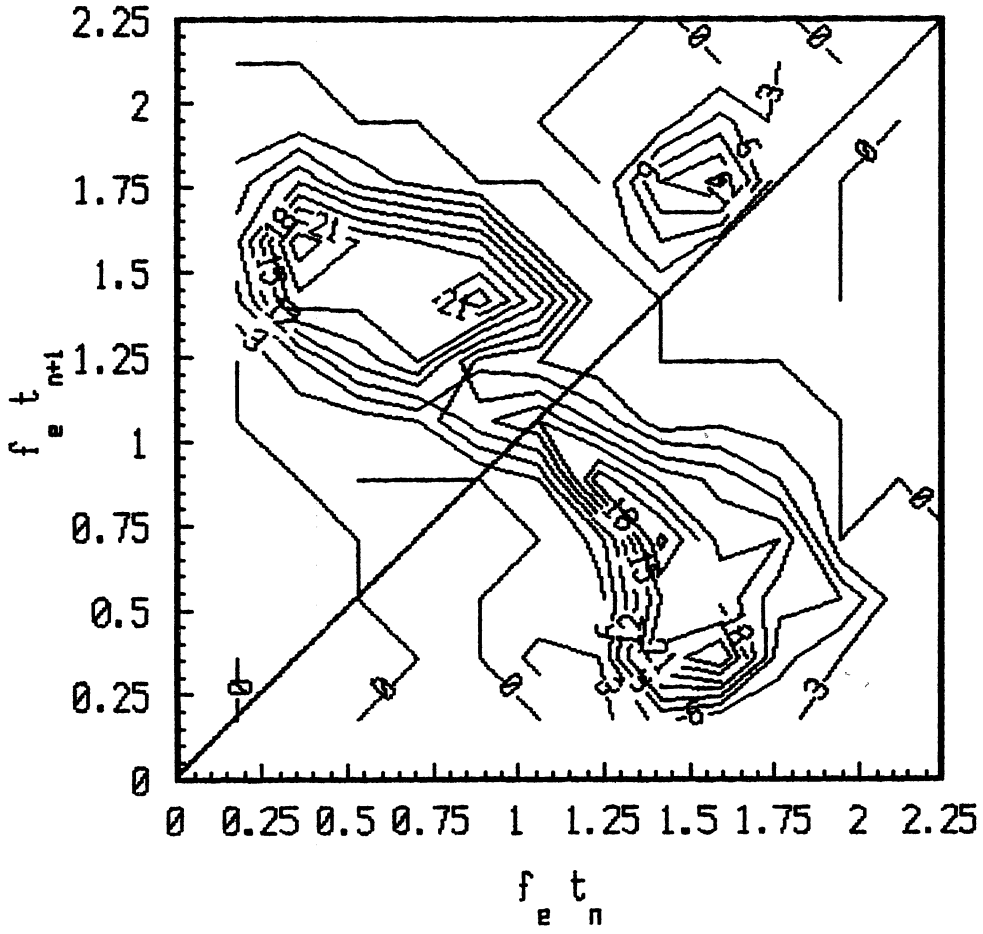

Figure 59. Poincare Section, f=5.3 Hz, x/D=2.0

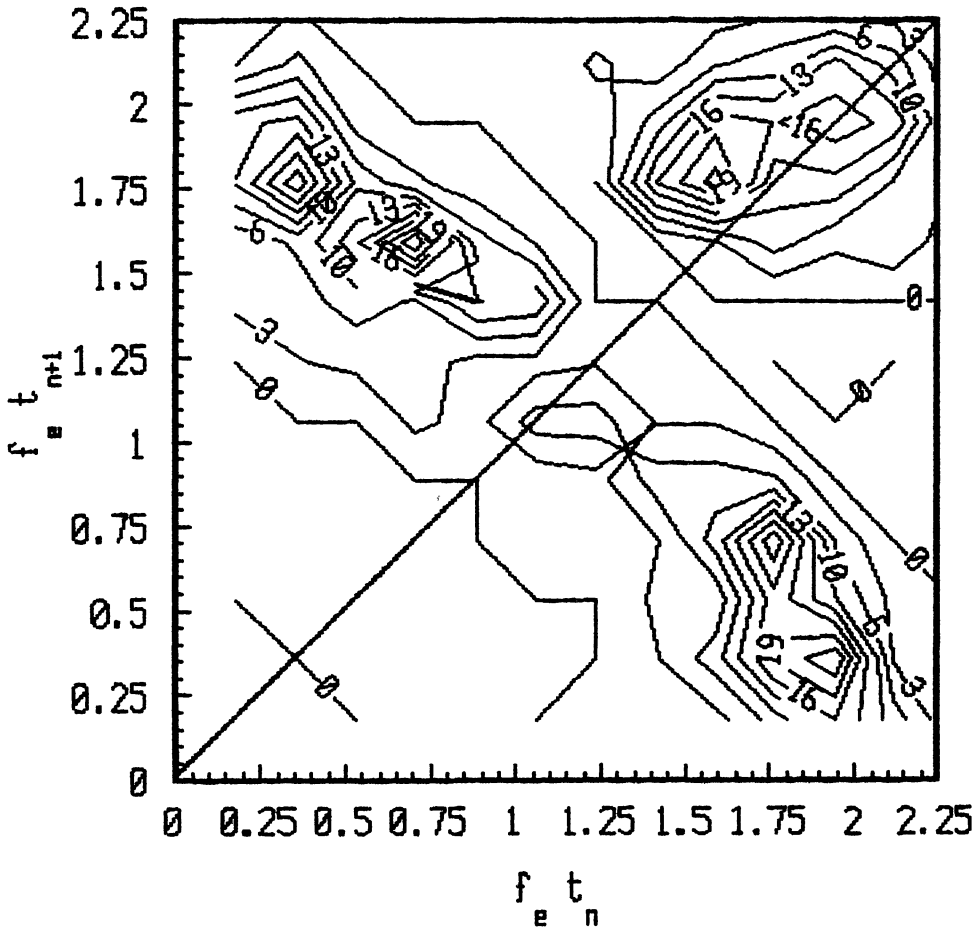

Figure 60. Poincare Section, f=5.3 Hz, x/D=2.5

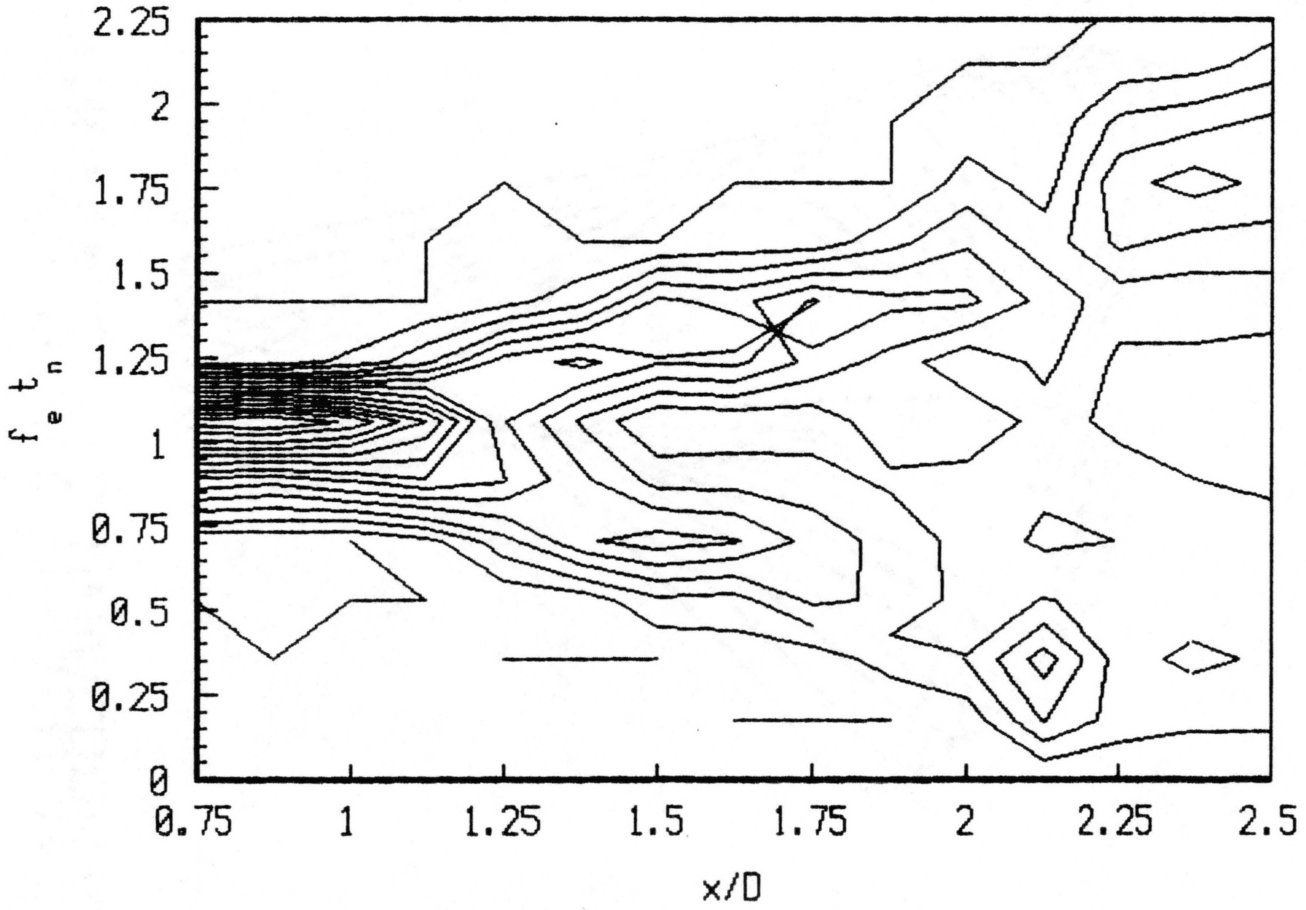

Figure 61. Bifurcation Diagram, f=5.3 Hz

produced using scale factors based on the x/D location and the number of bifurcations before that location. There appears to be a classic pitchfork bifurcation (figure 53) near the critical value of x/d = 1.25. The upper branch continues and another bifurcation is apparent near x/D = 2.25. The bottom arm simply disappears as the flow approaches chaos. This probably is the result of the relatively low number of data points or data scatter and not an indication that the bifurcation was a saddle-node bifurcation instead of the pitchfork bifurcation.

Figure 54 shows that for the 5.3 Hz case the flow is almost periodic at x/D = 0.75 as evidenced by the single peak. As with the 7 Hz case, there is considerable data scatter. However, the Poincare section is nearly symmetric about the 45 degree line; again indicating an invertable map. The peak is fairly broad and is therefore in agreement with indications from the 'vortex tracking' plot regarding fluctuations in the location of vortex rollup and initial convective velocities. A bifurcation begins between x/D = 0.875 and 1.0 (figures 55 and 56) and by x/D=1.25 (figure 56) the pattern clearly bifurcates (compare with the bifurcation diagram, figure 61). Thus, by x/D = 1.25, the motion is biperiodic indicating two competing frequencies whose ratio is rational. The pattern remains highly symmetric (invertable) past x/D=1.75 (figures 57-59). A new peak appears by x/D=2.0 and eventually results in the second bifurcation near x/D=2.15

(figures 60 and 61). This new peak is slightly off the centerline but the other peaks remain symmetric. These bifurcations definitely appear to be pitchfork bifurcations. Both arms of each bifurcation remain distinct (although the lower arms do overlap) indicating stable branches.

Schuster (1984) makes an interesting comparison between a bifurcation map of the logistic equation and the same data in the presence of external noise. When noise is present, only two bifurcations are distinguishable and the clean lines and patterns of the noise-free case are broad and blurred. This seems to explain why the bifurcations derived from the current experimental data do not appear as 'clean lines' and why only two bifurcations could be identified. Undoubtedly, the data under consideration is a combination of deterministic data and non-deterministic noise. The result is a broad band pattern on the bifurcation map.

In a later section, the location of these bifurcations will be used to estimate the location where chaotic vortical motion begins.

Onset of Chaos

Power Spectra. One of the important clues (especially for low-dimensional systems) to detecting chaotic motion is the appearance of a broad spectrum of frequencies when the input is a single-frequency harmonic motion (Lundqvist and

March, 1988; Moon, 1987). Figures 62 and 63 show that for both excitation frequencies, there is a discrete frequency power spectrum at x/D=0.25 with very little background noise. By x/D=2, there is a substantial increase in the broad spectrum. This indicates possible chaotic motion. It should be emphasized that this test for chaos is qualitative. It is only an indication that chaotic flow may exist.

Fractal Dimension. This is a quantitative test for chaos. A noninteger fractal dimension is the hallmark of a strange attractor and implies chaotic motion (Ciliberto and Gollub, 1985; Moon, 1987). In general terms, the fractal dimension is a measure of the extent to which orbits fill a certain subspace. Thus, as discussed in Chapter I, a dimension of zero represents a single point and a dimension of one represents a line.

There are several measures of fractal dimensions (Farmer, Ott, and Yorke 1983; Grassberger and Procaccia, 1983; Berge, Pomeau, and Vidal, 1986). The correlation dimension appears to be best suited for a time series and is used in this study. This fractal dimension is defined as

$$d = \lim_{r \to 0} \frac{\log C(r)}{\log r} \qquad (3.3)$$

where C(r) is a correlation function

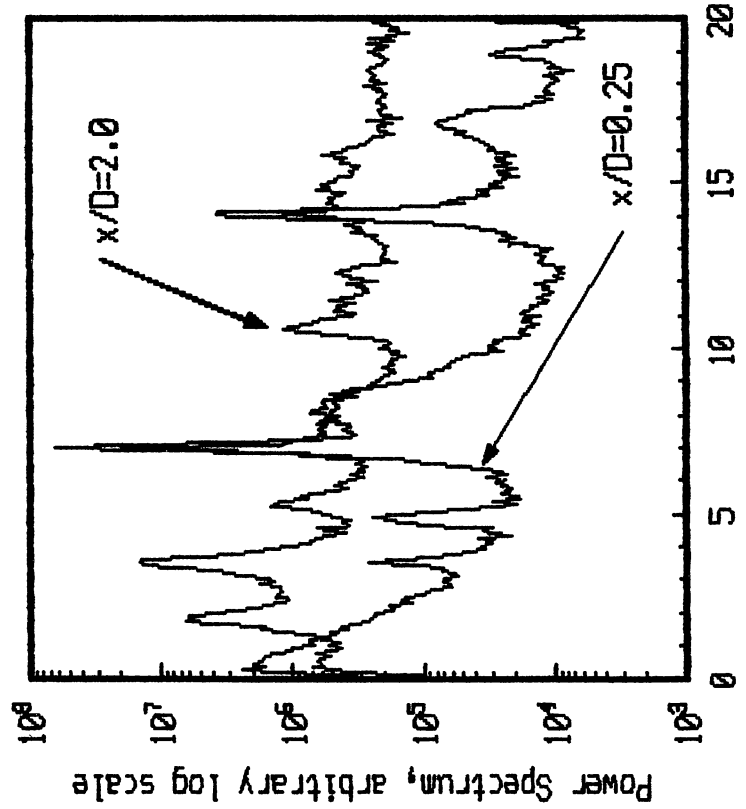

Figure 62. Power Spectrum Comparison
f=7 Hz

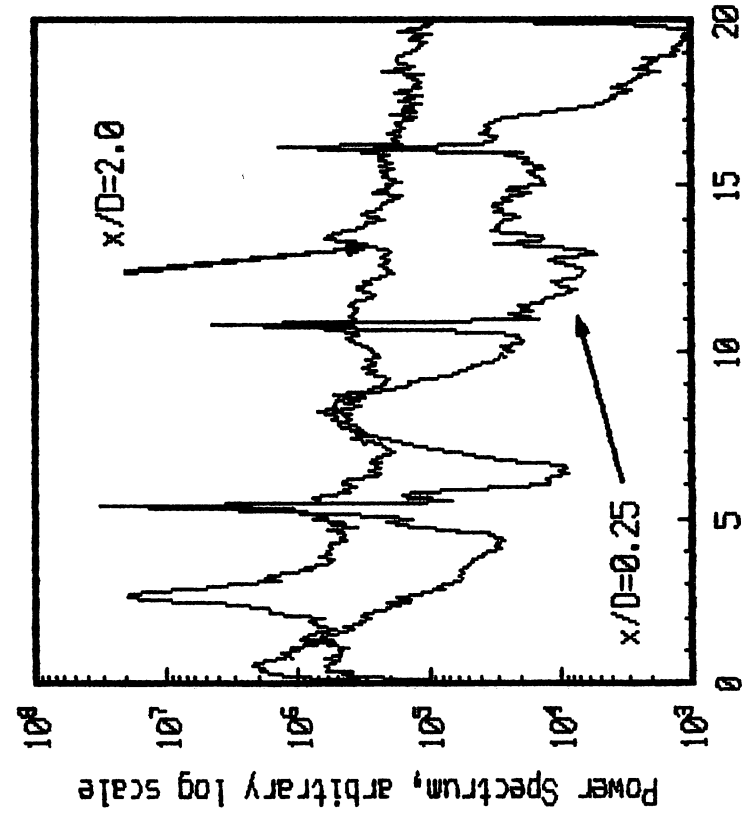

Figure 63. Power Spectrum Comparison
f=5.3 Hz

r is the radius of a circle

and d is the fractal dimension.

The correlation function is generated by producing a circle of radius r about the origin and counting the number of data pairs that lie inside the circle. Eventually, for some value of r, all of the pairs will lie inside the circle and C(r) will attain and remain at a value of 1.0. For smaller values of r, the slope (d) of the function when plotted (log C(r)) vs (log r) will be a straight line. If the trajectory is reconstructed in a p-dimensional space, the slope may change for increasing values of p (where p is the bifurcation parameter). For instance, if the function is white noise, the slope will always continue to change as p increases. If there exists some limiting value on the slope as p increases (d becomes independent of p), then the chaos is deterministic and the corresponding attractor strange. Mathematically, the correlation function is defined as

$$C(r) = \lim_{N\to\infty} \frac{1}{N^2} * \text{number of pairs}(i,j) \text{ with distance } s_{ij} < r \qquad (3.4)$$

For the current study, data sets were generated by calculating the time interval between vortex passages at a given x/D location. The time interval s_{ij} (i.e. $|t_1 - t_j|$) between all vortex pairs (vi, vj) was tabulated. A simple computer program was written which would examine each set of data and calculate the correlation term as a function of r (where r was the time interval t_n and varied

from 0.0333 seconds to 0.4333 seconds in increments of 0.0333). Plots of log C(r) vs log r are presented as figures 65 and 66. There exists a portion of the curves which is approximately linear. This slope of the linear section is the fractal dimension (d). As the longitudinal location approaches x/D=2.5 the slope approaches a limiting value of approximately 0.55 for a forcing frequency of 5.3 Hz and 0.58 for 7 Hz. The fact that a limit exists, and the slope at this limit is a noninteger, indicates that the attractors are strange for both initial conditions. For f=7 Hz, the slope (d) becomes independent of the bifurcation parameter (x/D or p) near x/D=2.25 indicating the onset of chaotic motion. The pattern is almost identical for the 5.3 Hz case and also indicates chaotic motion near x/D=2.25.

These data compare favorably (within 8%) with the logistic equation at the onset of chaos where a non-integer fractal dimension of 0.538 is calculated. The non-integer fractal dimension is generally accepted to be a clear indicator for the existence of chaotic behavior.

Estimation Based on the Feigenbaum Number. By knowing two successive bifurcation values of a quadratic map, an estimate of location of the onset of chaos (λ_∞) can be made (Moon, 1987). This relationship is

$$\lambda_\infty = \frac{1}{(\delta-1)} [\delta \lambda_{n+1} - \lambda_n] \qquad (3.5)$$

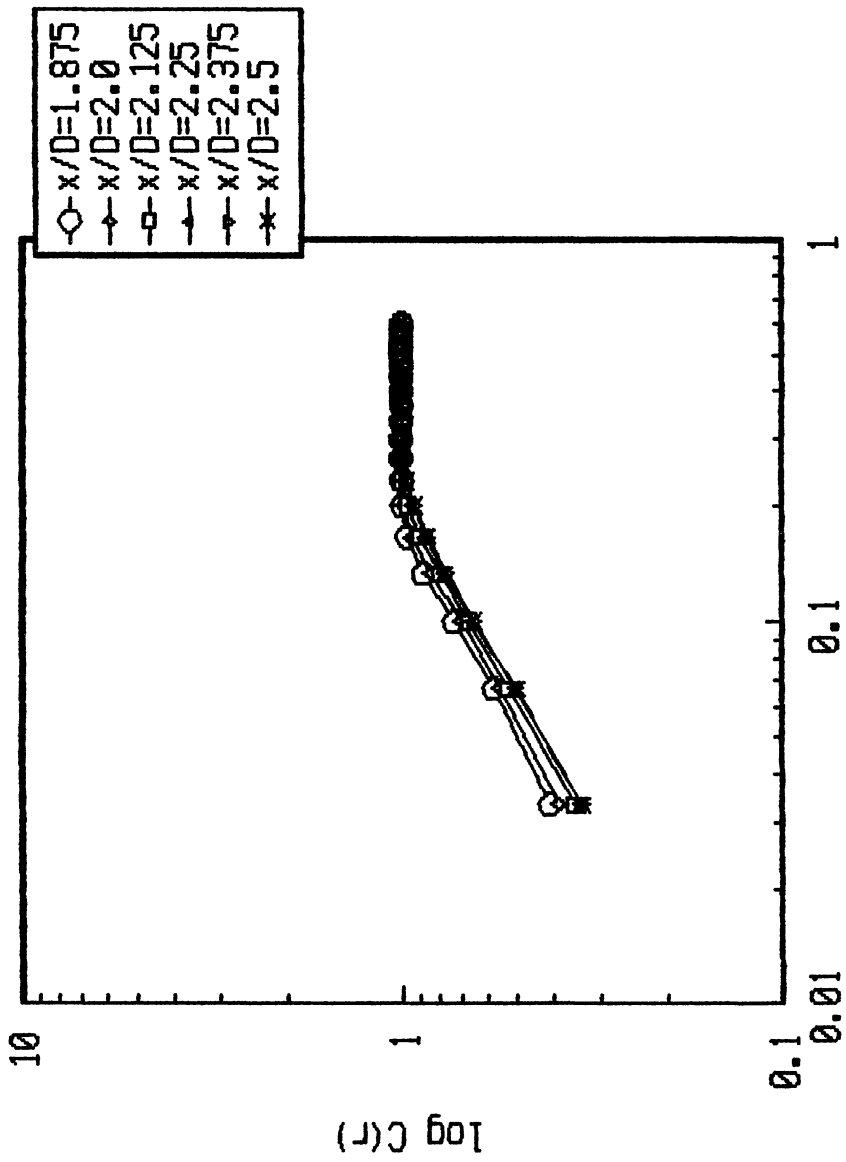

Figure 64. Fractal Dimension, f=7 Hz

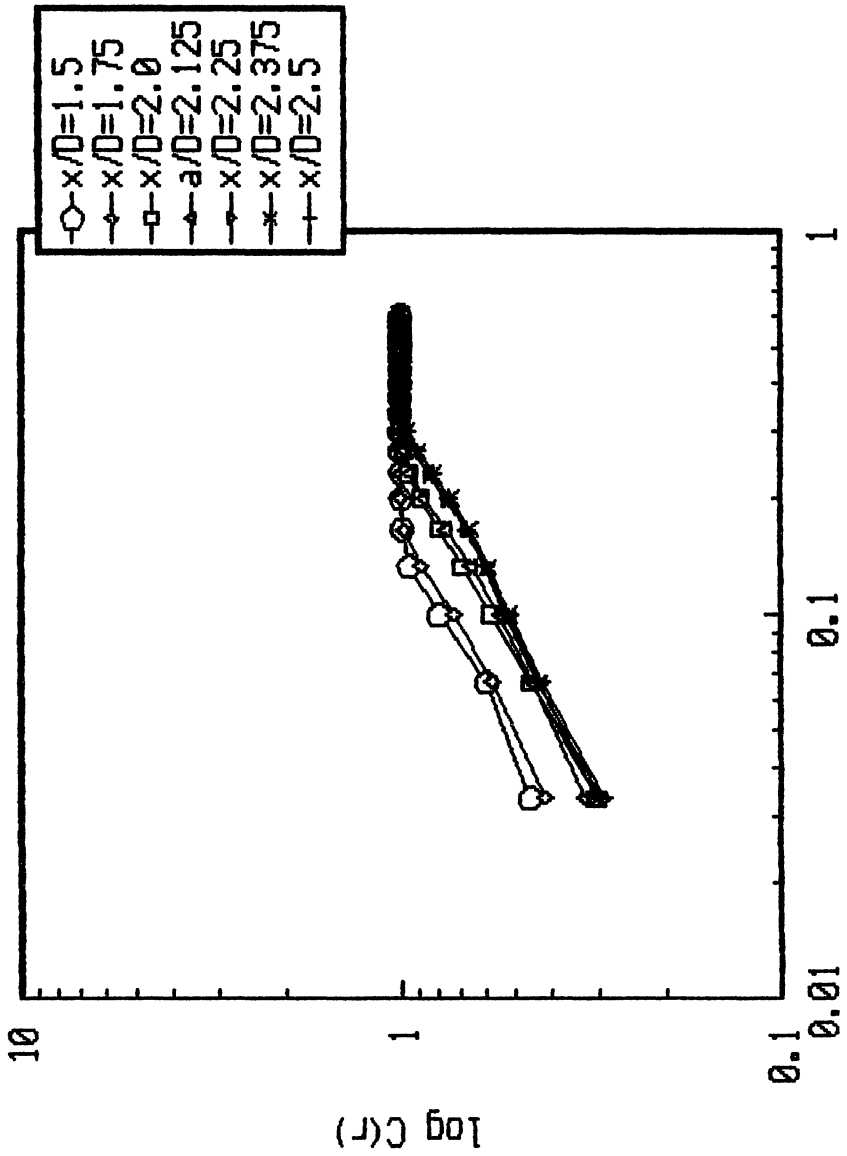

Figure 65. Fractal Dimension, f=5.3 Hz

where δ - Feigenbaum number = 4.6692...

λ_{n+1} and λ_n - location of two successive bifurcations

The Feigenbaum number is generally accepted to be a universal number and specifically apply to all one-dimensional maps of quadratic functions. Equation 3.5 is valid for any two successive bifurcations.

Application of this equation to the logistic equation with (see figure 66)

$$\lambda_n = \lambda_1 = 3.0$$

$$\lambda_{n+1} = \lambda_2 = 3.44949$$

$$\delta = 4.66920$$

gives an estimate for λ_∞ of 3.57199. This is within 0.2% of the correct value (3.56694...).

Fortunately the first two bifurcations can be clearly identified in the bifurcation diagram for both the 7 Hz and the 5.3 Hz cases. Unfortunately, random noise blends the data and makes it impossible to identify exact locations. Nevertheless, ballpark approximations for the location of onset of chaos can be obtained.

For the data with an external excitation at 5.3 Hz, the first bifurcation occurs between x/D=1.13 and 1.4 and is estimated to be approximately x/D = 1.38. The second bifurcation is between x/D=1.9 and 2.2 and is estimated at x/D = 2.13 (figure 61) Assuming the bifurcation parameter x/D starts with an initial value of zero, equation 3.5 can be used to obtain an estimate of x/D = 2.3 for the onset of

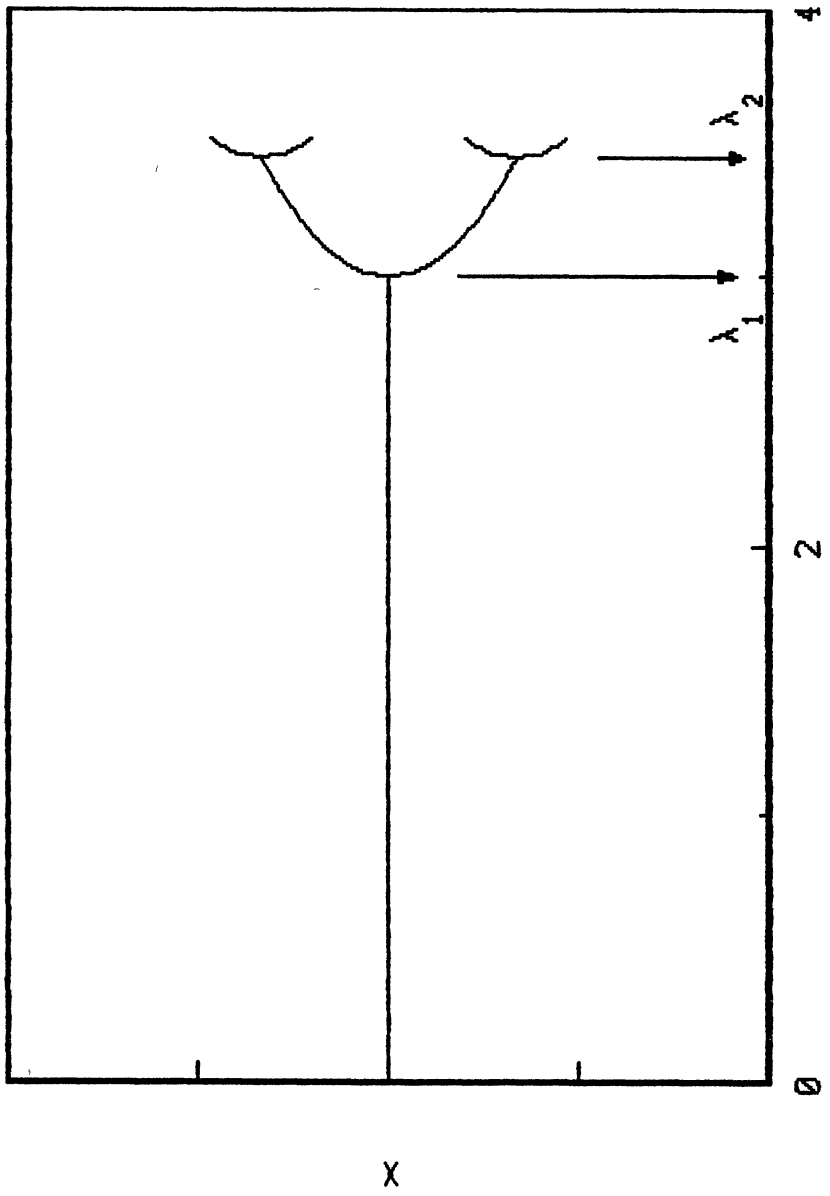

Figure 66. Schematic of Bifurcation Diagram for the Logistic Equation

chaos. Based on the uncertainty of the location of the first and second bifurcations, the onset of chaos can be calculated to be bounded between x/D=2.04 and 2.43. Similar calculations for the 7 Hz data, with λ_1=1.25 and λ_2=2.25 (Figure 52), gives an estimate for λ_∞ of 2.45. If λ_1 is between x/D=1.1 and 1.5 and λ_2 is between x/D=2.2 and 2.35, the onset of chaos is bounded between x/D=2.4 and 2.7. Thus, forcing at the 7 Hz frequency appears to organize the flow, delaying both the first and second bifurcations, and moves the location at which chaos is initiated. However, chaos is inevitable. Chaos was expected to exist when the flow was fully turbulent. External forcing was expected to organize the structure motion at least to the end of the potential core and perhaps well into the interaction region. Therefore, it is surprising that chaotic motion occurs so early in the flow field, substantially before the break down of the two-dimensional structures or the end of the potential core.

Lyapunov Exponent. As has been previously stated, chaos in a deterministic system implies extreme sensitivity to initial conditions. Thus, on the average, two trajectories that start close to each other will move exponentially away from each other for small times. For an experimental time series, the relationship is

$$d_n = d_o \, 2^{\lambda n} \qquad (3.6)$$

where d_n = distance between the trajectories n data points later

d_o = initial distance

λ = Lyapunov exponent

It is commonly accepted that a positive exponent implies chaotic behavior. Numerous authors have compared this quantitative analysis with the logistic equation (Moon, 1987; Thompson and Stewart, 1986; and Schuster, 1984). The onset of chaos is predicted exactly at $\lambda_n = 3.56994...$

A procedure for calculating the Lyapunov exponent for experimental data is suggested by Wolf, Swift, Swinney, and Vastano (1985). Unfortunately, negative exponents cannot be calculated by this procedure. However, chaos is inferred by a rapid rise and subsequent leveling in the positive value of the exponent. The procedure involves first selecting a reference (fuduciary) trajectory and a point on a nearby trajectory. The ratio d_n/d_o is then measured. When d_n becomes too large, a new 'nearby' trajectory is selected and the process continues. The exponent is calculated by a summation of the form

$$\lambda = \frac{1}{N} \sum_{k=1}^{N} \text{LOG}_2 \frac{d_n}{d_o} \qquad (3.7)$$

where N is the number of data points in that sequence.

Wolf provides a computer program to calculate the Lyapunov exponent from experimental data. This program was modified slightly to better fit the data under analysis. In its original form, the program would 'crash' when single data points were found to be outside of an expected range

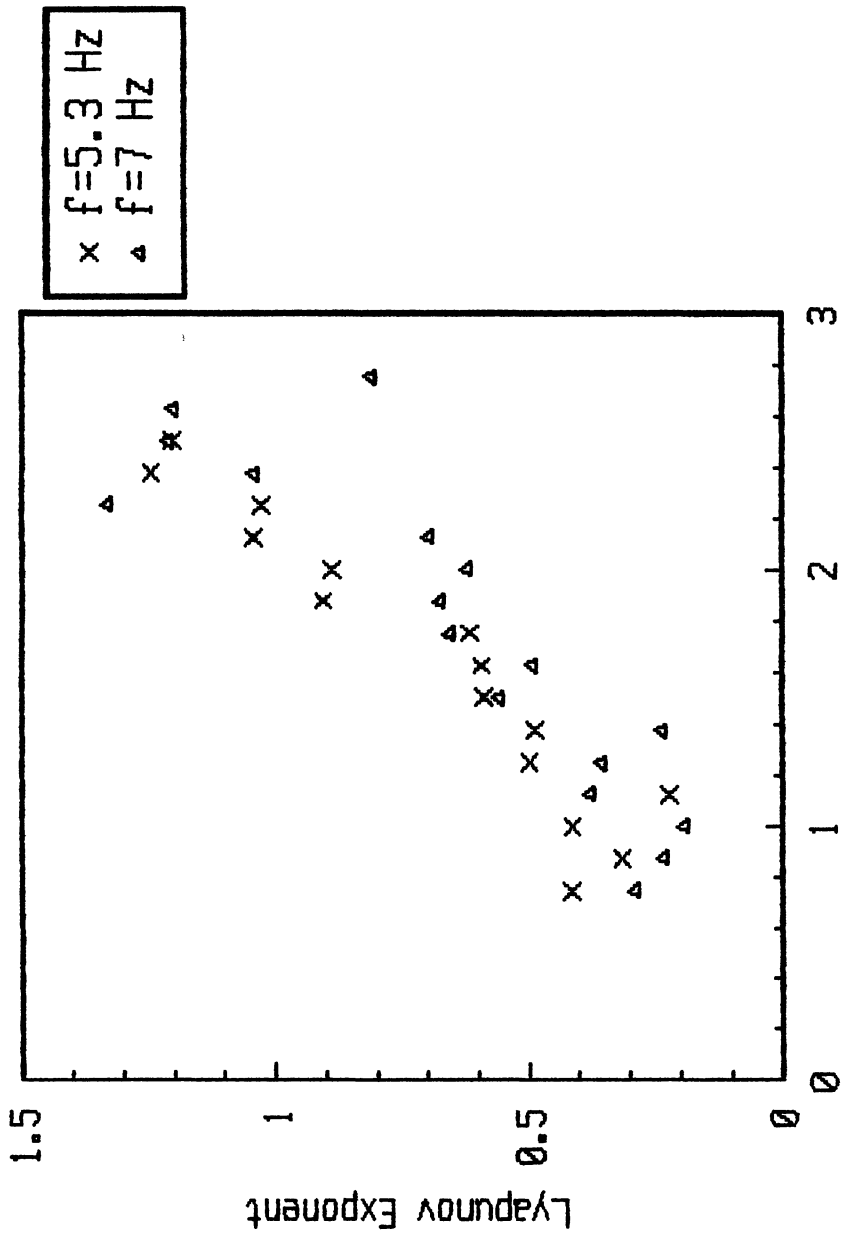

Figure 67. Onset of Chaos - Lyapunov Exponent

(especially when d_n would decrease suddenly). A section was added which allowed the program to ignore these occasional outlier points. The results are presented as Figure 67. For the 5.3 Hz case, the rapid rise in the value of λ levels out at about x/D=2.3. This leveling appears to occur at about x/D=2.4 for the 7 Hz case. These locations agree favorably with the analysis from the previous section. Again, the conclusion can be reached that external forcing can at best delay the onset of chaos. The eventual existence of chaos is inevitable.

Difference Between Chaotic Motion of the Vortical Structures and Turbulence

It has been shown that the motion of the two-dimensional coherent structures becomes chaotic before the jet becomes fully turbulent. This fact should not be too surprising. Turbulent flow is generally assumed to be chaotic. However, the reverse is not always true. Deterministic chaos applies to algebraic maps and dynamical systems where time is the only variable. Turbulence is both a temporally and spatially varying phenomenon.

These observations agree with a study performed by Aref (1983) involving vortex motion in two-dimensional flows. It was found that for a point-vortex system in unbounded flow, a system containing more than 3 point vortices is chaotic but not necessarily turbulent.

Turbulence was found to occur only in chaotic flows with many degrees of freedom.

CHAPTER IV

CONCLUSIONS AND RECOMMENDATIONS

Conclusions

Conclusions based on the experimental work presented are next summarized.

1. Onset of turbulence seems to be associated with the interaction of the shear layers near the end of the potential core. Fully turbulent flow did not occur until slightly after x/D=4 for either the tuned or untuned jets. It seems to be more than just coincidence that the average end of the potential core and the location of the first vortex pairing was between x/D=2.5 and 3.5. Therefore, the pairing mechanism may be related to the end of the potential core but does not appear to have a direct influence on the breakdown of the two-dimensional structures and the establishment of fully turbulent flow.

2. Initial vortex roll-up, and subsequent pairing can be strongly influenced by low amplitude external forcing. This forcing helps to organize the flow and isolate specific mechanisms. A natural jet appears to be a random combination of numerous vortex movements and pairing patterns. By forcing at a frequency which is near

the shear layer most unstable frequency and an even power of two times the jet column mode, a 'classic' pairing pattern is emphasized. The distance between each subsequent pairing doubles (for 7 Hz roll-up was at x/D=1, first pairing between 2.5 and 3, second pairing near x/D=5.5) and the frequency is halved at each pairing (7 Hz and roll-up, 3.5 Hz after the first pairing, 1.75 Hz after the second pairing). Forcing at other frequencies results in substantial adjustments in the shear layer in order to roll-up at the desired frequency.

3. No long term, continuously repeating pattern of vortex movements or interaction was found for the natural jet or even more importantly, the excited jet. Non-periodic behavior appears to exist as early as vortex roll-up. Certainly, the visualized structures were slightly non-periodic at the location where they were first distinguishable. The exact location where the vortex movements established chaotic behavior was difficult to establish. However, strong evidence that chaotic behavior does exist has been presented. Forcing to produce a tuned jet may slightly delay the onset of chaotic movements as compared to the untuned jet ($x/D \approx 2.4$ vs $x/D \approx 2.3$). The really important point is that chaotic vortical motion begins near the same location for both cased under study. Therefore, it is concluded that chaotic behavior is inevitable and will occur near the same location for any

flow condition. This confirms that downstream of some x/D location, no purely periodic motion exists.

4. There does not seem to be any correlation between the onset of chaotic vortical motion and the breakdown of the structures into turbulence.

Recommendations

1. A better procedure needs to be developed to monitor the vortex motions. The current procedure used a video camera with a maximum 'shutter' speed of 30 per second. This resolution needs to be improved to obtain clearer poincare maps and to more accurately examine the non-periodic roll-up of the vortices. An additional procedure is needed to more precisely locate the vortex structure. A computer data imaging system might accomplish this task.

2. No information is available regarding the influence of several variables on the vortex movements and onset of chaotic behavior. Two of these parameters are Reynold's number (slot width and /or flow velocity) and external forcing amplitude.

3. An experimental test needs to be conducted to more closely relate the spectral frequencies with visual observations of dye images. A complete description of the nonrotating dye marks in the untuned jet is also desired. A hot film probe could be placed in the shear to compute velocity fluctuations in both the longitudal and lateral

directions. Simultaneous video and hot film data could be taken to better isolate the location of vortex rollup and pairing.

REFERENCES

Antonia, R. A., Browne, L. W. B., Rajagopalan, S., Chambers, A. J. (1983). On the Organized Motion of a Turbulent Plane Jet. Journal of Fluid Mechanics, 134, 49-66.

Aref, H. (1983). Integrable, Chaotic, and Turbulent Vortex Motion in Two-Dimensional Flows. Ann. Rev. Fluid Mech., 15, 345-389.

Aref, H., Kambe, T. (1988). Report on the IUTAM Symposium: Fundamental aspects of Vortex Motion. J. Fluid Mech., 190, 571-595.

Aref, H. (1983). Integrable, Chaotic, and Turbulent Vortex Motion in Two-Dimensional Flows. Ann. Rev. Fluid Mech., 15, 345-389.

Aref, H., Kambe, T. (1988). Report on the IUTAM Symposium: Fundamental aspects of Vortex Motion, J. Fluid Mech., (190), 571-595.

Becker, H. A., Massaro T. A. (1988). Vortex Evolution in a Round Jet, J. Fluid Mech., 31, 435-448.

Berge P., Pomeau Y., Vidal, C. (1986). Order Within Chaos, New York: John Wiley and Sons.

Bradbury, L. J. S. (1965). The Structure of a Preserving Turbulent Plane Jet. J. Fluid Mech., 23, (1), 31-65.

Browand, F. K., Weidman, P. D.(1976). Large Scales in the Developing Mixing Layer. J. Fluid Mechanics, 76,(1), 127-144.

Brown, G. L., Roshko, A. (1974). On Density Effects and Large Structure in Turbulent Mixing Layers. J. Fluid Mechanics, 64, 775-806.

Bruun, H. H. (1977). A Time Domain Analysis of the Large Scale Flow Structure in a Circular Jet. J. Fluid Mechanics, 83, (4), 641-671.

Cervantes De Gortari, J. G. (1978). An Experimental Study of the Flapping Motion of a Turbulent PLane Jet. Purdue University: Ph.D. dissertation.

Chambers, F. W. (1977). Acoustic Interaction With a Turbulent Plane Jet. Purdue University: Ph.D. dissertation.

Ciliberto, S., Gollub, J. P. (1985) Chaotic Mode Competition in Parametrically Forced Surface Waves. J. Fluid Mech., 158, 381-398.

Chu Huan-Chang (1987). Quantitive Measurement of Nonlinear Wave Interactions Characterizing the Transition of a Planar Turbulent Jet. Oklahoma State Univ.: M.S. Thesis.

Crow, S. C. and Champagne, F. H. (1971). Orderly Structures in Jet Turbulence. J. Fluid Mech., 48, (3), 547-591.

Donaldson, C. duP and Snedeker, R. S. and Margolis, D. P. (1971). A study of free Jet Impingement. Part 2. Free Jet Turbulent Structure and Impingement Heat Transfer. J. Fluid Mech., 45,(3), 477-512.

Everıtt, K. W. and Robins, A. G.(1978). The Development and Structure of Turbulent Plane Jets. J. Fluid Mech., 88,(3), 563-568.

Farmer, J. D., Ott, E., Yorke, J. A. (1983). The Dimension of Chaotic Attractors, Physica, 7D, 153-180.

Flora, J. J. Jr., and Goldschmidt, V. W. (1969). Virtual Origins of a Free Plane Turbulent Jet. AIAA Journal, 7, (12), 2344-2346.

Foss, F. J. (1965). A Study of Incompressible Bounded Turbulent Jets. Purdue University: Ph.D. Dissertation.

Gleick, J. (1987). Chaos: Making a New Science. Viking: New York.

Grassberger, P., Procaccia, I. (1983). Characterization of Strange Attractors. Physical Review Letters, 50,(5), 346-349.

Gutmark, E. and Wygnanski, I.(1976). The Planar Turbulent Jet. J. Fluid Mech., 73, 465-495.

Hinze, J. O. (1975). Turbulence. New York: McGraw-Hill, Inc.

Ho C.M., Huang L.S.(1982). Subharmonics and Vortex Merging in Mixing Layers. J. Fluid Mechanics, 119, 443-73.

Ho Chih-Ming, Huerre P. (1984). Perturbed Free Shear Layers. Annual Review of Fluid Mechanics, 16, 365-425.

Hussain, A.K.M.F. (1986). Coherent Structures and Turbulence. J. Fluid Mechanics, 173, 1986, 303-356.

Hussain, A.K.M.F. (1986). Coherent Structures-Reality and Myth. Phys Fluids, 26,(10) 2816-2850.

Hussain, A.K.M.F., Zaman, K.B.M.Q. (1985). An Experimental Study of Organized Motion in the Turbulent Plane Mixing Layer. J. Fluid Mechanics, 85-104.

Jenkins, P. E., Goldschmidt, V. M.(1974). Study of the Intermittent Region of a Two-Dimensional Plane Jet. Herrick Lab Report, HL 74-75. Purdue University.

Jimenez, J. (1980). On the Visual Growth of a Turbulent Mixing Layer. J Fluid Mech., 96, 447-460.

Jones, S. W., Aref, H. (1988). Chaotic Advection on Pulsed Source-Sink Systems. Phys. Fliuds, 31, 469-485.

Kaiser, K. F. (1971). An Experimental Investigation of Interaction of an Acoustic Field and a Plane Turbulent Jet. Purdue University: M.S. Thesis.

Kline, S. J. , McClintock, F. A. (1953). Describing Uncertainties in Single-Sample Experiments. Mech. Engr., 75, 3.

Lasheras J.C., Choi H. (1988). Three Dimensional Instability of a Plane Free Shear Layer: An Experimental Study of the Formation and Evolution of Streamwise Vortices. J. Fluid Mechanics., 189, 53-86.

Lundqvist, S., March, N. H., Tosi, M. P. (1988). Order and Chaos in Nonlinear Physical Systems, (eds), New York: Plenum Press.

Mandelbrot, B. B. (1983). The Fractal Geometry of Nature, New York: W.H. Freeman and Company.

McInville R. M., Gatski T. B., Hassan H. A. (1985). Analysis of Large Vortical Structures in Shear Layers. AIAA J., 23, (8), 1165-1171.

Monkewitz, P. A. (1988). Subharmonic Resonance Pairing and Shredding in the Mixing Layer. J. Fluid Mech., 188, 223-252.

Moon, F. C. (1987). Chaotic Vibrations, An Introduction for Applied Scientists and Engineers. New York: John Wiley & Sons.

Mulej, K. J. (1975). The Velocity of the Interface. Purdue University: M.S. Thesis.

Oler J. W., Goldschmidt V. W. (1982). A Vortex-Street Model of the Flow in the Similarity Region Of A Two-Dimensional Free Turbulent Jet. J. Fluid Mech., 123, 523-535.

Oler J. W., Goldschmidt V. W. (1984). Coherent Structures in the Similarity Region of Two Dimensional Turbulent Jets. J. Fluids Engineering, 106, (6) 187-192.

Ott, E. S. (1972). Convective Velocities in a Turbulent Plane Jet. Purdue University: M.S. Thesis.

Peterson R.A. (1978). Influence of Wave Dispersion on Vortex Pairing in a Jet. J. Fluid Mechanics, 89, 469-495.

Prasad, R. R., Meneveau, C., Sreenivasan, K. R. (1988). Multifractal Nature of the Dissipation Field of Passive Scalars in Fully Turbulent Flows, 61,(1), 74-77.

Prakash, K. M. K. (1986). Influence of a Global Resonance Mechanism on the Structural Development of a Planar Turbulent Jet. Oklahoma State University: M.S. Thesis.

Ramaprian B. R., Patel V. C., Sastry M. S. (1982). The Symmetric Turbulent Wake of a Flat Plate. AIAA, 20, 1228-1235.

Rockwell D.O. (1972). External Excitation of Planar Jets. J of Applied Mechanics, Dec., 883-890.

Rockwell D.O., Niccolls W.O. (1972). Natural Breakdown of Planar Jets. Transaction of the ASME J. of Basic Engineering, Dec. 720-730.

Sato, H. (1960). The stability and Transition of a Two-Dimensional Jet, J. Fluid Mech., 7, 53-80.

Schuster, H. G. (1984). Deterministic Chaos. Physik-Verlag, GmbH, Weinheim (Federal Republic of Germany).

Shaw, R. (1984). The Dripping Faucet as a Model Chaotic System. Santa Cruz, Ca.: Aerial Press.

Sreenivasan, K. R., Meneveau, C. (1986). The Fractal Facets of Turbulence, J. Fliud Mech., 173, 357-386.

Thomas, F. O. (1980). Effect of Nozzle Geometry of Acoustic Interaction With a Turbulent Jet. Purdue University: M.S. Thesis.

Thomas, F. O. (1983). Development of a Two-Dimensional Turbulent Jet Under Natural and Excited Conditions. Purdue University: Ph.D. Dissertation.

Thomas F. O., Brehob E. G. (1986). An Investigation of Large-scale Structure in the Similarity Region of a Two Dimensional Trubulent Jet. Phys of Fluids, 29, 1986, 1788-1795.

Thomas, F. O., Chu H. C. An experimental Investigation of the Transition of a Planar Jet: Subharmonic Suppression and Upstream Feedback. Physics of Fluids A, Vol 1, No. 9, Sept 1989, 1566-1587.

Thomas, F. O., Goldschmidt V. W. (1986). Structural Characteriscics of a Developing Turbulent Planar Jet. J. Fluid Mechanics, 227-256.

Thompson, J. M. T., Stewart, H. B. (1986). Nonlinear Dynamics and Chaos. New York: John Wiley & Sons.

Van Der Hegge Zijnen, B. G. (1958). Measurements of Turbulence in a Plane Jet of Air by the Diffusion Method and by the Hot-Wire Meghod. Applied Science Rec. Section A,, 7, 256-276.

Winant C. D., Browand F. K.(1974). Vortex Pairing: the Mechanism of Trbulent Mixing Layer Growth at Moderate Reynolds Number. J. of Fluid Mechanics, 63, (2), 237-255.

Wolf, A., Swift, J. B., Swinney, H. L, Vastano, J. A. (1985) Determining Lyapunov Exponents From a Time Series. Physica, 16D, 285-317.

APPENDIX

UNCERTAINTY ANALYSIS

In order to determine the experimental uncertainties associated with measurements performed in this investigation, an analysis based on the method of Kline and McClintock (1953) was used. The following results were obtained

1. Uncertainty in Mean Velocity Measurements

The water velocity was set using a calibrated rotometer using the equation

$$Um = [(r*a + b)/c]^{0.45}$$

where r = rotometer setting
a = 0.00202
b = 0.000275
c = 0.01788

The uncertainty in setting the rotometer was 0.1 and the mean setting was 2.5.

Then the uncertainty due to the rotometer setting is

$$\frac{\partial Um}{\partial r} = 0.45 * (a/c) * [(r*a + b)/c]^{-0.55} = 0.099$$

$$\text{uncertainty} = \left[\left(\frac{\partial Um}{\partial r}\right)^2 * (0.1)^2\right] = 0.0099 \text{ or } 1.7\%$$

Repeatability was found to be within 2%, therefore the total uncertainty is estimated to be

$$Um = Um \pm 3.7\%$$

2. Uncertainty in setting the Reynolds Number

$$Re = Um*D/\nu$$

The mean velocity has an uncertainty of 3.7%

(0.021 ft/sec) and a mean value of 0.581 ft/sec

The viscosity has an uncertainty of 6%

(7.32×10^{-7} ft^2/sec) due to temperature

fluctuations and a mean value of

1.22×10^{-5} ft^2/sec

The Reynolds Number uncertainty due to mean

velocity is

$$\frac{\partial Re}{\partial Um} = D/\nu = 3415$$

The Reynolds Number uncertainty due to viscosity

is

$$\frac{\partial Re}{\partial \nu} = (Um*D) * m^{-2} = -162,650,000$$

Then the total uncertainty w is estimated to be

$$w = [(3415)^2 * (0.0099)^2 + (1.627 \times 10^8)^2 * (7.32 \times 10^{-7})^2]^{0.5}$$

$$= 139 \quad \text{or } 6.9\%$$

3. Uncertainty in RMS Velocity Measurements is estimated based on repeatability to be

$$u = 5\%$$

VITA

JAMES W. CUTBIRTH

Candidate for the degree of

Doctor of Philosophy

Thesis: CHAOTIC VORTICAL MOTION IN THE NEAR REGION OF A PLANE JET

Major Field: Mechanical Engineering

Biographical:

Personal Data: Born in Monahans, Texas, August 4, 1946, the son of Wilbert and Mary Cutbirth.

Education: Graduated from Monahans High School, Monahans, Texas in May 1964; received Bachelor of Science in Aerospace Engineering from the University of Texas at Austin in January, 1969; received Master of Science in Engineering from the University of Texas at Austin in August, 1973; completed requirements for the Doctor of Philosophy degree at Oklahoma State University in December, 1991.

Professional Experience: Experimental Test Engineer, Pratt and Whitney Aircraft, West Palm Beach, Florida, January 1969 to May 1972; Teaching and Research Assistant, University of Texas, Austin, Texas, September 1972 to January 1975; Aerodynamics Engineer at The Boeing Company, Renton, Washington, January 1975 to May 1979; Associate Professor at Oklahoma Christian University of Science and Arts, Oklahoma City, Oklahoma, August 1983 to December 1991.